

**CHARACTERIZATION OF SUGAR
TRANSPORTERS AND CATABOLIZING
ENZYMES INVOLVED IN *ARABIDOPSIS-
PSEUDOMONAS/BOTRYTIS* INTERACTIONS**

Inaugural dissertation

for the attainment of the title of doctor
in the Faculty of Mathematics and Natural Sciences
at the Heinrich Heine University Düsseldorf

presented by

Chen Deng

from Hsinchu, Taiwan (R.O.C.)

Düsseldorf, March 2025

from the institute for Molecular Physiology
at the Heinrich Heine University Düsseldorf

Published by permission of the
Faculty of Mathematics and Natural Sciences at
Heinrich Heine University Düsseldorf

Supervisor: Prof. Dr. Wolf B. Frommer
Co-supervisor: Prof. Dr. Jane E. Parker

Date of the oral examination: 2025.03.17

TABLE OF CONTENTS

Abstract.....	1
Introduction	2
The transport and metabolic processes of sucrose in Arabidopsis.....	2
Beneficial microorganisms depend on sugars derived from host plants for their sustenance	6
Sugars play a significant role in enhancing the virulence of phytopathogenic microorganisms.....	8
Phytopathogenic microorganisms create a niche within plants that is enriched with sugars	9
Sugars play a crucial role in enhancing the immune systems of plants.....	11
Plant defense inhibit the formation of suitable habitats.....	12
Objectives of the research.....	13
Sugars derived from Arabidopsis are proposed to function as potential virulence- inducing signals and nutritional metabolites for <i>Pst</i> DC3000.....	14
Transcriptional reprogramming of Arabidopsis STP13 in response to the challenge posed by <i>Pst</i> DC3000.....	15
The sugar transporters and invertases found in Arabidopsis may influence the plant's susceptibility to <i>B. cinerea</i>	16
Materials and Methods.....	18
Evaluations of the proliferation of <i>Pst</i> DC3000 mutant strains cultured in a modified <i>hrp</i> derepressing medium.....	18
Assessment of Arabidopsis susceptibility to mutant strains of <i>Pst</i> DC3000	19
Evaluation of the susceptibility of Arabidopsis mutant to <i>Pst</i> DC3000.....	20
Histochemical analysis of GUS fusions in Arabidopsis infected with <i>Pst</i> DC3000	21
Analysis of the subcellular localization of dCas9-TurboID-mVenus	23
Evaluation of the biotin ligase activity of the dCas9-TurboID-mVenus.....	26
Identification of proteins associated with the STP13 promoter during <i>Pst</i> DC3000 infection	27
Confocal imaging of GFP fusions in Arabidopsis infected with <i>B. cinerea</i>	31
Histochemical analysis of GUS fusions in Arabidopsis infected with <i>B. cinerea</i>	36
Assessment of the susceptibility of Arabidopsis mutants to <i>B. cinerea</i> B05.10.....	37
Results.....	40
<i>Pst</i> DC3000 relies on the sucrose porin precursor ScrY to facilitate the rapid uptake of sucrose.....	40
<i>Pst</i> DC3000 utilizes the enzyme sucrose-6-phosphate hydrolase ScrB and the sucrose uniporters SWEET11, SWEET12, and SWEET13 to promote its rapid proliferation within the leaves of Arabidopsis	41
The hexose uniporter SWEET4 is observed to accumulate in the leaf veins in response to the challenge posed by <i>Pst</i> DC3000	43

Investigating the transcriptional regulation of STP13 in Arabidopsis leaves infected by <i>Pst</i> DC3000.....	45
Hexose/proton symporters STP3 and STP4 are dispensable for Arabidopsis susceptibility to <i>B. cinerea</i> infection.....	50
Vacuolar invertases VIN1 and VIN2 might contribute Arabidopsis resistance to <i>B. cinerea</i> infection.....	56
Cell wall/vacuolar inhibitor of fructosidase C/VIF1 and C/VIF2 are dispensable for Arabidopsis susceptibility to <i>B. cinerea</i> infection.....	58
Tonoplast-localized hexose uniporter SWEET2 and SWEET17 are dispensable for Arabidopsis susceptibility to <i>B. cinerea</i> infection.....	60
Cytosolic invertase 1 contributes Arabidopsis susceptibility to <i>B. cinerea</i> infection.....	62
Plasma membrane-localized sucrose uniporters SWEET11, SWEET12 and SWEET13 contribute Arabidopsis susceptibility to <i>B. cinerea</i> infection.....	63
Sucrose/proton symporters SUC1 and SUC3 are dispensable for Arabidopsis susceptibility to <i>B. cinerea</i> infection.....	65
Discussion.....	68
Sugars influence the susceptibility of Arabidopsis to infection by <i>Pst</i> DC3000.....	68
Identifying proteins associated with the Arabidopsis STP13 promoter through proximity labeling continues to present significant challenges.....	70
Sugar modulates the susceptibility of Arabidopsis to infection by <i>B. cinerea</i>	72
Conclusion.....	78
References.....	79
Appendix.....	90

Abstract

Phytopathogenic microorganisms colonizing plant leaves significantly reduce crop yields, and sugar reallocation plays a crucial role in influencing plant susceptibility to these pathogens. However, the mechanisms underlying sugar transport and metabolism alterations in various leaf cell types during pathogen invasion remain largely unexplored. This study utilized confocal imaging techniques on *Arabidopsis thaliana* (*Arabidopsis*) reporter lines infected with *Botrytis cinerea* (*B. cinerea*) to investigate sugar transport and metabolism in different leaf cell types. The results revealed that sucrose hydrolysis mediated by cytosolic, vacuolar, and cell wall invertases occurs in multiple cell types, while the activities of vacuolar and cell wall invertases are inhibited in mesophyll and phloem cells. Furthermore, genetic analyses identified key genes involved in mediating *Arabidopsis* susceptibility to pathogen infection, including cytosolic invertase 1, vacuolar invertases, and plasma membrane-localized sucrose uniporters. Additionally, the study found that *Pseudomonas syringae* pv. tomato DC3000 (*Pst* DC3000) utilizes its sucrose porin precursor and sucrose-6-phosphate hydrolase for sucrose assimilation and bacterial proliferation. A CRISPR/dCas9-TurboID-based proximity labeling approach was developed in *Arabidopsis* to identify transcriptional activators of the proton/hexose symporter STP13 during *Pst* DC3000 infection, although further optimization is necessary. This research provides novel insights into the genetic factors coordinating pathogen virulence, plant immune responses, and cellular survival in *Arabidopsis* leaves infected by *B. cinerea* and *Pst* DC3000, ultimately contributing to the development of strategies to improve crop resistance to phytopathogenic microorganisms.

Introduction

The transport and metabolic processes of sucrose in Arabidopsis

Photosynthesis, conducted by plants, algae, and cyanobacteria, serves as the principal source of fixed carbon for all life on Earth. During the process of photosynthesis in plants, triose phosphates (triose-P) are generated when carbon dioxide is assimilated in the chloroplasts via the Calvin cycle. A triose-P/phosphate translocator facilitates the transport of triose-P into the cytosol. Within the cytosol, the enzyme aldolase catalyzes a reaction that converts two molecules of triose-P into one molecule of fructose 1,6-bisphosphate (F1,6BP). Subsequently, F1,6BP is further metabolized to yield various hexose phosphates, such as glucose 6-phosphate (G6P) and fructose 6-phosphate (F6P). G6P can be utilized to synthesize nucleotide sugars, including uridine diphosphate glucose (UDP-G). The enzyme sucrose phosphate synthase (SPS) catalyzes the reaction between UDP-G and F6P, resulting in the formation of sucrose-6-phosphate (S6P). Finally, sucrose phosphate phosphatase (SPP) catalyzes the dephosphorylation of S6P to yield sucrose (Ruan, 2014).

In the model dicotyledonous plant *Arabidopsis*, sucrose is distributed within the leaves as follows: approximately 50% in the cytosol, 15% in the vacuole, and 35% in the chloroplast (Vu et al., 2020). The sucrose present in the cytosol can be metabolized by cytosolic invertases (CINVs) and sucrose synthases, thereby facilitating cellular metabolic processes. CINVs are responsible for the hydrolytic cleavage of sucrose, resulting in the production of glucose and fructose. These enzymes are classified as neutral invertases, exhibiting an optimal pH range of 7.0 to 8.0, and belong to the glycoside hydrolase family 100 (GH100). Structural analysis through X-ray crystallography has demonstrated that *AtCINV2* adopts a (α/α)₆-barrel conformation, characterized by surface loops that include short β -hairpins (Tarkowski et al., 2020). Comparative structural alignment with *Anabaena* invertase A indicates that specific residues within *AtCINV2*—namely Phe124, Arg126, Asp127, Asp263, Tyr445, His446, Gln507, and Trp509—constitute the sucrose binding pocket, while residues Asp263 and Glu489 are implicated in the catalytic hydrolysis of sucrose (Xie et al., 2016). Additionally, sucrose synthase functions as a glycosyl transferase enzyme, catalyzing the reversible conversion of sucrose into fructose and UDP-G, which serves as a precursor for cellulose and starch biosynthesis (Stein and Granot, 2019).

The uptake of sucrose into the vacuole is facilitated by the tonoplast-localized sugar transporters TONOPLAST MONOSACCHARIDE TRANSPORTER 1 (*AtTMT1*) and *AtTMT2*, while the efflux of vacuolar sucrose is mediated by the tonoplast-localized sucrose/proton symporter SUCROSE TRANSPORTER 4 (*AtSUC4*) (Schulz et al., 2011). Sucrose transporters (SUTs/SUCs) are classified as sucrose/proton symporters within the major facilitator superfamily (Riesmeier et al., 1992; Sauer and Stolz, 1994). *AtSUC1* is characterized by twelve transmembrane domains (TMDs) and features a nine-amino acid amphipathic alpha helix located in the core cytoplasmic loop between TMDs 6 and 7, as well as a short extracellular amphipathic alpha helical domain situated between TMDs 5 and 6 in its outward-open conformation (Bavnhøj et al., 2023). Through the integration of crystal structure analysis, molecular dynamics simulations, and biochemical characterization, Bavnhøj et al. suggest that the sucrose transport cycles mediated by *AtSUC1* adhere to the alternating access model (Latorraca et al., 2017). The protonated residues Asp152, Arg163, and other binding pocket constituents (e.g., Trp47, Gly75) facilitate the binding of the glucosyl moiety of sucrose within the expansive cavity of the outward-opened *AtSUC1*. During the transition from the outward-open to the inward-open state, the intracellular network of salt bridges is disrupted, while charged and polar residues likely establish interactions between helices on the extracellular side. A change in the acid dissociation constant (pKa) directed by Gln50 leads to the deprotonation of Asp152, thereby promoting the release of sucrose into the cytosol.

Vacuolar sucrose can undergo conversion into fructans through the action of fructosyltransferases or can be hydrolyzed by vacuolar invertases (VINs), subsequently being stored as hexose. VINs, which belong to the GH32 family, are categorized as acid invertases, with an optimal pH range of 4.0 to 5.5. These enzymes are characterized by an N-terminal five-bladed β -propeller domain and a C-terminal two β -sheet domain (Alberto et al., 2004). The hydrolysis of sucrose is facilitated by three highly conserved acidic residues located within the WMNDPNG, RDP, and EC motifs of the β -propeller domain. Specifically, the asparagine (D) residue in the WMNDPNG motif acts as a nucleophile, while D in the RDP motif is proposed to stabilize the transition state. Additionally, the glutamic acid (E) residue in the EC motif serves as an acid/base catalyst (Van den Ende et al., 2009).

The transport of hexose between the vacuole and the cytosol is regulated by the tonoplast-localized hexose uniporters *AtSWEET2*, *AtSWEET16*, and *AtSWEET17* (Chardon et al., 2013; Guo et al., 2014; Chen et al., 2015a). Members of the SWEET family, which belong to the MtN3/saliva group, function as sugar uniporters that enable the passive diffusion of sugars across the plasma membrane and tonoplast (Chen et al., 2010). The rice vacuolar hexose uniporter *OsSWEET2b* features an inversion linker helix (TM4) that connects an asymmetric pair of triple-helix bundles (THBs) and is proposed to function as an alternating access transporter (Tao et al., 2015).

In *Arabidopsis*, sucrose serves as the principal carbohydrate that is transported from source tissues to sink tissues through the phloem. The phloem, which is the vascular tissue responsible for the long-distance transport of sucrose in higher plants, is composed of sieve elements, companion cells, and phloem parenchyma cells. For sucrose derived from mesophyll cells to enter the sieve element-companion cell complex (SECC) for long-distance transport, it must first be transferred into the phloem parenchyma cells adjacent to the SECC, potentially via plasmodesmata. *Arabidopsis* lines that overexpress PLASMODESMATA-LOCATED PROTEIN 5 (*AtPDLP5*) or *AtPDLP6* exhibit elevated starch accumulation in their leaves, which may be attributed to a reduction in intercellular sugar transport (Li et al., 2024). The process of phloem loading involves two essential steps. The initial step entails the efflux of sucrose into the apoplasm, facilitated by phloem parenchyma cell-specific sucrose uniporters, namely *AtSWEET11* and *AtSWEET12* (Chen et al., 2012). The sucrose uniporter *AtSWEET13* exhibits a similar inward-open conformation to that of *OsSWEET2b* (Han et al., 2017). The subsequent step of phloem loading involves the uptake of sucrose from the apoplasm into the SECC, mediated by the companion cell-specific SUCROSE TRANSPORTER 1/SUCROSE-PROTON SYMPORTER 2 (*AtSUT1/AtSUC2*) (Stadler and Sauer, 1996).

In the context of fruit physiology, sucrose is transported from the phloem and subsequently hydrolyzed by cell wall invertases (CWINVs), leading to the production of hexose sugars that are absorbed by sink tissues via hexose/proton symporters known as SUGAR TRANSPORT PROTEINS (STPs). CWINVs are classified as acid invertases within the glycoside hydrolase family GH32. The crystal structure of *AtCWINV1* reveals a fivefold β -propeller domain at the N-terminus and a C-terminal

domain composed of two β -sheets (Verhaest et al., 2006). The nucleophilic residue Asp23 and the acid/base catalytic residue Glu203, located within the fivefold β -propeller domain, play critical roles in the hydrolysis of sucrose. The sucrose hydrolyzing activity of the tobacco (*Nicotiana tabacum*) CWINV, *Nt*CWINV, is subject to inhibition by cell wall inhibitors of fructosidase (CIFs) in a manner that is strictly dependent on pH (Weil et al., 1994). The structure of *Nt*CIF is characterized by a four-helix bundle core, accompanied by an extended α -hairpin module at the N-terminus, and it inhibits *Nt*CWINV through direct binding to its catalytic site (Hothorn et al., 2004; Hothorn et al., 2010).

STPs are proton-driven hexose transporters that are classified within the major facilitator superfamily (Sauer et al., 1990). The structure of *At*STP10 consists of twelve transmembrane helices, which are interconnected by a cytosolic helical bundle domain (IC1–IC5) that links the N-terminal domain (helices M1–M6) to the C-terminal domain (helices M7–M12). Additionally, an extracellular helix-helix-loop-helix (Lid) domain connects helices M1 and M2 (Paulsen et al., 2019; Bavnhøj et al., 2021). Bavnhøj et al. suggest that *At*STP10 operates as an alternating access transporter. In its outward-open conformation, the lid domain is open, facilitating the entry of hexose and protons into the water-filled inlet channel. Following this, the protonation and neutralization of Asp42 lead to the formation of a high-affinity glucose binding pocket, which is comprised of Phe39, Leu43, Ile184, and Gln177. The residues Tyr76 and Tyr306 are critical for maintaining hydrophobic interactions among the central helices during the transition from the outward-occluded state to the inward-open state. Ultimately, the movement of N-domain residues Leu43, Ile184, Phe39, and Gln177 facilitates the release of sugar into the cytosol. In summary, the transport and metabolism of sucrose in *Arabidopsis* necessitate the involvement of invertases, sucrose synthase, plasmodesmata, and sugar transporters (see Fig. 1).

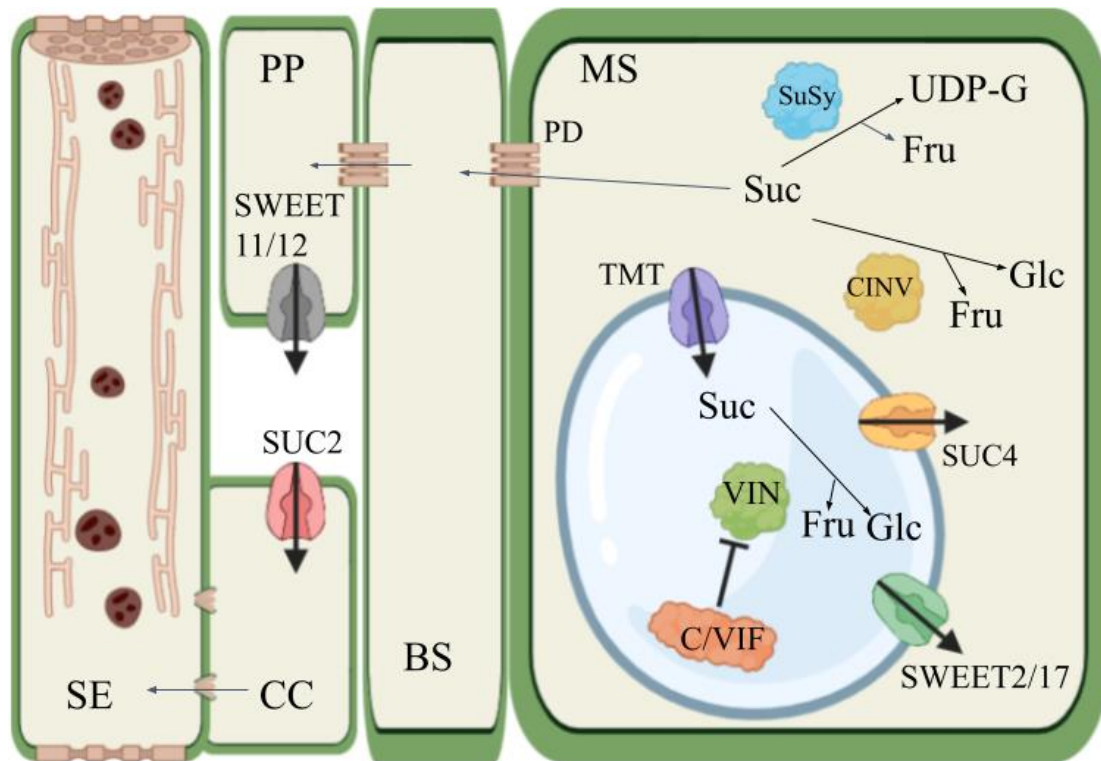


Fig. 1. Sucrose transport and metabolism in Arabidopsis leaves. In the cytosol, sucrose (Suc) undergoes conversion into glucose (Glc) and fructose (Fru) through the action of cytosolic invertase (CINV), or alternatively, it can be converted into Fru and uridine diphosphate (UDP-G) via sucrose synthase (SuSy). The transport of sucrose across the tonoplast is facilitated by the tonoplast monosaccharide transporter (TMT) and the tonoplast-localized sucrose/proton symporter SUC4. Within the vacuole, vacuolar invertase (VIN) catalyzes the hydrolysis of vacuolar Suc into Glc and Fru, although this enzymatic activity is inhibited by the cell wall/vacuolar inhibitor of fructosidase (C/VIF). Additionally, tonoplast-localized hexose uniporters, such as SWEET2 and SWEET17, regulate the movement of hexoses across the tonoplast. Sucrose is transported from mesophyll cells (MS) into phloem parenchyma cells (PP) through plasmodesmata (PD). Furthermore, plasma membrane-localized sucrose uniporters, including SWEET11 and SWEET12, work in conjunction with the plasma membrane-localized sucrose/proton symporter SUC2 to facilitate the translocation of sucrose from PP into companion cells (CC). BS, bundle sheath cells. SE, sieve element. Created with BioRender.com.

Beneficial microorganisms depend on sugars derived from host plants for their sustenance

In the natural environment, plants exist not in isolation but as hosts to a diverse array of microorganisms collectively referred to as the plant microbiota. This microbiota plays a significant role in various plant processes, including growth and resilience to both biotic and abiotic stressors.

Arbuscular mycorrhizal fungi (AMF) represent a vital component of the root microbiota for approximately 72% of terrestrial plant species (Duan et al., 2024). The extraradical

hyphae of AMF facilitate the acquisition of otherwise inaccessible nutrients such as phosphate (Pi), nitrogen, and micronutrients from the soil. AMF establish colonization of root cortical cells through the formation of intraradical hyphae and arbuscules. The peri-arbuscular space, which is defined as the region between the fungal cell wall and the plant's peri-arbuscular membrane, serves as the primary site for the bidirectional exchange of nutrients between the plant and AMF. Due to their limited saprotrophic capabilities, AMF depend on their host plants for a supply of carbon, including lipids and sugars. It is widely accepted that plants may compensate their most effective AMF partners by providing additional carbon (Bever et al., 2009). The significance of host-derived sugars in the process of mycorrhization has been substantiated through genetic studies. For instance, the colonization of plant roots by AMF and the subsequent development of arbuscules are dependent on the presence of the arbuscular membrane-localized monosaccharide transporter *RiMST2*, which is derived from the fungus *Rhizophagus irregularis* (Helber et al., 2011). Moreover, plant sugar uniporters found in the peri-arbuscular membrane, like *MtSWEET1b* from *Medicago truncatula* and *StSWEET7a* from *Solanum tuberosum*, have been demonstrated to improve mycorrhizal colonization. (An et al., 2019; Tamayo et al., 2022).

In a manner analogous to arbuscular mycorrhizal (AM) symbiosis, leguminous plants supply rhizobial bacteria with carbon in exchange for nitrogen. Research indicates that legume plants impose sanctions on rhizobial strains that fail to effectively fix nitrogen. Specifically, ineffective nodules exhibit reduced sucrose concentrations, indicating that bacteria lacking a functional nitrogenase receive diminished carbon resources due to these sanctions (Pini et al., 2017; Westhoek et al., 2021). The proposed plant sugar transporters *MtSWEET11* and *LjSWEET3* (from *Lotus japonicus*) are thought to aid in the movement of sugars to nitrogen-fixing bacteria (Kim et al., 2021a).

To facilitate the associated microbiota, plants release a portion of their photosynthetic products into the rhizosphere and phyllosphere (Lindow and Brandl, 2003; von Bodman et al., 2003). It is not surprising that glucose, fructose, and sucrose serve as some of the most fertile carbon sources for 224 bacterial strains that inhabit the leaves of wild *Arabidopsis* plants (Schäfer et al., 2023). Distinct bacterial communities, both in the rhizosphere and endosphere, colonize different root segments of *Arabidopsis* (Loo et al., 2024). Notably, the sugar uniporters *AtSWEET2*, *AtSWEET4*, *AtSWEET11*, and

AtSWEET12 play a significant role in shaping the spatial metabolic profiles and endospheric root microbiota along the root axis. Consequently, the close association between plants and microbes is fundamentally linked to the availability of sugars, a relationship that has persisted since the advent of terrestrial plants.

Sugars play a significant role in enhancing the virulence of phytopathogenic microorganisms

The synthesis of virulence factors imposes significant energetic demands on phytopathogenic microorganisms (Platt et al., 2012; Sturm et al., 2011). Furthermore, the untimely release of these virulence factors can inadvertently alert the host to the presence of the pathogen (Oh et al., 2010). In order to effectively circumvent plant defense mechanisms and establish a suitable environment for survival, phytopathogenic microbes must possess the ability to accurately identify their host and strategically deploy their virulence factors at optimal moments and locations.

Sugars have been identified as factors that enhance virulence in the bacterial pathogen *Pseudomonas syringae* pv. *glycinea* (Huynh et al., 1989). A number of genes associated with sugar uptake and catabolism in phytopathogenic microorganisms have been correlated with the activation of virulence. For instance, the fructose-induced activation of the *hrp/hrc* (*hypersensitive response and pathogenicity/hypersensitive response and conserved*) system in the hemibiotrophic bacterial pathogen *Pst* DC3000 necessitates the involvement of a putative enzyme component of the fructose-specific phosphoenolpyruvate-dependent phosphotransferase system (Anderson, 2023). Similarly, the germination of spores in the necrotrophic fungal pathogen *B. cinerea* is stimulated by the influx of fructose mediated by the fructose transporter *BcFRT1* (Doehlemann et al., 2005). Additionally, the complete fitness of *Pseudomonas syringae* pv. *syringae* B728a during leaf infection is contingent upon the expression of multiple genes that encode enzymes involved in sugar catabolism (Helmann et al., 2019).

Phytopathogenic bacteria utilize cell surface receptors, such as two-component system (TCS) sensor kinases, to perceive environmental stimuli and modulate the expression of virulence-related genes, among other cellular functions. In the biotrophic bacterial pathogen *Agrobacterium tumefaciens* (*A. tumefaciens*), the expression of virulence genes induced by sugars necessitates the involvement of TCS sensor kinase VirA, response regulator protein VirG, and periplasmic sugar-binding protein ChvE (Nester,

2014). The interaction between the sugar-ChvE complex and VirA leads to the phosphorylation of VirG, which subsequently activates the expression of virulence genes. A recent investigation has revealed that the expression of virulence genes in the hemibiotrophic bacterial pathogen *Xanthomonas campestris* pv. *campestris* (*Xcc*) is contingent upon the intracellular sensing of glucose by the transcription factor XccR (Zhang et al., 2023). The glucose-bound form of XccR exhibits an increased affinity for the *luxXc* box located in the promoter region of the virulence factor proline iminopeptidase. Furthermore, the overexpression of a constitutively active hexose transceptor (Hxt1^{R164K}) in the biotrophic fungal pathogen *Ustilago maydis* has been shown to inhibit its development following penetration of maize epidermal cells (Schuler et al., 2015). Thus, it is evident that plant-derived sugars play a crucial role in activating the virulence of phytopathogenic microorganisms with varying lifestyles.

Phytopathogenic microorganisms create a niche within plants that is enriched with sugars

Plants have developed both preformed and inducible defense mechanisms to protect their nutritional metabolites from opportunistic microbial threats. In response, phytopathogenic microbes have adapted characteristics that enable them to extract these nutritional resources from plant hosts. Among these metabolites, sugars, particularly sucrose, are the most prevalent in plant tissues. Recent research indicates that water present in the apoplast facilitates the accumulation of nutritional metabolites, such as amino acids, within the leaf apoplast (Gentzel et al., 2022).

Plants utilize plasma membrane-localized sugar uniporters, such as SWEET, and sugar/proton symporters, including SUC and STP, to regulate the efflux of intracellular sugars along their concentration gradient and the influx of extracellular sugars against their concentration gradient, respectively. The phenomenon of microbe-induced hydrosis, characterized by water-soaked conditions, reduces the concentration of sugars in the apoplast and dilutes the protons necessary for the operation of sugar/proton symporters, thereby promoting sugar efflux into the apoplast while impeding sugar influx into plant cells (Roussin-Léveillé et al., 2024). This hydrosis may facilitate a heightened level of microbial proliferation by elevating sugar concentrations in the apoplast.

Hydrosis is facilitated by two primary sources of water: liquid water present on the leaf

surface and water derived from the mesophyll and vascular bundles. The hemibiotrophic bacterial pathogen *Xanthomonas gardneri* introduces the transcription activator-like effector (TALE) AvrHah1 into tomato (*Solanum lycopersicum*) cells, which subsequently triggers the expression of the basic helix-loop-helix (bHLH) transcription factors *S/bHLH3* and *S/bHLH6* (Schwartz et al., 2017). Following this induction, *S/bHLH3* and *S/bHLH6* promote the expression of a pectate lyase, thereby facilitating hydrosis through the absorption of water from the leaf surface.

Plants regulate stomatal closure to mitigate water loss through evaporation from their leaves. The phytohormone abscisic acid (ABA) plays a crucial role in this process by inducing stomatal closure in guard cells and facilitating water retention within the leaf apoplast. *Pst* DC3000 can manipulate the host's ABA-mediated stomatal closure by introducing the effector proteins HopM1 and AvrE into the plant cytoplasm (Hu et al., 2022; Roussin-Léveillé et al., 2022). Specifically, HopM1 utilizes the host ATP-BINDING CASSETTE (ABC) transporter G family member 40 (*AtABCG40*) to enhance the influx of ABA into guard cells (Roussin-Léveillé et al., 2022). Additionally, AvrE interacts with type I protein phosphatases, thereby derepressing the SNF1-related protein kinase 2 (SnRK2)-dependent expression of ABA-responsive genes (Hu et al., 2022). Moreover, AvrE directly forms a channel in the plant plasma membrane that is permeable to water and solutes, which promotes hydrosis (Nomura et al., 2023).

In addition to inducing hydrosis, phytopathogenic microorganisms have developed traits to reprogram the plant sugar transport system, thereby enhancing sugar availability. The rice pathogen *Xanthomonas oryzae* pv. *oryzae* (*Xoo*) colonizes the leaf xylem vessels, which are deficient in carbon resources. To acquire carbon from rice, *Xoo* promotes the expression of plasma membrane-localized sucrose uniporters, specifically *OsSWEETs*, in xylem parenchyma cells through TALEs-mediated gene activation (Gupta et al., 2021). Similarly, the soilborne fungal pathogen *Rhizoctonia solani* induces the expression of *OsSWEET2a* and *OsSWEET3a* via its AG1-IA effector *RsAOS2*, which interacts with rice transcription factors *OsWRKY53* and *OsGT1* to form a transcriptional complex in the nucleus (Yang et al., 2023). Notably, the TAL20 protein Xam668 from the cassava (*Manihot esculenta*) pathogen *Xanthomonas axonopodis* pv. *manihotis* exhibits a dual role in promoting hydrosis and

activating the expression of *MeSWEET10a* (Cohn et al., 2014). Collectively, phytopathogenic microorganisms manipulate the host's water and sugar transport systems to create a conducive environment enriched with water and sugars.

Sugars play a crucial role in enhancing the immune systems of plants

Priming refers to the mechanism by which a plant is conditioned to mount a defense response that is more rapid and/or robust than it would typically be, without triggering the defense mechanism prior to the onset of a stressor (Conrath, 2011). A significant benefit of this priming process is that it allows the plant to circumvent the energetic expenditures associated with a full defense response, thereby preserving its overall fitness and yield.

Soluble sugars are recognized for their role in inducing the expression of defense marker genes and are classified as priming agents for plant immunity (Herbers et al., 1996; Yamada and Mine, 2024). In conditions where glucose is abundant in the apoplast, the glucose-bound plasma membrane-based regulator of G protein signaling 1 (*S/RGS1*) is internalized through endocytosis. This process promotes the dissociation of the RGS1-G protein α subunit (*S/GPA1*) from the GPA1-G protein β subunit (*S/GB1*), thereby activating G protein signaling pathways and liberating free *S/GB1*, which enhances the defense mechanisms of tomato plants against *Pst* DC3000 (Wang et al., 2022b). Additionally, the efficacy of plant defense against the virulent strain *Pst* DC3000, the nonvirulent strain *Pst* DC3000 *hrcC*⁻, and the avirulent strain *Pst* DC3000 *avrRpm1* is contingent upon the intracellular glucose sensing mediated by hexokinase 1 (*AtHXK1*) (Jing et al., 2020).

In addition to its role in glucose sensing, HXK1 catalyzes the conversion of glucose to G6P. G6P has been shown to directly inhibit the phosphatase activity of ABSCISIC ACID-INSENSITIVE 1 (*AtABI1*), which in turn enhances the trans-phosphorylation activity of calcium-dependent protein kinase 5 (*AtCPK5*) (Yamada and Mine, 2024). The active form of *AtCPK5* phosphorylates Thr-229 of the transcription factor *AtWRKY33*, resulting in an upregulation of camalexin biosynthetic gene expression (Zhou et al., 2020). Camalexin is subsequently secreted into the apoplast via the plasma membrane-localized transporter ABCG34, where it functions to eliminate necrotrophic fungal pathogens, such as *Alternaria brassicicola* (Khare et al., 2017;

Yamada and Mine, 2024). Additionally, the influx of glucose mediated by *AtSTP1,4,13* enhances the plant's defense against *Pst* DC3000 Δ avrPto Δ avrPtoB (Yamada and Mine, 2024). Collectively, these findings underscore the significant role that sugars play in priming plant defense responses.

Plant defense inhibit the formation of suitable habitats

The immune system of plants is fundamentally characterized by two primary branches that exhibit mutual potentiation (Ngou et al., 2021; Pruitt et al., 2021; Tian et al., 2021; Yuan et al., 2021). Extracellular immunity receptors, which are localized in the plasma membrane and include transmembrane receptor-like kinases and transmembrane receptor-like proteins, are responsible for detecting infection-associated ligands, such as flagellin, found in the apoplasm. This recognition triggers pattern-triggered immunity (PTI). Following ligand detection, these extracellular receptors activate a series of downstream defense, including the production of reactive oxygen species, the expression of defense-related genes, calcium ion influx, the activation of mitogen-activated protein kinases, and the synthesis of defense hormones. In contrast, intracellular immunity receptors, predominantly composed of nucleotide-binding leucine-rich-repeat (NLR) proteins, are tasked with monitoring intracellular effectors to initiate effector-triggered immunity (ETI). For example, the Arabidopsis NLR protein ZAR1 (HOPZ-ACTIVATED RESISTANCE1) detects the uridylyl transferase activity of the *Xcc* effector AvrAC, subsequently forming a Ca²⁺-permeable channel localized in the plasma membrane upon recognition of AvrAC (Wang et al., 2019; Bi et al., 2021).

As previously noted, *Pst* DC3000 manipulates the ABA signaling pathway in the host to promote hydrosis. PTI activates the expression of secreted peptides known as SMALL PHYTOCYTOKINES REGULATING DEFENSE AND WATER LOSS (*AtSCREWs*), which serve to mitigate the stomatal closure induced by *Pst* DC3000 (Liu et al., 2022). The action of *AtSCREWs* leads to the phosphorylation of *AtABI1* and *AtABI2* in a manner dependent on the receptor kinase PLANT SCREW UNRESPONSIVE RECEPTOR (*AtNUT*). This phosphorylation subsequently enhances the activity of ABI phosphatases towards OPEN STOMATA 1 (*AtOST1*), a key kinase involved in regulating stomatal closure in response to infection-related

ligands and ABA. Furthermore, under continuous light conditions, the plant defense hormone salicylic acid (SA) effectively negates the stomatal closure induced by *Pst* DC3000 in an ABA-dependent manner (Lajeunesse et al., 2023).

Similar to PTI, ETI also inhibits microbe-induced hydrosis. For example, the activation of ETI has been shown to prevent hydrosis caused by *Xanthomonas* spp. TALEs AvrBs3 and AvrHah1 (Schenstnyi et al., 2022). In comparison to the virulent strain *Pst* DC3000 and the nonvirulent strain *Pst* DC3000 *hrcC*⁻, the avirulent strain *Pst* DC3000 *avrRpm1* experiences lower water potential in host plants, which may be attributed to a restricted water supply from the vascular bundle (Wright and Beattie, 2004; Freeman and Beattie, 2009). Consequently, both PTI and ETI serve to mitigate microbe-induced hydrosis.

PTI not only inhibits hydrosis induced by *Pst* DC3000 but also curtails bacterial growth in the apoplast by diminishing sugar availability. The receptor FLAGELLIN-SENSITIVE 2 (*AtFLS2*), which is localized to the plasma membrane and recognizes the flagellin peptide flg22, forms a complex with BRASSINOSTEROID INSENSITIVE 1-associated kinase 1 (*AtBAK1*) upon flg22 binding (Sun et al., 2013). A pivotal study has demonstrated that the *AtFLS2-AtBAK1* complex can directly facilitate hexose uptake into plant epidermal and mesophyll cells by phosphorylating the plasma membrane-localized hexose/proton symporter, sugar transport protein 13 (*AtSTP13*) (Yamada et al., 2016). In conclusion, plant immune systems mitigate the proliferation of phytopathogenic microorganisms by altering the quality of their ecological niche.

Objectives of the research

Like all complex organisms, plants are vulnerable to diseases caused by infections from microbial pathogens. Plant diseases pose a significant and ongoing threat to agricultural productivity and ecological biodiversity. The phyllosphere, characterized as an oligotrophic environment, primarily harbors carbon sources within host cells. In response, phytopathogenic microbes have developed specific traits that enable them to access this sugar-rich plant tissue, resulting in considerable damage. Consequently, the phyllosphere serves as an ideal context for investigating the impact of sugar allocation on plant-microbe interactions. In this section, I will outline the existing knowledge gaps

regarding sugar reallocation within the Arabidopsis-*Pst* DC3000/*B. cinerea* pathosystems, as well as the three principal objectives of my dissertation.

Sugars derived from Arabidopsis are proposed to function as potential virulence-inducing signals and nutritional metabolites for *Pst* DC3000

Sugars represent one of the primary carbon sources utilized by the leaf microbiota of Arabidopsis (Schäfer et al., 2023). The invasion of *Pst* DC3000 leads to a decrease in disaccharide levels in Arabidopsis leaves, indicating that *Pst* DC3000 is actively utilizing sugars obtained from Arabidopsis (Ryffel et al., 2016). Genetic studies show that the sucrose uniporter SWEET11, along with the hexose uniporters SWEET5 and SWEET7, plays a significant role in modulating Arabidopsis susceptibility to *Pst* DC3000 infection (Fatima and Senthil-Kumar, 2021). Furthermore, sugars have been shown to enhance the virulence of *Pst* DC3000 in vitro (Stauber et al., 2012; Turner et al., 2020). Consequently, the Arabidopsis-*Pst* DC3000 pathosystem serves as an appropriate model for investigating the dynamics of sugar reallocation during the bacterial colonization of leaf tissues.

The genome of *Pst* DC3000 encodes sucrose-6-phosphate hydrolase ScrB and sucrose porin precursor ScrY, implying that this bacterium can metabolize sucrose derived from plants in a manner that does not depend on levansucrase (Laue et al., 2006). Both *ScrB* and *ScrY* are located within a lineage-specific region, indicating their potential role in enhancing bacterial fitness (Hacker and Carniel, 2001; Joardar et al., 2005). ScrY is characterized by a hydrophilic pore structure formed by 18 anti-parallel β -strands, which facilitates the diffusion of sucrose across the outer membrane of the bacterium (Forst et al., 1998). Once in the periplasmic space, sucrose can be phosphorylated and subsequently transported into the bacterial cytoplasm through the phosphoenolpyruvate-dependent carbohydrate:phosphotransferase systems (PTSs) (Wang et al., 2001). Within the cytoplasm, ScrB catalyzes the hydrolysis of S6P, resulting in the production of fructose and G6P (Chassy et al., 1979). Nonetheless, it remains uncertain whether *Pst* DC3000 relies on ScrY and ScrB for the utilization of plant-derived sucrose.

In addition to sucrose, glucose serves as a carbon source and a virulence-inducing ligand for *Pst* DC3000 (Stauber et al., 2012; McCraw et al., 2016; Turner et al., 2020).

Moreover, G6P has been identified as a significant enhancer of antibacterial defense mechanisms (Yamada and Mine, 2024). It is plausible that the hexose uniporters SWEET4, SWEET5, SWEET7, or SWEET8 in Arabidopsis, which are induced by *Pst* DC3000 infection, may facilitate the coordination of glucose transport and signaling among various leaf cell types.

The first objective of my dissertation is to clarify the functions of ScrY and ScrB within the framework of pathogenesis, in addition to examining the spatial distribution of SWEET4, SWEET5, SWEET7, and SWEET8 in leaves infected by *Pst* DC3000. To achieve these objectives, I utilized genetic methodologies, translational β -glucuronidase (GUS) fusions, and GUS histochemical analysis.

Transcriptional reprogramming of Arabidopsis STP13 in response to the challenge posed by *Pst* DC3000

Transcriptional reprogramming of defense-related genes constitutes a fundamental aspect of both PTI and ETI. The influx and signaling of hexoses mediated by STP1,4,13 is critical for antibacterial defense mechanisms (Yamada et al., 2016; Yamada and Mine, 2024). A particularly intriguing area of research is the accumulation of STP13 in epidermal and mesophyll cells during the invasion by *Pst* DC3000. Notably, 24 hours following *Pst* DC3000 inoculation, STP13 exhibits a correlation between messenger ribonucleic acid (mRNA) levels and chromatin accessibility, implying that its transcription is induced (Nobori et al., 2025). The R2R3-type transcription factor MYB96, along with the WRKY transcription factors WRKY18, WRKY33, and WRKY40, have been identified as transcriptional activators of STP13 in response to flg22 treatment (Birkenbihl et al., 2017; Lee and Seo, 2021). It is plausible to hypothesize that the complete induction of STP13 in response to *Pst* DC3000 challenge necessitates chromatin remodeling and the involvement of additional, yet unidentified, transcription factors.

The second objective of my dissertation is to investigate the protein complex responsible for the activation of STP13 expression in response to the invasion of *Pst* DC3000. To accomplish this, I have employed a clustered regularly interspaced short palindromic repeats (CRISPR)/dCas9-TurboID-mediated proximity labeling approach, followed by comprehensive proteomic analyses.

The sugar transporters and invertases found in Arabidopsis may influence the plant's susceptibility to *B. cinerea*

Utilizing ^{13}C -nuclear magnetic resonance spectroscopy, Dulermo et al. (2009) demonstrated that *B. cinerea* acquires sugars from the cotyledons of sunflower (*Helianthus annuus* L.). Following this, Veillet et al. (2016) identified glucose as the predominant sugar absorbed by *B. cinerea*. Furthermore, genetic knockout studies of either the SWEET4 or the STP13 has been shown to affect the susceptibility of Arabidopsis to infection by *B. cinerea* (Chong et al., 2014; Lemonnier et al., 2014).

The infectious process of *B. cinerea* on leaf tissue is categorized into three distinct phases (Bi et al., 2023). During the initial phase (0–36 hours post-infection), *B. cinerea* exists as an epiphytic organism, employing cell-death-inducing proteins to eliminate a limited number of leaf cells. In the subsequent intermediate phase (36–48 hours post-infection), the fungal hyphae penetrate further, resulting in the death of additional leaf cells. Concurrently, the presence of antifungal plant metabolites, such as camalexin, instigates significant cell death within the fungal population. In the final phase (48 hours post-infection), the surviving fungal cells proliferate within the necrotic leaf tissues, leading to the formation of extensive lesions, which are characteristic of this stage of infection.

Hexose/proton symporters STP1, STP3, STP4, STP13, and cell wall invertase 1 (CWINV1) exhibit increased mRNA levels during the early phase, likely contributing to the reduction of hexose concentrations in the apoplasm and the enhancement of antifungal immunity (Lemonnier et al., 2014; Sham et al., 2014; Sham et al., 2017). In the later phase, there is an increased of mRNA levels for hexose uniporter SWEET4, sucrose/proton symporters SUC1 and SUC3, vacuolar invertases VIN1 and VIN2, as well as cell wall/vacuolar inhibitor of fructosidase 1 (C/VIF1), while mRNA levels of C/VIF2 are diminished (Veillet et al., 2016). This increase in invertase mRNA levels correlates with heightened invertase activity observed in the late phase (Veillet et al., 2016). It is plausible to hypothesize that *B. cinerea* may manipulate leaf cells to retain higher sugar levels within the expanding lesions. Alternatively, leaf cells may be reallocating their carbon reserves towards antifungal defense mechanisms or actively removing sugars from the advancing lesions.

The third objective of my dissertation is to examine the coordination of sucrose and hexose transport, as well as sucrose hydrolysis, during the invasion of *B. cinerea*. To address this inquiry, I employed genetic techniques, translational green fluorescent protein (GFP) fusions, and confocal imaging. The primary research questions are encapsulated in Figure 2.

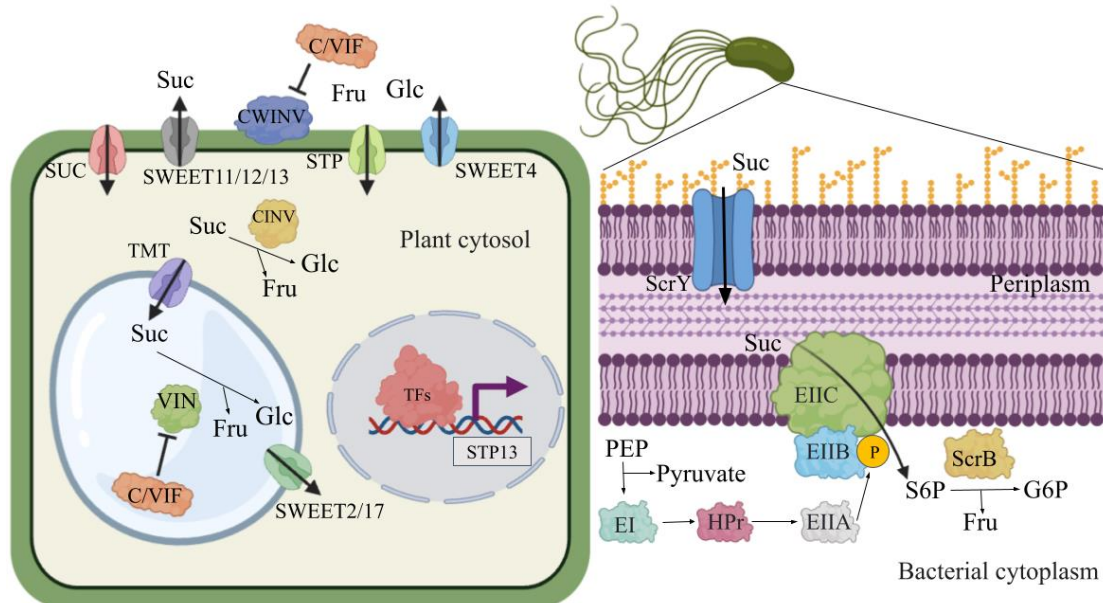


Fig. 2. This study investigates the potential genetic factors involved in the reallocation of sugars in *Arabidopsis* leaves during the invasion by *Pseudomonas syringae* pv. tomato DC3000 (*Pst* DC3000) and *Botrytis cinerea* (*B. cinerea*). In the leaf apoplast, sucrose (Suc) is transported through the sucrose porin (ScrY) situated in the outer membrane of *Pst* DC3000 into the periplasmic space. Following this, Suc undergoes phosphorylation and is subsequently transferred into the cytoplasm via the phosphoenolpyruvate (PEP)-dependent carbohydrate:phosphotransferase systems, which include Enzyme I (EI), heat-stable protein (HPr), and Enzyme II (EIIA, EIIB, and EIIC). Within the cytoplasm, sucrose-6-phosphate (S6P) is hydrolyzed by S6P hydrolase (ScrB) to yield glucose-6-phosphate (G6P) and fructose (Fru). Both ScrY and ScrB may facilitate bacterial proliferation within plant tissues. In *Arabidopsis* leaves infected by *Pst* DC3000, the hexose/proton symporter STP13 is transcriptionally activated by transcription factors (TFs), including the R2R3-type transcription factor MYB96 and several WRKY transcription factors (WRKY18, WRKY33, and WRKY40), which contribute to hexose retrieval and bolster antibacterial immunity. During the invasion by *B. cinerea*, sucrose uniporters (SWEET11, SWEET12 and SWEET13) and a hexose uniporter (SWEET4) localized in the plasma membrane may promote the efflux of sugars into the leaf apoplast. Conversely, plasma membrane-localized sucrose (SUC) and hexose (STP) symporters facilitate the influx of sugars from the apoplast into the plant cytoplasm. Additionally, tonoplast-localized hexose uniporters (SWEET2 and SWEET17) regulate the exchange of hexoses between the cytosol and vacuole of leaf cells. The hydrolysis of sucrose into glucose and fructose is mediated by cytosolic (CINV), vacuolar (VIN), and cell wall (CWINV) invertases. The activities of VIN and CWINV are inhibited by the cell wall/vacuolar inhibitor of fructosidase (C/VIF). The interplay between sugar transporters and sucrose metabolism enzymes across various leaf cell types is likely to affect the susceptibility of *Arabidopsis* to *B. cinerea*. Created with BioRender.com.

Materials and Methods

Evaluations of the proliferation of *Pst* DC3000 mutant strains cultured in a modified *hrp* derepressing medium

The design of the CRISPR ribonucleic acid (crRNA) was conducted using the CRISPR Guide RNA Design tool available on Benchling.com. This process involved the creation of a specific crRNA protospacer sequence for the genes *ScrB* (PSPTO_0885) and *ScrY* (PSPTO_0890). To achieve this, two synthesized 24 nucleotide complementary DNA oligonucleotides, obtained from Integrated DNA Technology, were annealed to form a double-stranded DNA oligonucleotide (dsDNA). This dsDNA featured a 5' overhang of GTGG on the sense strand and a 5' overhang of AAAC on the antisense strand, as detailed in Table A1.

The double-stranded DNAs crRNA^{ScrB} and crRNA^{ScrY} were separately incorporated into the cytidine deaminase-mediated base-editing vector pnCAsPA-BEC (Chen et al., 2018) utilizing the Golden Gate Assembly method (NEB, MA, United States). This assembly reaction was subsequently introduced into *Escherichia coli* One Shot TOP10 chemically competent cells (hereafter referred to as *E. coli* TOP10) (Catalog No. C404003, Thermo Fisher Scientific, Darmstadt, Germany) through a heat shock protocol (see Table A2). The resulting plasmids, pnCAsPA-BEC-sgRNA^{ScrB} and pnCAsPA-BEC-sgRNA^{ScrY}, were extracted from *E. coli* TOP10 using the NucleoSpin® Plasmid isolation kit (Catalog No. 740588.50, Macherey-Nagel, Düren, Germany) and their identities were verified via Sanger sequencing (Microsynth Seqlab GmbH, Göttingen, Germany).

Three days prior to the electroporation process, *Pst* DC3000 was streaked from glycerol stocks, which had been stored at -80°C, onto King's medium B (KB) agar plates (Catalog No. K5165, Duchefa Biochemie) supplemented with 50 µg mL⁻¹ rifampicin (see Table A2). The *Pst* DC3000 was incubated at 28°C for a duration of two days. A single colony of *Pst* DC3000 was subsequently used to inoculate 10 mL of dYT medium [composed of tryptone at 16 g L⁻¹, yeast extract at 10 g L⁻¹, sodium chloride (NaCl) at 5 g L⁻¹, pH = 7] containing 50 µg mL⁻¹ rifampicin, and the culture was grown at 28°C with shaking at 200 revolutions per minute (rpm) for 16 hours. Following this incubation, *Pst* DC3000 cells in dYT medium were harvested via centrifugation at 22°C (4000 rpm for 2 minutes). The cell density of *Pst* DC3000 was then adjusted to an

optical density of 600 (OD₆₀₀) approximately 0.3 in 2 mL of fresh dYT medium, followed by an additional incubation period of 1.5 hours at 28°C with shaking at 200 rpm. The cells from the 2 mL subculture were again harvested by centrifugation at 22°C (4000 rpm for 2 minutes) and subsequently washed three times with 50 µL of 0.3 M sucrose. A total of 50 ng of pCasPA-BEC-sgRNA^{ScrB} or pCasPA-BEC-sgRNA^{ScrY} was then combined with the *Pst* DC3000 cells in 50 µL of 0.3 M sucrose on ice for 20 minutes. The constructs pCasPA-BEC-sgRNA^{ScrB} and pCasPA-BEC-sgRNA^{ScrY} were introduced into *Pst* DC3000 via electroporation using a 1 mm cuvette with parameters set at 1250 voltage, 100 ohm, and 25 microfarads (Chen et al., 2018). Following electroporation, *Pst* DC3000 was allowed to recover in 1 mL of dYT medium for 2.5 hours at 28°C with shaking at 200 rpm before being plated on dYT agar containing 50 µg mL⁻¹ rifampicin and 10 µg mL⁻¹ gentamicin for selection. To verify mutations in the *ScrB* or *ScrY* genes, gene-specific primers were employed to amplify the regions of interest (refer to Table A1), and the resulting amplicons were subjected to analysis via Sanger sequencing.

Pst DC3000 and its mutant strains, *scrB*^{cr} and *scrY*^{cr}, were cultured from glycerol stocks maintained at -80°C onto KB agar plates supplemented with 50 µg mL⁻¹ rifampicin (see Table A2). All strains were incubated at 28°C for a duration of two days, followed by a subsequent incubation period at 4°C for an additional two days. For the preparation of starting cultures, the *Pst* DC3000, *scrB*^{cr}, and *scrY*^{cr} strains grown on KB agar were resuspended in a 10 mM magnesium chloride (MgCl₂) solution. The bacterial cell density was adjusted to an OD₆₀₀ of approximately 0.05 in 200 µL of a modified *hypersensitive response and pathogenicity* (*hrp*) derepressing medium, which consisted of 7.5 mM sucrose, 50 mM potassium phosphate (KH₂PO₄), 7.6 mM ammonium sulfate [(NH₄)₂SO₄], 1.7 mM MgCl₂, 1.7 mM NaCl, 50 µg mL⁻¹ rifampicin, and was adjusted to a pH of 6. The growth of *Pst* DC3000, *scrB*^{cr}, and *scrY*^{cr} (each with three technical replicates) in the modified *hrp* derepressing medium was monitored over a period of 46 hours using a TECAN Spark microplate reader, set at 150 rpm and maintained at 28°C.

Assessment of Arabidopsis susceptibility to mutant strains of *Pst* DC3000

Arabidopsis Columbia ecotype Col-0 (Col-0) plants were cultivated in a peat-based substrate composed of peat moss, perlite, and vermiculite in a ratio of 8:1:1 (see Table A3). The plants were maintained under a photoperiod of 16 hours of light and 8 hours

of darkness at a temperature of 22°C, with a relative humidity (RH) of 60%. The photosynthetic photon flux density (PPFD) was set at 80 $\mu\text{mol m}^{-2} \text{s}^{-1}$ for a duration of five weeks.

Pst DC3000 and its mutant strains, *scrbc^{cr}* and *scry^{cr}*, were cultured from glycerol stocks maintained at -80°C onto KB agar plates supplemented with 50 $\mu\text{g mL}^{-1}$ rifampicin. All strains were incubated at 28°C for a duration of two days, followed by a subsequent incubation period at 4°C for an additional two days. For the preparation of bacterial inoculums, the *Pst* DC3000, *scrbc^{cr}*, and *scry^{cr}* strains grown on KB agar were resuspended in a 10 mM MgCl_2 solution. The bacterial cell density was adjusted to an OD_{600} of approximately 0.002 (10^6 colony-forming unit, CFU mL^{-1}). Bacterial inoculums were introduced into the abaxial surface of the leaves utilizing a 1 mL syringe, with three leaves per plant and eight plants per strain. The infiltrated plants were subsequently positioned in a tray that was covered with a transparent lid and cultivated under a photoperiod of 12 hours of light followed by 12 hours of darkness, maintained at a temperature of 22°C, with a RH of 60% and a PPFD of 80 $\mu\text{mol m}^{-2} \text{s}^{-1}$.

One hour following infiltration, three leaf discs collected from three infiltrated plants were homogenized in water using a pestle and mortar to create a single biological replicate, with a total of four biological replicates per strain. At three days post-infiltration, five leaf discs pooled from five infiltrated plants were similarly homogenized in water to produce another biological replicate, again with four biological replicates per strain. The homogenized leaf solutions underwent serial dilution (tenfold) in autoclaved water, and 5 μL of each leaf solution was applied to KB agar supplemented with 50 $\mu\text{g mL}^{-1}$ rifampicin. All *Pst* DC3000 strains were incubated at 28°C for a duration of one day. To assess the bacterial population present in the infiltrated leaves, colonies that formed on the KB agar were counted manually with the aid of a stereo microscope.

Evaluation of the susceptibility of Arabidopsis mutant to *Pst* DC3000

Col-0 and the transfer DNA (T-DNA) insertion mutant *sweet11;12;13* (SALK_073269; SALK_031696; SALK_087791), which was generously provided by Li-Qing Chen from the University of Illinois, Urbana-Champaign, were cultivated on half-strength

Murashige & Skoog basic salt ($\frac{1}{2}$ MS) (Catalog No. M0221, Duchefa Biochemie) under controlled conditions of 16 hours of light and 8 hours of darkness at a temperature of 23°C, with a RH of 60% and a PPFD of 120 $\mu\text{mol m}^{-2} \text{s}^{-1}$ for a duration of 14 days (see Table A3) (Alonso et al., 2003). Subsequently, the seedlings were transferred to a peat-based substrate and maintained under a regime of 8 hours of light and 16 hours of darkness at the same temperature and humidity conditions, with a reduced PPFD of 80 $\mu\text{mol m}^{-2} \text{s}^{-1}$ for an additional 20 days.

Pst DC3000 was cultured from glycerol stock maintained at -80°C onto KB agar plates supplemented with 50 $\mu\text{g mL}^{-1}$ rifampicin. *Pst* DC3000 was incubated at 28°C for a duration of two days. For the preparation of bacterial inoculum, the *Pst* DC3000 grown on KB agar were resuspended in a 10 mM MgCl_2 solution. The bacterial cell density was adjusted to an OD_{600} of approximately 0.002 (10^6 CFU mL^{-1}). Bacterial inoculum was introduced into the abaxial surface of the leaves utilizing a 1 mL syringe, with three leaves per plant and eight plants per genotype. The infiltrated plants were subsequently positioned in a tray that was covered with a transparent lid and cultivated under a photoperiod of 12 hours of light followed by 12 hours of darkness, maintained at a temperature of 22°C, with a RH of 60% and a PPFD of 80 $\mu\text{mol m}^{-2} \text{s}^{-1}$.

One hour following infiltration, four leaf discs collected from three infiltrated plants were homogenized in water using a pestle and mortar to create a single biological replicate, with a total of four biological replicates per genotype. At three days post-infiltration, eight leaf discs pooled from five infiltrated plants were similarly homogenized in water to produce another biological replicate, again with four biological replicates per genotype. The homogenized leaf solutions underwent serial dilution (tenfold) in autoclaved water, and 5 μL of each leaf solution was applied to KB agar supplemented with 50 $\mu\text{g mL}^{-1}$ rifampicin. *Pst* DC3000 was incubated at 28°C for a duration of one day. To assess the bacterial population presents in the infiltrated leaves, colonies that formed on the KB agar were counted manually with the aid of a stereo microscope.

Histochemical analysis of GUS fusions in Arabidopsis infected with *Pst* DC3000

To investigate the accumulation patterns of SWEET4 (AT3G28007), SWEET5 (AT5G62850), and SWEET7 (AT4G10850), genomic fragments encompassing the

putative promoter, 5' untranslated regions, and open reading frames were amplified via polymerase chain reaction (PCR) utilizing CloneAmp HiFi PCR Premix (Catalog No. 639298, Takara Bio, USA), Col-0 genomic DNA, and gene-specific primers featuring 15-base-pair extensions that are complementary to the ends of linearized vectors (refer to Table A1). In the case of SWEET8 (AT5G40260), a genomic fragment containing the putative promoter, 5' untranslated region, and open reading frame was amplified using a three-step PCR approach with PrimeSTAR GXL DNA Polymerase (Catalog No. R050A, Takara Bio, USA), Col-0 genomic DNA, and gene-specific primers with 15-base-pair extensions complementary to the linearized vector ends (refer to Table A1). Each amplified product, along with the linearized GUS expression vector $P_{OsSWEET13}:OsSWEET13$ -GUSplus (digested with *Bam*HI and *Xba*I), was combined in an In-Fusion HD Cloning enzyme mix (Takara Bio, USA) and subsequently introduced into *E. coli* TOP10 through a heat shock method (Eom et al., 2019). The resulting plasmids (pP_{SWEET4}:SWEET4-GUS, pP_{SWEET5}:SWEET5-GUS, pP_{SWEET7}:SWEET7-GUS, and pP_{SWEET8}:SWEET8-GUS) were extracted from *E. coli* TOP10 using the NucleoSpin® Plasmid kit and were verified through Sanger sequencing.

The constructs pP_{SWEET4}:SWEET4-GUS, pP_{SWEET5}:SWEET5-GUS, pP_{SWEET7}:SWEET7-GUS, and pP_{SWEET8}:SWEET8-GUS were introduced into chemically competent *A. tumefaciens* GV3101 cells through a heat shock method (see Table A2). The resulting strains of *A. tumefaciens* GV3101 were subsequently employed in the floral dip transformation technique (Clough & Bent, 1998). Individual T1 transformants of the Col-0 line were selected on ½ MS supplemented with 50 mg mL⁻¹ hygromycin (see Table A3).

T2 seeds were planted in a medium consisting of ½ MS supplemented with 50 mg mL⁻¹ hygromycin, and the resulting seedlings were cultivated under a photoperiod of 12 hours of light and 12 hours of darkness at a temperature of 22°C, with a RH of 60% and a PPFD of 120 μmol m⁻² s⁻¹ for a duration of either 10 days (prior to transplanting) or 21 days. The surviving seedlings were subsequently transferred to a peat-based substrate and continued to be grown under the same light and environmental conditions for an additional 18 days.

Two days prior to the spray inoculation, *Pst* DC3000 and its *hrpL* mutant (*Pst* DC3000 *hrpL*⁻) were streaked from glycerol stocks, which had been stored at -80°C, onto

peptone yeast glycerol (NYG) agar plates (see Table A2). The composition of the NYG agar plates included 5 g L⁻¹ peptone, 3 g L⁻¹ yeast extract, 20 g L⁻¹ glycerol, and 10 g L⁻¹ bacto agar, supplemented with 50 µg mL⁻¹ rifampicin for *Pst* DC3000 and with both 50 µg mL⁻¹ rifampicin and 50 µg mL⁻¹ spectinomycin for *Pst* DC3000 hrpL⁻. Both strains were incubated at 28 °C. To prepare the bacterial inoculums at a concentration of 10⁸ CFU mL⁻¹, the strains were scraped from the NYG agar plates and resuspended in either 10 mM MgCl₂ or autoclaved water. Subsequently, plants were spray-inoculated with either *Pst* DC3000, *Pst* DC3000 hrpL⁻, autoclaved water, or 10 mM MgCl₂. Following the inoculation, the potted plants were placed in a plastic tray with a lid and maintained under a photoperiod of 12 hours light and 12 hours dark at a temperature of 22°C and 60% RH, with a PPFD of 120 µmol m⁻² s⁻¹ for a duration of two days.

In accordance with the histochemical GUS analysis protocol established by Yang et al. (2018), whole plants or the aerial portions of pot-grown plants were subjected to fixation in 90% cold acetone for a duration of 10 minutes. Subsequently, the samples underwent vacuum infiltration in a GUS staining solution composed of 0.5 M ethylenediaminetetraacetic acid (EDTA), 100 mM phosphate buffer, 10% Triton-X 100 [C₁₄H₂₂O(C₂H₄O)₉₋₁₀], 50 mM potassium ferrocyanide (C₆FeK₄N₆), and 50 mM potassium ferricyanide (C₆N₆FeK₃) for an additional 10 minutes on ice. Following this, the samples were again vacuum infiltrated in a GUS staining solution containing 400 mM 5-bromo-4-chloro-3-indolyl-beta-D-glucuronic acid (X-Gluc) for 10 minutes on ice. The samples were then incubated at 37°C until the formation of a blue precipitate was observed, which took approximately 3 hours for P_{SWEET4}:SWEET4-GUS, 5 hours for P_{SWEET5}:SWEET5-GUS, and 16 hours for both P_{SWEET7}:SWEET7-GUS and P_{SWEET8}:SWEET8-GUS. Following GUS staining, the samples were sequentially dehydrated and cleared using 30%, 50%, and 70% ethanol (C₂H₆O). Imaging of the cleared samples was performed using a canon digital single lens reflex camera.

Analysis of the subcellular localization of dCas9-TurboID-mVenus

To construct the dCas9-TurboID-mVenus fusion protein, the coding sequence of TurboID-mVenus was amplified through PCR utilizing CloneAmp HiFi PCR Premix, the vector pDONR_P2R-P3_R2-Turbo-mVenus-STOP-L3 (Mair et al., 2019), and gene-specific primers that included 15-base-pair extensions complementary to the ends

of the linearized vector (refer to Table A1). The resulting amplified product, along with the linearized MultiSite Gateway *attL1-attR5* entry vector pYPQ173 (which had been digested with *SaII* and *AatII*) (Lowder et al., 2018), was subsequently combined in an In-Fusion HD Cloning enzyme mix. This reaction mixture was then introduced into *E. coli* TOP10 cells via a heat shock method.

To excise the P_{AtU6} :sgRNA sequence from the MultiSite Gateway *attL5-attL2* entry vector pYPQ141A (Lowder et al., 2015), the vector was linearized through inverse PCR utilizing CloneAmp HiFi PCR Premix and primers designed with 15-base-pair extensions that are complementary to the ends of the linearized vector (refer to Table A1). The resulting amplified product was subsequently combined in an In-Fusion HD Cloning enzyme mix, and the reaction mixture was introduced into *E. coli* TOP10 cells via a heat shock method.

The promoter for ubiquitin 10 from Col-0 ($P_{AtUBQ10}$) was amplified via PCR from the vector pGPTVII-Bar-U-iGluSnFR (a laboratory stock) utilizing CloneAmp HiFi PCR Premix and gene-specific primers that included 15-base-pair extensions complementary to the ends of the linearized vector (refer to Table A1). The linearized MultiSite Gateway *attR1-attR2* destination vector pYPQ203 (Tang et al., 2017), which had been digested with *HindIII* and *AscI*, was combined with the amplified product in an In-Fusion HD Cloning enzyme mix. This reaction mixture was subsequently introduced into *E. coli* TOP10 through a heat shock method. Plasmids *pattL1-dCas9-TurboID-mVenus-attR5*, *pattL5-attL2*, and $pP_{AtUBQ10}:attR1-attR2$ were extracted from *E. coli* TOP10 using the NucleoSpin® Plasmid kit and were verified through Sanger sequencing.

The entry vectors *pattL1-dCas9-TurboID-mVenus-attR5*, *pattL5-attL2*, and the destination vector $pP_{AtUBQ10}:attR1-attR2$ were utilized in a Gateway™ LR Clonase™ II enzyme mix (Invitrogen™, USA). This reaction was subsequently introduced into *E. coli* TOP10 through a heat shock method. The plasmid $pP_{AtUBQ10}:dCas9-TurboID-mVenus$ was then extracted from *E. coli* TOP10 using the NucleoSpin® Plasmid isolation kit and was verified through Sanger sequencing.

The construct $pP_{AtUBQ10}:dCas9-TurboID-mVenus$ was introduced into *A. tumefaciens* strain GV3101 through a heat shock method. The transformed *A. tumefaciens* GV3101

strains were subsequently employed in the floral dip transformation. Individual T1 transformants of the Col-0 line were selected on ½ MS medium supplemented with 50 mg mL⁻¹ hygromycin (see Table A3). The presence of mVenus fluorescence in the T1 transformants was detected using a ZEISS Axio Zoom stereo microscope.

To create the intronized dCas9, double point mutations (D10A and H840A) were incorporated into the intronized Cas9 sequence through PCR utilizing CloneAmp HiFi PCR Premix, the vector pAGM55261 (Grützner et al., 2021), and primers featuring 15-base-pair extensions that are complementary to the ends of the linearized vector (refer to Table A1). The resulting amplified product, along with the linearized pUC19-based entry vector pGD146 (which was amplified via inverse PCR using CloneAmp HiFi PCR Premix and pGD146 as the DNA template), was subsequently combined in NEBuilder® HiFi DNA assembly master mix (New England Biolabs, MA, USA). This reaction mixture was then introduced into *E. coli* TOP10 through a heat shock method. The pGD146 vector was generously provided by Rüdiger Simon from Heinrich Heine University Düsseldorf, Germany.

To create the TurboID-mVenus-NLS fusion protein, the nuclear localization signal (NLS) from the simian vacuolating virus 40 was incorporated into the coding sequence of TurboID-mVenus through PCR. This process utilized CloneAmp HiFi PCR Premix, the vector pDONR_P2R-P3_R2-Turbo-mVenus-STOP-L3, and primers designed with 15-base-pair extensions that were complementary to the ends of the linearized vector (refer to Table A1). The resulting amplified product, along with the linearized pUC19-based entry vector pGGD002 (which was generated via inverse PCR using CloneAmp HiFi PCR Premix and pGGD002 as the DNA template), was combined in an In-Fusion HD Cloning enzyme mix (Lamprouopoulos et al., 2013). The resultant reaction was subsequently introduced into *E. coli* TOP10 through a heat shock method. Plasmids pGGC-dCas9i and pGGD-TurboID-mVenus-NLS were extracted from *E. coli* TOP10 using the NucleoSpin® Plasmid kit and were verified through Sanger sequencing.

The DNA-binding domain of the bacterial repressor LexA (X), the acidic transactivating domain of VP16 (V), and the regulatory region of the human estrogen receptor (E) have been combined to form a chimeric transcription activator known as XVE (Zuo et al., 2000). In order to produce a β-estradiol-inducible dCas9-TurboID-mVenus-NLS fusion, a series of pUC19-based entry vectors, including pBLA001-

LexA-35S, pGGB002, pGGC-dCas9i, pGGD-TurboID-mVenus-NLS, pGGE001, and pGGF-RT-FAST-red fluorescent protein (RFP), were assembled into the destination vector pGD283 utilizing Golden Gate assembly (Lampropoulos et al., 2013; Denay et al., 2019; Rossmann et al., 2020). This assembly was subsequently introduced into *E. coli* TOP10 through a heat shock method. The plasmid pP_{CaMV35S}:XVE-P_{LexA}:dCas9-TurboID-mVenus-NLS-FAST-RFP was extracted from *E. coli* TOP10 using the NucleoSpin® Plasmid kit and was verified through Sanger sequencing.

The construct pP_{CaMV35S}:XVE-P_{LexA}:dCas9-TurboID-mVenus-NLS-FAST-RFP was introduced into *A. tumefaciens* strain GV3101 through a heat shock method. The Col-0 ecotype was utilized for floral dipping. T1 transgenic plants, designated as XVE-dCas9-Tb, were selected based on the presence of seed-coat specific RFP fluorescence (see Table A3). T2 seeds exhibiting RFP fluorescence were subsequently sown in a peat-based substrate and cultivated under controlled conditions of 12 hours of light and 12 hours of darkness at a temperature of 22°C, with a RH of 60% and a PPFD of 80 $\mu\text{mol m}^{-2} \text{s}^{-1}$ for a duration of four weeks.

To assess the expression of the dCas9-TurboID-mVenus-NLS fusion protein, fully expanded rosette leaves from T2 plants were infiltrated with a 20 μM solution of β -estradiol using a syringe. The mVenus fluorescence in the T2 transformants was detected 24 hours post-infiltration using a ZEISS Axio Zoom stereo microscope. For the investigation of the subcellular localization of the dCas9-TurboID-mVenus-NLS fusion within adaxial epidermal cells, fluorescence images of mVenus were captured using a Leica TCS SP8 microscope, employing the following settings: excitation at 488 nm (white light laser) and emission between 492-552 nm for mVenus, and excitation at 638 nm with emission between 645-738 nm for chlorophyll autofluorescence.

Evaluation of the biotin ligase activity of the dCas9-TurboID-mVenus

In order to evaluate the biotin ligase activity of the dCas9-TurboID-mVenus-NLS fusion protein, XVE-dCas9-Tb leaves were subjected to incubation in a 50 μM biotin ($\text{C}_{10}\text{H}_{16}\text{N}_2\text{O}_3\text{S}$) solution for a duration of one hour at a temperature of 22°C. Following biotin treatment, the leaves were homogenized in liquid nitrogen utilizing a pestle and mortar. The resulting homogenate was combined with 1 mL of freshly prepared radioimmunoprecipitation assay (RIPA) buffer, which consisted of 50 mM

trisaminomethane (Tris)-HCl ($\text{NH}_2\text{C}(\text{CH}_2\text{OH})_3\cdot\text{HCl}$) (pH 7.4), 150 mM NaCl, 0.5% sodium deoxycholate ($\text{C}_{24}\text{H}_{39}\text{NaO}_4$), 1 mM EDTA (pH = 8), 0.1% sodium dodecyl sulfate ($\text{NaC}_{12}\text{H}_{25}\text{SO}_4$), 1% Triton-X 100, 1 mM phenylmethanesulfonylfluoride ($\text{C}_7\text{H}_7\text{FO}_2\text{S}$), and half a Roche cOmplete™ Protease Inhibitor Cocktail tablet. This mixture was then incubated on ice for 10 minutes. Following this incubation, the sample was centrifuged at 13,300 rpm for 30 minutes at 4°C, and the protein concentration in the supernatant was determined using the Quick Start™ Bradford Protein Assay Kit (Cat. No. 5000201, Bio-Rad, CA, USA). A total of 3 mg of protein from each sample was then resolved using 12% Mini-PROTEAN® TGX™ Precast Protein Gels (Cat. No. 4561043, Bio-Rad, CA, USA) at a current of 200 milliamperes (mA) for 60 minutes at room temperature.

Proteins were transferred from the gel to a polyvinylidene fluoride membrane by applying a current of 80 mA at a temperature of 4°C for a duration of 60 minutes. Subsequently, the membrane was subjected to two washes with tris buffered saline with Tween 20 (TBST), which consisted of 20 mM Tris, 150 mM NaCl, and 0.1% Tween 20 ($\text{C}_{58}\text{H}_{114}\text{O}_{26}$), followed by a blocking step in TBST supplemented with 5% bovine serum albumin for 60 minutes at 22°C with gentle agitation at 30 rpm. To facilitate the detection of biotinylated proteins on the membrane, the blocked membranes were incubated overnight at 4°C with a Streptavidin-horseradish peroxidase solution diluted to 1:2500 (Catalog No. ab7403, Abcam, MA, USA). After four washes with TBST, 1 mL of SuperSignal™ West Femto Maximum Sensitivity Substrate (Catalog No. 34094, Thermo Fisher Scientific, MA, USA) was applied, and the resulting chemiluminescence was captured using the UVP ChemStudio PLUS Touch (Analytik Jena, Jena, Germany).

Identification of proteins associated with the STP13 promoter during *Pst* DC3000 infection

To incorporate two *Paq*CI sites in front of the trans-activating crRNA (trRNA), the DNA sequence designated as 2X *Paq*CI-trRNA was amplified via PCR utilizing CloneAmp HiFi PCR Premix, the vector pEE515 (Ellison et al., 2020), and primers featuring 16-base-pair extensions that are complementary to the ends of the linearized vector (refer to Table A1). The resulting amplified product, along with the linearized tobacco rattle virus (TRV) RNA2 vector pTRV-RNA2-*P_{PEBV}*-MCS-*tRNA^{Atlleu}* (which

had been digested with *Xba*I and *Sac*I (Ellison et al., 2020), was subsequently combined in NEBuilder HiFi DNA assembly master mix. This reaction mixture was then introduced into *E. coli* TOP10 cells through a heat shock transformation method. The plasmid pTRV-RNA2-P_{PEBV}:2XPaqCI-trRNA-tRNA^{Atlleu} was extracted from the *E. coli* TOP10 cells using the NucleoSpin® Plasmid isolation kit and was verified through Sanger sequencing.

CHOPCHOP (<http://chopchop.cbu.uib.no>) was utilized to design the crRNA protospacer sequence targeting the STP13 (AT5G26340) promoter located on chromosome 5 (positions 9312835-9312854) (Labun et al., 2019). For the construction of a specific crRNA protospacer, two synthesized complementary DNA oligonucleotides, each consisting of 24 nucleotides, were purchased from Integrated DNA Technology and subsequently annealed. This process resulted in the formation of a dsDNA characterized by a 5' overhang of AGTC on the sense strand and a 5' overhang of AAAC on the antisense strand (refer to Table A1).

The dsDNA crRNA^{PAtSTP13} was incorporated into the linearized vector pTRV-RNA2-P_{PEBV}:2XPaqCI-trRNA-tRNA^{Atlleu}, which had been restricted with *Paq*CI, following a DNA ligation protocol utilizing T4 DNA ligase (NEB, MA, USA). The resulting reaction mixture was subsequently introduced into *E. coli* StellaTM chemical competent cells (hereafter referred to as *E. coli* Stella) (Takara, USA) through a heat shock method (see Table A2). Plasmid pTRV-RNA2-P_{PEBV}:sgRNA^{PAtSTP13}-tRNA^{Atlleu} was extracted from *E. coli* Stella using the NucleoSpin® Plasmid isolation kit and was verified via Sanger sequencing. The vector pTRV-RNA2-P_{PEBV}:sgRNA^{PAtSTP13}-tRNA^{Atlleu}, as well as the TRV RNA1 vector pYL192 (Liu et al., 2002), were introduced into *A. tumefaciens* strain GV3101 utilizing a heat shock method.

For the agroflooding experiment, seeds of T2 (XVE-dCas9-Tb) exhibiting RFP fluorescence were planted in ½ MS medium and cultivated under a photoperiod of 12 hours light and 12 hours dark at a temperature of 22°C, with a RH of 60% and a PPFD of 120 µmol m⁻² s⁻¹ for a duration of two weeks. Strains of *A. tumefaciens* GV3101 (specifically pTRV-RNA2-P_{PEBV}:sgRNA^{PAtSTP13}-tRNA^{Atlleu} or pYL192) were inoculated from glycerol stocks, which had been preserved at -80°C, onto Lysogeny Broth (LB) agar plates supplemented with 50 µg mL⁻¹ rifampicin and 50 µg mL⁻¹ kanamycin. Both strains of *A. tumefaciens* GV3101 were incubated at 28°C for a period of two days.

Subsequently, a single colony of *A. tumefaciens* GV3101 was utilized to inoculate 5 mL of LB medium containing 50 $\mu\text{g mL}^{-1}$ rifampicin and 50 $\mu\text{g mL}^{-1}$ kanamycin, and both strains were cultured at 28°C with shaking at 200 rpm for 16 hours.

The bacterial cultures were collected through centrifugation at a force of 4000 g for a duration of 2 minutes. The harvested cells were then washed with 1 mL of water under the same centrifugation conditions. Following this, the *A. tumefaciens* GV3101 pellets were resuspended in 1 mL of water. The cell density of *A. tumefaciens* GV3101 was adjusted to an OD₆₀₀ of 0.5 in an agroflooding buffer composed of 10 mM MgCl₂, 10 mM 2-(N-morpholino) ethanesulfonic acid (C₆H₁₃NO₄S), and 250 μM acetosyringone (C₁₀H₁₂O₄). The resuspended cells were incubated at 22°C with shaking at 30 rpm for a duration of 2 hours. Subsequently, 2 mL of *A. tumefaciens* GV3101 containing the construct pTRV-RNA2-P_{PEBV}:sgRNA^{PAiSTP13}-tRNA^{AtIleu} was combined with 2 mL of *A. tumefaciens* GV3101 harboring the pYL192 plasmid to create the inoculum. XVE-dCas9-Tb seedlings, which had been cultivated on ½ MS agar plates, were then exposed to the *A. tumefaciens* GV3101 inoculum under controlled conditions of 12 hours of light and 12 hours of darkness at 22°C and 60% RH, with a PPF of approximately 80 $\mu\text{mol m}^{-2} \text{s}^{-1}$ for four days. Following agroflooding, the XVE-dCas9-Tb seedlings were transplanted into a peat-based substrate and maintained under the same light and temperature conditions for an additional three weeks.

Three days prior to the infection with *Pst* DC3000, the bacterium was streaked from glycerol stocks, which had been stored at -80 °C, onto a KB agar plate supplemented with 50 $\mu\text{g mL}^{-1}$ rifampicin. The *Pst* DC3000 was subsequently incubated at 28 °C for a duration of two days. A single colony of *Pst* DC3000 was then utilized to inoculate 4 mL of *hrp* derepressing medium, which consisted of 10 mM fructose, 50 mM KH₂PO₄, 7.6 mM (NH₄)₂SO₄, 1.7 mM MgCl₂, 1.7 mM NaCl, and 50 $\mu\text{g mL}^{-1}$ rifampicin, adjusted to a pH of 6. The culture was maintained at 28 °C with shaking at 200 rpm for 16 hours. Following this incubation, the *Pst* DC3000 cells in the *hrp* derepressing medium were harvested via centrifugation (2 minutes at 4000 g), and the resulting pellet was resuspended in 2 mL of 10 mM MgCl₂. To prepare the inoculum of *Pst* DC3000 at a concentration of 10⁶ CFU mL⁻¹, the cell density was adjusted to an OD₆₀₀ of 0.002 in 10 mM MgCl₂. Subsequently, either the *Pst* DC3000 suspension or 10 mM MgCl₂ (as a mock treatment) was infiltrated into the abaxial leaf surface of XVE-dCas9-Tb plants,

with nine plants allocated to each treatment group, using a 1 mL syringe. The infiltrated plants were then placed in a plastic tray covered with a transparent lid and were grown under controlled conditions of 12 hours of light and 12 hours of darkness at 22 °C, with a RH of 60% and a PPFD of 80 $\mu\text{mol m}^{-2} \text{s}^{-1}$.

Two days following infiltration, XVE-dCas9-Tb plants were treated with a 20 μM solution of β -estradiol to induce the expression of dCas9-TurboID-mVenus-NLS. Subsequently, three days post-infiltration, leaves from the XVE-dCas9-Tb plants exhibiting mVenus (yellow fluorescent protein) fluorescence were incubated in a 50 μM biotin solution at 22°C for a duration of two hours. The biotin-treated tissues, comprising three biological replicates per treatment (with each biological replicate consisting of three plants), were then homogenized in liquid nitrogen to a fine powder using a pestle and mortar.

A homogenized leaf sample was subjected to incubation in 500 μL of freshly prepared RIPA buffer on ice for a duration of 30 minutes, followed by centrifugation at 13,300 rpm for 15 minutes at 4°C. The resulting supernatant, totaling 200 μL , was desalted on ice utilizing a PD SpinTrap G-25 column (Catalog No. 28918004, Cytiva, MA, USA), which had been equilibrated with a wash buffer composed of 20 mM Tris-HCl (pH 7.5), 1 mM EDTA, and 200 mM NaCl. The 200 μL flowthrough was subsequently incubated with 20 μL of equilibrated Streptavidin Sepharose High Performance (Catalog No. 17-5113-01, Cytiva, MA, USA) at 4°C for a period of two hours. The agarose beads were then subjected to three washes with 400 μL of wash buffer, followed by an additional three washes with 400 μL of 50 mM ammonium bicarbonate (NH_4HCO_3). The washed agarose beads were incubated in 50 μL of 50 mM NH_4HCO_3 containing 0.5 μg of SoLu-Trypsin (Catalog No. EMS0004, Sigma-Aldrich, MO, USA) at 37°C for 16 hours. Finally, the supernatant was transferred to a new 1.5 mL tube and stored at -70°C.

Frozen peptide samples were analyzed at the Molecular Proteomics Laboratory at Heinrich Heine University Düsseldorf using liquid chromatography–mass spectrometry (LC-MS). The peptide solutions, which had been digested with trypsin, were subjected to vacuum centrifugation to remove solvent, resulting in a dried form. These samples were subsequently reconstituted in 17 μL of 0.1% trifluoroacetic acid. For the LC-MS analysis, 15 μL of the reconstituted peptide mixtures were injected into a Q Exactive Plus Hybrid Quadrupole-Orbitrap mass spectrometer (Thermo Fisher Scientific, MA,

USA), which was coupled with a nanoelectrospray ionization source (Sinatra et al., 2022). The mass spectrometer operated in positive ion mode and was integrated with an Ultimate 3000 Rapid Separation liquid chromatography system (Dionex/Thermo Fisher Scientific, Germany). The liquid chromatography system utilized an Acclaim PepMap 100 C18 column (75 μm inner diameter, 25 cm length, 2 μm particle size, Thermo Fisher Scientific, MA, USA) and implemented a 60-minute liquid chromatography gradient. The capillary temperature was maintained at 250°C, with a source voltage of 1.4 kV. Mass spectrometry survey scans were conducted over a mass-to-charge ratio (m/z) range of 200 to 2000 at a resolution of 140,000. The automatic gain control was configured to 3,000,000, with a maximum fill time of 50 ms. The ten most intense peptide ions were isolated and subjected to fragmentation via higher-energy collisional dissociation.

The protein identification and quantification software MaxQuant (version 2.2.0.0, Max Planck Institute for Biochemistry, Planegg, Germany) was employed for the mass spectrometry-based proteomics data analysis. Mass spectrometry-derived spectra were matched against the reference proteomes of *Arabidopsis thaliana* cv. Columbia (UP000006548_3702.fasta) and *Pseudomonas syringae* pv. tomato strain ATCC BAA-871/DC3000 (UP000002515_223283.fasta), both sourced from UniProtKB (retrieved from <https://www.uniprot.org/>). The protein sequence of dCas9-TurboID-mVenus was utilized for the search. The analysis accounted for variable modifications, specifically methionine oxidation and N-terminal acetylation, while cysteine residues were designated as fixed carbamidomethyl modifications. The criteria for protein and peptide identification were established at a 1% false discovery rate. To predict the subcellular localization of the identified proteins, the multiple marker abundance profiling (MMAP) tool from the subcellular localization database for Arabidopsis proteins version 5 (SUBA5) was utilized (accessible at <https://suba.live/>).

Confocal imaging of GFP fusions in Arabidopsis infected with *B. cinerea*

To construct a GreenGate cloning pUC19-based entry vector containing the $P_{SWEET4}:SWEET4$ sequence, an A overhang (ACCT) and a D overhang (TCAG) were incorporated into the $P_{SWEET4}:SWEET4$ sequence through PCR utilizing CloneAmp HiFi PCR Premix, the vector $pP_{SWEET4}:SWEET4$ -GUS, and primers featuring 21-base-pair extensions that are complementary to the ends of the linearized vector (refer to

Table A1). The resulting amplified product, along with the linearized vector pGGA000 (which had been digested with *Bsa*I), was combined in the NEBuilder® HiFi DNA assembly master mix (Lampropoulos et al. in 2013). This reaction mixture was subsequently introduced into *E. coli* TOP10 cells via a heat shock protocol. The plasmid pGGAD-P_{SWEET4}:*SWEET4* was then extracted from the *E. coli* TOP10 cells using the NucleoSpin® Plasmid isolation kit and was verified through Sanger sequencing.

The pUC19-based entry vectors pGGAD- P_{SWEET4}:*SWEET4*, pGGD001, pGGE009, and pGGF-RT-FAST-RFP were assembled into the destination vector pGGZ003 utilizing Golden Gate assembly (Lampropoulos et al. in 2013; Rossmann et al., 2020). This assembly reaction was subsequently introduced into *E. coli* TOP10 through a heat shock method. The plasmid pP_{SWEET4}:*SWEET4*-eGFP was then isolated from *E. coli* TOP10 using the NucleoSpin® Plasmid extraction kit and was verified through Sanger sequencing.

Similarly, the pUC19-based entry vectors pGGA012, pGGB002, pGGC-dCas9i, pGGD-TurboID-mVenus-NLS, pGGE001, and pGGF-RT-FAST-RFP were also assembled into the destination vector pGGZ003 via Golden Gate assembly (Lampropoulos et al., 2013; Denay et al., 2019; Rossmann et al., 2020). This reaction was introduced into *E. coli* TOP10 using the heat shock method. The plasmid pP_{AtRPS5A}:dCas9i-TurboID-mVenus-rbcS-FAST-RFP was isolated from *E. coli* TOP10 using the NucleoSpin® Plasmid extraction kit and was confirmed through Sanger sequencing.

To construct the eGFP-GUS reporter vector, the porcine teschovirus-1 2A (P2A)-eGFP-GUS sequence was PCR amplified from the vector pP_{AtSWEET11}:*AtSWEET11*-P2A-eGFP-GUS (Kim et al., 2021) utilizing CloneAmp HiFi PCR Premix and primers featuring 16-base-pair extensions that were complementary to the ends of the linearized vector (refer to Table A1). The resulting amplified product, along with the linearized vector pP_{AtRPS5A}:dCas9i-TurboID-mVenus-rbcS-FAST-RFP (which had been digested with *Kpn*I) (Lampropoulos et al., 2013), was combined in NEBuilder® HiFi DNA assembly master mix. This reaction mixture was subsequently introduced into *E. coli* TOP10 through a heat shock method. The plasmid pGreenII-P2A-eGFP-GUS-rbcS-FAST-RFP was then extracted from *E. coli* TOP10 using NucleoSpin® Plasmid purification and was verified through Sanger sequencing.

To investigate the accumulation patterns of CINV2(AT4G09510), VIN2(AT1G12240), C/VIF2(AT5G64620), and SUC1(AT1G71880), genomic fragments encompassing the putative promoter, 5' untranslated regions, and open reading frames were amplified via PCR utilizing CloneAmp HiFi PCR Premix, genomic DNA from Col-0, and gene-specific primers featuring 15-base-pair extensions that are complementary to the influenza hemagglutinin (HA) peptide and the linearized ends of the vector (refer to Table A1). The resulting amplicons were subsequently combined with single-stranded DNA oligonucleotides HA and the linearized vector pGreenII-P2A-eGFP-GUS-rbcS-T-FAST-RFP (which had been restricted with *KpnI*) in the NEBuilder® HiFi DNA assembly master mix. The assembled reactions were then introduced into *E. coli* TOP10 through a heat shock method. Plasmids pP_{CINV2}:CINV2-P2A-eGFP-GUS, pP_{VIN2}:VIN2-P2A-eGFP-GUS, pP_{C/VIF2}:C/VIF2-P2A-eGFP-GUS, and pP_{SUC1}:SUC1-P2A-eGFP-GUS were subsequently isolated from *E. coli* TOP10 using the NucleoSpin® Plasmid extraction kit and were verified through Sanger sequencing.

To investigate the accumulation patterns of STP1(AT1G11260), STP4 (AT3G19930), STP13, VIN1(AT1G62660), CWINV1(AT3G13790), C/VIF1(AT1G47960), and SUC3(AT2G02860), genomic fragments encompassing the putative promoter, 5' untranslated regions, and open reading frames were amplified via PCR utilizing CloneAmp HiFi PCR Premix, genomic DNA from Col-0, and gene-specific primers featuring 15-base-pair extensions that are complementary to the ends of the linearized vector (refer to Table A1). The resulting amplicons were subsequently combined with the linearized vector pGreenII-P2A-eGFP-GUS-rbcS-T-FAST-RFP, which was amplified through inverse PCR using CloneAmp HiFi PCR Premix and pP_{VIN2}:VIN2-P2A-eGFP-GUS as the DNA template, within the In-Fusion HD Cloning enzyme mix. These reactions were then introduced into *E. coli* TOP10 (for STP13 and CWINV1) or *E. coli* Stellar (for STP1, STP4, VIN1, SUC3, and C/VIF1) via heat shock. The plasmids pP_{STP1}:STP1-P2A-eGFP-GUS, pP_{STP4}:STP4-P2A-eGFP-GUS, pP_{STP13}:STP13-P2A-eGFP-GUS, pP_{VIN1}:VIN1-P2A-eGFP-GUS, pP_{CWINV1}:CWINV1-P2A-eGFP-GUS, pP_{C/VIF1}:C/VIF1-P2A-eGFP-GUS, and pP_{SUC3}:SUC3-P2A-eGFP-GUS were subsequently isolated from *E. coli* TOP10 or *E. coli* Stellar using the NucleoSpin® Plasmid kit and were verified through Sanger sequencing.

To investigate the accumulation pattern of STP3 (AT5G61520), a genomic fragment

encompassing the putative promoter, 5' untranslated regions, and an open reading frame was amplified via PCR utilizing CloneAmp HiFi PCR Premix, genomic DNA from Col-0, and gene-specific primers containing the *SapI* restriction site (refer to Table A1). The resulting amplicon was subsequently assembled into a linearized vector, pGreenII-P2A-eGFP-GUS-rbcst-FAST-RFP, which had been amplified through inverse PCR using CloneAmp HiFi PCR Premix and pP_{CINV2}:CINV2-P2A-eGFP-GUS as the DNA template. This assembly was performed using Golden Gate assembly techniques, and the resultant reaction was introduced into *E. coli* strain TOP10 via a heat shock method. The plasmid pP_{STP3}:STP3-P2A-eGFP-GUS was then isolated from *E. coli* TOP10 using the NucleoSpin® Plasmid isolation kit and was subsequently verified through Sanger sequencing.

To investigate the accumulation pattern of CINV1 (AT1G35580), a genomic fragment encompassing the putative promoter, 5' untranslated regions, and an open reading frame was amplified via PCR utilizing CloneAmp HiFi PCR Premix, genomic DNA from Col-0, and primers featuring 15-base-pair extensions that are complementary to the ends of the linearized vector (refer to Table A1). The resultant amplicon was subsequently integrated with the linearized vector pDONR221, which had been amplified via inverse PCR utilizing CloneAmp HiFi PCR Premix and pDONR221-SWEET4 as the DNA template, within the NEBuilder® HiFi DNA assembly master mix. The resultant reaction was introduced into *E. coli* TOP10 through a heat shock method. Subsequently, the plasmid pDONR221-P_{CINV1}:CINV1 was extracted from *E. coli* TOP10 using NucleoSpin® Plasmid purification and was verified through Sanger sequencing.

To produce the HA-P2A fusion, the HA-P2A sequence was amplified via PCR from the vector pP_{STP13}:STP13-P2A-eGFP-GUS utilizing CloneAmp HiFi PCR Premix and primers featuring 15-base-pair extensions that were complementary to the ends of the linearized vector (refer to Table A1). The resulting amplicon, along with the linearized vector pDONR221-P_{CINV1}:CINV1 (which was amplified through inverse PCR using CloneAmp HiFi PCR Premix with pDONR221-P_{CINV1}:CINV1 as the DNA template), was subsequently combined in an In-Fusion HD Cloning enzyme mix. This reaction mixture was then introduced into *E. coli* TOP10 through a heat shock method. The plasmid pDONR221-P_{CINV1}:CINV1-HA-P2A was extracted from *E. coli* TOP10 using

the NucleoSpin® Plasmid extraction kit and was verified through Sanger sequencing.

The entry vector pDONR221-P_{CINVI}:CINVI-HA-P2A was then combined with the destination vector pBGWFS7.0 (Karimi et al., 2002) in a Gateway™ LR Clonase™ II enzyme mix, and this reaction was also introduced into *E. coli* TOP10 via heat shock. The plasmid pP_{CINVI}:CINVI-P2A-eGFP-GUS was isolated from *E. coli* TOP10 using the NucleoSpin® Plasmid extraction kit and was confirmed through Sanger sequencing.

The constructs pP_{SWEET4}:SWEET4-eGFP, pP_{CINVI}:CINVI-P2A-eGFP-GUS, pP_{CINV2}:CINV2-P2A-eGFP-GUS, pP_{VINI}:VINI-P2A-eGFP-GUS, pP_{VIN2}:VIN2-P2A-eGFP-GUS, pP_{CWINV1}:CWINV1-P2A-eGFP-GUS, pP_{CVIF1}:C/VIF1-P2A-eGFP-GUS, pP_{CVIF2}:C/VIF2-P2A-eGFP-GUS, pP_{SUC1}:SUC1-P2A-eGFP-GUS, pP_{SUC3}:SUC3-P2A-eGFP-GUS, pP_{STP1}:STP1-P2A-eGFP-GUS, pP_{STP3}:STP3-P2A-eGFP-GUS, pP_{STP4}:STP4-P2A-eGFP-GUS, and pP_{STP13}:STP13-P2A-eGFP-GUS were introduced into *A. tumefaciens* strain GV3101 through a heat shock method. The Col-0 ecotype was utilized for floral dipping, with the exception of the construct pP_{CINVI}:CINVI-P2A-eGFP-GUS, for which the T-DNA insertion mutant *cinvl* (SALK_095807) was employed (see Table A3). T1 transgenic plants were identified based on seed-coat specific RFP fluorescence, with the exception of the P_{CINVI}:CINVI-P2A-eGFP-GUS/*cinvl* plants. For the selection of T1 transgenic plants P_{CINVI}:CINVI-P2A-eGFP-GUS/*cinvl*, a medium consisting of ½ MS agar supplemented with 10 µg mL⁻¹ glufosinate ammonium (C₅H₁₅N₂O₄P) was utilized.

For the purpose of *B. cinerea* infection, T2 seeds exhibiting RFP fluorescence were cultivated in a peat-based substrate. The plants were maintained under a photoperiod of 12 hours of light and 12 hours of darkness at a temperature of 22°C, with a RH of 60% and a PPFD of 80 µmol m⁻² s⁻¹ for a duration of four weeks. For the transgenic plants P_{CINVI}:CINVI-P2A-eGFP-GUS/*cinvl*, T2 seeds were sown in ½ MS medium supplemented with 10 µg mL⁻¹ glufosinate ammonium. The seedlings were grown under identical light and temperature conditions for a period of seven days, after which the surviving seedlings were transferred to a peat-based substrate. These plants were subsequently grown under the same environmental conditions for an additional three weeks. In the case of the transgenic plants P_{SWEET12}:SWEET12, seeds were also sown in a peat-based substrate and subjected to the same growth conditions as previously described for four weeks (Chen et al., 2012).

The mycelium of *B. cinerea* B05.10 (Van Kan et al., 2017), which had been stored at -20°C, was cultured on potato dextrose agar (PDA) (Catalog No. 1101300500, Merck) and incubated at 22°C for a duration of two weeks. To collect conidia, the mycelium on the PDA was suspended in water and subsequently filtered through Miracloth. A 10 µL aliquot of the conidia suspension was introduced into a counting chamber (Catalog No. 718605, BRAND, Wertheim, Germany) to determine the conidia density within the suspension. Inoculums of *B. cinerea* were prepared by diluting the conidia suspension to achieve concentrations of 2 or 2.5 x 10⁵ conidia mL⁻¹ in a ½ malt extract medium supplemented with 100 mM glucose. For the purpose of *B. cinerea* infection, 2 or 4 µL of the inoculum was applied to each half leaf (three rosette leaves per plant) across all reporter lines. The inoculated plants were then placed in a tray covered with a transparent lid and maintained under conditions of 12 hours of light and 12 hours of darkness at 22°C, with a RH of 60% and a PPFD of 6 µmol m⁻² s⁻¹.

A leaf disc was excised from the region adjacent to the droplet of conidia suspension for the purpose of confocal imaging. To visualize the leaf vasculature, the abaxial epidermis was carefully removed utilizing 3M Magic tape. Fluorescence images were acquired using the Leica TCS SP8 microscope, configured with the following parameters: for green fluorescent protein (GFP), excitation was set at 488 nm (employing a white light laser) and emission was recorded between 492-552 nm; for chlorophyll autofluorescence, excitation occurred at 638 nm, with emission captured in the range of 645-738 nm.

Histochemical analysis of GUS fusions in Arabidopsis infected with *B. cinerea*

Transgenic plants P_{SWEET2}:SWEET2-GUS (Chen et al., 2015a), P_{SWEET12}:SWEET12-GUS (Chen et al., 2012), and P_{SWEET17}:SWEET17-GUS (Guo et al., 2014) were cultivated in a peat-based substrate under controlled environmental conditions of 16 hours of light and 8 hours of darkness at a temperature of 22°C, with a RH of 60% and a PPFD of 80 µmol m⁻² s⁻¹ for a duration of three weeks (see Table A3). T2 seeds from the P_{SWEET4}:SWEET4-GUS line 6 were sown onto ½ MS medium supplemented with 50 mg mL⁻¹ hygromycin, and the seedlings were maintained under a 12-hour light and 12-hour dark photoperiod at 22°C, 60% RH, and a PPFD of 120 µmol m⁻² s⁻¹ for ten days. The surviving seedlings were then transplanted into a peat-based substrate and continued to grow under the same 12-hour light/12-hour dark conditions at 22°C, 60%

RH, and a PPFD of $80 \mu\text{mol m}^{-2} \text{s}^{-1}$ for an additional three weeks.

The mycelium of *B. cinerea* B05.10, which had been stored at -20°C , was cultured on PDA at a temperature of 22°C for a duration of two weeks. To collect conidia, the mycelium was suspended in water and subsequently filtered through Miracloth. A $10 \mu\text{L}$ aliquot of the conidia suspension was introduced into a counting chamber to determine the conidia density. Inoculum of *B. cinerea* was prepared at a concentration of 5×10^5 conidia mL^{-1} by diluting the conidia suspension in an inoculation buffer composed of 15 g sucrose, 3 g trisodium citrate dihydrate ($\text{Na}_3\text{C}_6\text{H}_5\text{O}_7$), 6.5 g K_2HPO_4 , 0.2 g $\text{MgSO}_4 \cdot 7\text{H}_2\text{O}$, 0.1 g $\text{CaCl}_2 \cdot 2\text{H}_2\text{O}$, 2 g NH_4NO_3 per liter, adjusted to a pH of 5.8. For the purpose of *B. cinerea* infection, $5 \mu\text{L}$ of the inoculum was applied to each half of the leaves (three rosette leaves per plant) for all reporter lines. The inoculated plants were then placed in a tray covered with a transparent lid and maintained under conditions of 12 hours of light and 12 hours of darkness at 22°C , with a RH of 60% and a PPFD of $6 \mu\text{mol m}^{-2} \text{s}^{-1}$.

In accordance with the histochemical GUS analysis protocol established by Yang et al. (2018), the leaves of pot-grown plants were subjected to fixation in 90% cold acetone for a duration of 10 minutes. Subsequently, the samples underwent vacuum infiltration in a GUS staining solution for an additional 10 minutes on ice. Following this, the samples were again vacuum infiltrated in a GUS staining solution containing 400 mM X-Gluc for 10 minutes on ice. The samples were then incubated at 37°C until the formation of a blue precipitate was observed, which occurred after approximately 2 hours for $P_{\text{SWEET2}}:\text{SWEET2-GUS}$, 2 hours for $P_{\text{SWEET4}}:\text{SWEET4-GUS}$, 5.5 hours for $P_{\text{SWEET12}}:\text{SWEET12-GUS}$, and 1.5 hours for $P_{\text{SWEET17}}:\text{SWEET17-GUS}$. Following staining, the samples were sequentially dehydrated and cleared using 30%, 50%, and 70% ethanol. Imaging of the cleared samples was performed using a ZEISS Axio Zoom stereo microscope.

Assessment of the susceptibility of Arabidopsis mutants to *B. cinerea* B05.10

The design of the crRNA was conducted using the CHOPCHOP tool (Labun et al., 2019). This process involved the creation of a specific crRNA protospacer sequence for the genes *SWEET4*, *UmamiT18* (AT1G44800), *UmamiT20* (AT4G08290), and *UmamiT29* (AT4G01430). To achieve this, two synthesized 24-nucleotide

complementary DNA oligonucleotides, obtained from Integrated DNA Technology, were annealed to form a dsDNA. This dsDNA featured a 5' overhang of ATTG on the sense strand and a 5' overhang of AAAC on the antisense strand (refer to Table A1).

The dsDNAs corresponding to crRNA^{SWEET4}, crRNA^{UmamiT18}, crRNA^{UmamiT20}, and crRNA^{UmamiT29} were individually incorporated into linearized pCR8-based entry vectors, which had been digested with *Bsm*BI (Zheng et al., 2020). Each vector contained a distinct small nuclear RNA promoter and a poly-T terminator. This insertion was performed in accordance with the DNA ligation protocol utilizing T4 DNA ligase. Subsequently, all reactions were introduced into *E. coli* TOP10 through a heat shock method. The resulting plasmids, namely pCR-P_{AtU6}:sgRNA^{SWEET4}, pCR-P_{OsU3b}:sgRNA^{UmamiT18}, pCR-P_{AtU6-1}:sgRNA^{UmamiT20}, and pCR-P_{OsU3d}:sgRNA^{UmamiT29}, were extracted from *E. coli* TOP10 using the NucleoSpin® Plasmid isolation kit and were verified through Sanger sequencing.

The entry vectors pP_{AtU6}:sgRNA^{SWEET4}, pP_{OsU3b}:sgRNA^{UmamiT18}, pP_{AtU6-1}:sgRNA^{UmamiT20}, and pP_{OsU3d}:sgRNA^{UmamiT29} were incorporated into the vector pENTR4-*ccdB* utilizing Golden Gate assembly. This assembly reaction was subsequently introduced into *E. coli* TOP10 through a heat shock method. The plasmid pENTR4-sgRNAs^{SWEET4,UmamiT18,20,29} was then extracted from *E. coli* TOP10 using the NucleoSpin® Plasmid isolation kit and was verified through Sanger sequencing.

The crRNA protospacers for *SWEET2* (AT3G14770), *SWEET17* (AT4G15920), *VIN1*, *VIN2*, *SUC1*, *SUC3*, *C/VIF1*, *C/VIF2*, *STP3*, and *STP4* were designed utilizing the CHOPCHOP tool (Labun et al., 2019). Primers, as detailed in Table A1, were constructed to include the crRNA protospacer sequence flanked by the *Bsa*I restriction site, facilitating the amplification of tracrRNA and the *OsU3b* promoter derived from the vector pENTR4-sgRNAs^{SWEET4,UmamiT18,20,29} through PCR. The resulting amplicons were subsequently inserted into the linearized vector pAGM55261 (Grützner et al., 2021) via Golden Gate assembly. All reactions were then transformed into *E. coli* TOP10 through a heat shock method. The plasmids pP_{AtRPS5A}:Cas9-P_{AtU6}:sgRNA^{SWEET2}-P_{OsU3b}:sgRNA^{SWEET17}, pP_{AtRPS5A}:Cas9-P_{AtU6}:sgRNA^{VIN1}-P_{OsU3b}:sgRNA^{VIN2}, pP_{AtRPS5A}:Cas9-P_{AtU6}:sgRNA^{SUC1}-P_{OsU3b}:sgRNA^{SUC3}, pP_{AtRPS5A}:Cas9-P_{AtU6}:sgRNA^{C/VIF1}-P_{OsU3b}:sgRNA^{C/VIF2}, pP_{AtRPS5A}:Cas9-P_{AtU6}:sgRNA^{STP3}-P_{OsU3b}:sgRNA^{STP4} were

subsequently isolated from *E. coli* TOP10 using the NucleoSpin® Plasmid extraction kit and were confirmed through Sanger sequencing.

The constructs $\text{pP}_{AtRPS5A}:\text{Cas9}-\text{P}_{AtU6}:\text{sgRNA}^{SWEET2}-\text{P}_{OsU3b}:\text{sgRNA}^{SWEET17}$, $\text{pP}_{AtRPS5A}:\text{Cas9}-\text{P}_{AtU6}:\text{sgRNA}^{VIN1}-\text{P}_{OsU3b}:\text{sgRNA}^{VIN2}$, $\text{pP}_{AtRPS5A}:\text{Cas9}-\text{P}_{AtU6}:\text{sgRNA}^{SUC1}-\text{P}_{OsU3b}:\text{sgRNA}^{SUC3}$, $\text{pP}_{AtRPS5A}:\text{Cas9}-\text{P}_{AtU6}:\text{sgRNA}^{C/VIF1}-\text{P}_{OsU3b}:\text{sgRNA}^{C/VIF2}$, $\text{pP}_{AtRPS5A}:\text{Cas9}-\text{P}_{AtU6}:\text{sgRNA}^{STP3}-\text{P}_{OsU3b}:\text{sgRNA}^{STP4}$ were introduced into *A. tumefaciens* strain GV3101 through a heat shock method. The Col-0 ecotype was utilized for floral dipping. Selection of T1 transgenic plants was conducted based on the presence of seed-coat specific RFP fluorescence. To verify mutations in the genes *SWEET2*, *SWEET17*, *VIN1*, *VIN2*, *SUC1*, *SUC3*, *C/VIF1*, *C/VIF2*, *STP3*, and *STP4*, gene-specific primers were employed to amplify the regions of interest, and the resulting amplicons were subjected to Sanger sequencing (refer to Table A1). Homozygous mutants that lacked seed-coat specific RFP fluorescence were subsequently utilized for infection assays with *B. cinerea*.

The Col-0 wild type, T-DNA insertion mutants *cinvl*, *sweet11;12;13*, and various double knockout mutants (*sweet2;17^{cr}*, *vin1;2^{cr}*, *suc1;3^{cr}*, *stp3;4^{cr}*, and *c/vif1;2^{cr}*) were cultivated in a peat-based substrate under controlled conditions of 12 hours of light and 12 hours of darkness at a temperature of 22°C, with a RH of 60% and a PPFD of 80 $\mu\text{mol m}^{-2} \text{s}^{-1}$ for a duration of five weeks. The *B. cinerea* strain B05.10, which had been stored at -20°C, was cultured on PDA at 22°C for two weeks. To collect conidia, the mycelium was suspended in sterile water and subsequently filtered through Miracloth. A 10 μL aliquot of the conidia suspension was introduced into a counting chamber to determine the conidia density. The inoculum for *B. cinerea* was prepared by diluting the conidia suspension to achieve a concentration of approximately 2 to 5 x 10⁵ conidia mL^{-1} in a ½ malt extract medium supplemented with 100 mM glucose. For the infection procedure, 5 μL of the inoculum was applied to each half leaf (three rosette leaves per plant) across all genotypes. The inoculated plants were then placed in a tray covered with a transparent lid and maintained under conditions of 12 hours of light and 12 hours of darkness at 22°C, with a RH of 60% and a PPFD of 6 $\mu\text{mol m}^{-2} \text{s}^{-1}$. Following this period, photographs of the *B. cinerea*-infected leaves were taken, and the sizes of the disease lesions were quantified using the freehand selection tool in ImageJ software.

Results

***Pst* DC3000 relies on the sucrose porin precursor ScrY to facilitate the rapid uptake of sucrose**

Sucrose has been shown to activate the expression of virulence genes in *Pst* DC3000 (Stauber et al., 2012; Turner et al., 2020). Additionally, *Pst* DC3000 is capable of metabolizing sucrose found in the extract of tomato leaf apoplasm (McCraw et al., 2016). The sucrose utilization system in *Pst* DC3000 is also stimulated in a *hrp*-inducing medium (Rico et al., 2008). It is posited that the S6P hydrolase ScrB and the sucrose porin precursor ScrY within this bacterium are essential for the effective utilization of sucrose (Joardar et al., 2005).

To investigate the necessity of ScrB and ScrY for sucrose utilization, I created knockout mutants for the *ScrB* gene (R28 codon CGA was altered to a premature stop codon TGA, designated as *scrB^{cr}*) and the *ScrY* gene (Q36 codon CAG was modified to a premature stop codon TAG, referred to as *scry^{cr}*) utilizing the CRISPR cytidine editor (Fig. A1) (Chen et al., 2018). Subsequently, I conducted *in vitro* bacterial growth assays.

For the purpose of inducing the sucrose utilization systems of *Pst* DC3000, I selected the *hrp* derepressing minimal (HDM) medium for the *in vitro* assays (Huynh et al., 1989). In this context, fructose in HDM was substituted with sucrose (designated as HDM_{Suc}) to assess the capacity of the *scrB^{cr}* and *scry^{cr}* to utilize sucrose as their sole carbon source (Stauber et al., 2012). *Pst* DC3000, *scrB^{cr}*, and *scry^{cr}* were cultured in HDM_{Suc} for a duration of 46 hours, during which the bacterial density was monitored by measuring OD₆₀₀.

At the 46-hour post-inoculation, the bacterial density of the *scry^{cr}* was observed to be lower than that of both *Pst* DC3000 and *scrB^{cr}* (Fig. 3). The findings from the *in vitro* bacterial growth assay indicate that the rapid proliferation of *Pst* DC3000 in HDM_{Suc} is contingent upon ScrY-mediated sucrose diffusion across the outer membrane. Despite the reduced growth of *scry^{cr}*, both *scrB^{cr}* and *scry^{cr}* were able to proliferate in HDM_{Suc}, indicating that *Pst* DC3000 likely employs alternative genetic components (such as sucrose transporters and levansucrase) to utilize the sucrose present in the HDM_{Suc} medium.

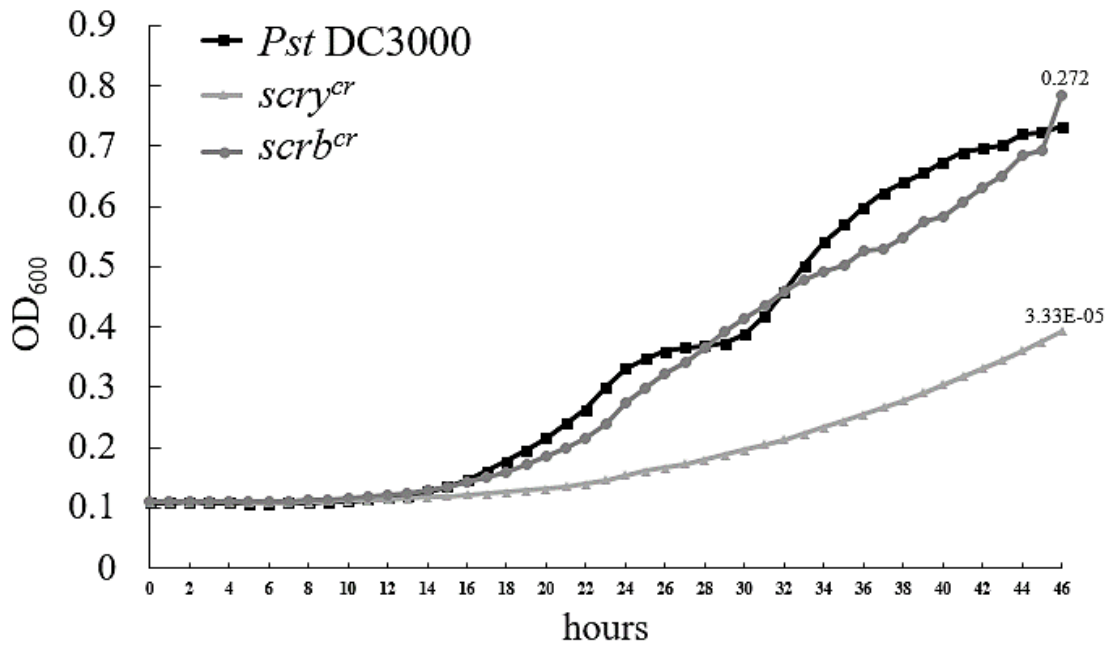


Fig. 3. The sucrose porin precursor ScrY in *Pst* DC3000 is essential for achieving optimal growth rates of this pathogen in modified hypersensitive response and pathogenicity derepressing medium (HDM_{Suc}). The growth curves of wild-type *Pst* DC3000, a sucrose-6-phosphate hydrolase knockout mutant (*scrbc*^{cr}), and a sucrose porin precursor knockout mutant (*scry*^{cr}) were analyzed during cultivation in HDM_{Suc}, which contained sucrose as the sole carbon source. The optical density at 600 nanometers (OD₆₀₀) of the bacterial cultures was recorded at one-hour intervals to estimate the bacterial cell population in HDM_{Suc}. Each data point is represented by a square for *Pst* DC3000, a triangle for *scry*^{cr}, and a dot for *scrbc*^{cr}, indicating the mean OD₆₀₀ at each time interval. Significant differences in comparison to *Pst* DC3000 at the 46-hour were assessed using the Student's *t*-test. The experiment was conducted twice, yielding consistent results.

***Pst* DC3000 utilizes the enzyme sucrose-6-phosphate hydrolase ScrB and the sucrose uniporters SWEET11, SWEET12, and SWEET13 to promote its rapid proliferation within the leaves of Arabidopsis**

To investigate the necessity of ScrB or ScrY for the *in planta* proliferation of *Pst* DC3000, I inoculated Col-0 with *Pst* DC3000, *scrbc*^{cr}, or *scry*^{cr} and subsequently quantified the viable bacterial cells present in the leaves 72 hours post-inoculation. The population of *scry*^{cr} did not exhibit a statistically significant difference compared to that of *Pst* DC3000 and *scrbc*^{cr}; however, the population of *scrbc*^{cr} was significantly lower than that of *Pst* DC3000. This finding shows that ScrB is essential for the proliferation of *Pst* DC3000 within the leaves of Arabidopsis (see Fig. 4a). Furthermore, ScrB was found to be non-essential for sucrose utilization when cultured in HDM_{Suc} (refer to Fig. 3). It is reasonable to propose that ScrB functions as the principal enzyme involved in sucrose metabolism in *Pst* DC3000 during the process of leaf colonization.

Sucrose plays a critical role in the virulence of *Pst* DC3000 and acts as a nutritional metabolite during the colonization of leaf tissues, as evidenced by the hypovirulent phenotype observed in the *scrB^{cr}* mutant. While the sucrose uniporter double mutant *sweet11;12* exhibited reduced susceptibility to *Pst* DC3000, it is possible that SWEET13 may partially compensate for the functions of SWEET11 and SWEET12 in this double mutant (Chen et al., 2012; Fatima and Senthil-Kumar, 2021). To further investigate the dependence of *Pst* DC3000 on sucrose efflux from living leaf cells, specifically phloem parenchyma cells, I employed the T-DNA triple mutant *sweet11;12;13*. The results indicated that the population of *Pst* DC3000 in the apoplasm of *sweet11;12;13* mutant plants was significantly lower compared to that in Col-0 plants (Fig. 4b). Collectively, these findings indicate that sucrose produced by the plant is a significant factor influencing the virulence of *Pst* DC3000 during the process of leaf colonization.

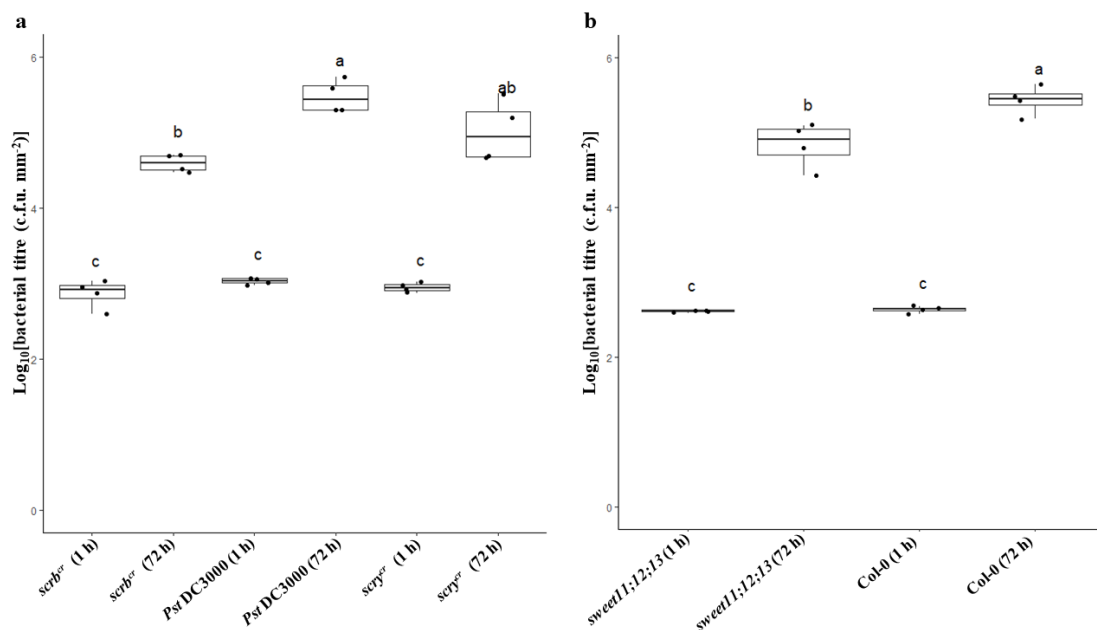


Fig. 4. *Pst* DC3000 sucrose-6-phosphate hydrolase ScrB and Arabidopsis plasma membrane-localized sucrose uniporter SWEET11, SWEET12, and SWEET13 were required for bacterial proliferation in leaves. (a) Arabidopsis plants of the Columbia ecotype (Col-0) were subjected to syringe infiltration with a concentration of 10^6 colony-forming units (c.f.u.) mL^{-1} of various strains of *Pst* DC3000, specifically the wild-type strain (*Pst* DC3000), a sucrose-6-phosphate hydrolase knockout mutant (*scrB^{cr}*), and a sucrose porin precursor knockout mutant (*scry^{cr}*). The boxplot illustrates the statistical distribution of bacterial titers, represented as log-transformed c.f.u. per millimeter squared (c.f.u. mm^{-2}), including the minimum (lower whisker), first quartile (lower edge), median (central line), third quartile (upper edge), and maximum (upper whisker). For samples collected one hour post-inoculation, each data point corresponds to a biological replicate, with four replicates per bacterial strain, where each replicate consists of three leaves pooled from three individual plants. For samples collected 72 hours post-inoculation, each data point also represents a biological replicate, with

four replicates per bacterial strain, and each replicate comprising five leaves pooled from five plants. (b) The Col-0 genotype and the triple mutant *sweet11;12;13* were similarly syringe-infiltrated with 10^6 c.f.u. mL⁻¹ of *Pst* DC3000. For the one-hour post-inoculation samples, each dot represents a biological replicate, with four replicates per genotype, where each replicate includes four leaves pooled from three plants. For the 72-hour post-inoculation samples, each dot again signifies a biological replicate, with four replicates per genotype, and each replicate containing eight leaves pooled from five plants. Distinct letters indicate statistically significant differences ($p < 0.05$) as determined by one-way analysis of variance followed by Tukey's honestly significant difference test. These experiments were conducted once.

The hexose uniporter SWEET4 is observed to accumulate in the leaf veins in response to the challenge posed by *Pst* DC3000

Pst DC3000 utilizes glucose not only as a carbon source but also as a ligand that induces virulence (Stauber et al., 2012; McCraw et al., 2016; Turner et al., 2020). Furthermore, glucose serves as a critical signaling molecule that facilitates the coordination of plant growth and the host's defense mechanisms against *Pst* DC3000 (Jing et al., 2020; Wang et al., 2022b; Yamada and Mine, 2024). The pathogen primarily enters the leaves of *Arabidopsis* through the stomatal openings. It is reasonable to anticipate that glucose signaling and pathogen feeding would occur in proximity to the leaf epidermal and mesophyll cells. Supporting this notion, Yamada et al. (2016) demonstrated that the STP13 accumulates in the epidermal and mesophyll cells in response to *Pst* DC3000 infection.

The mRNA levels of SWEET4, SWEET5, SWEET7, and SWEET8 are increased in *Pst* DC3000-infected-*Arabidopsis* leaves, implying that they function in glucose signaling and pathogen feeding (Chen et al., 2010). To see whether SWEETs-mediated glucose signaling/pathogen feeding are induced in certain leaf cell-types, I generated translational SWEET-GUS fusions of SWEET4 ($P_{SWEET4}:SWEET4$ -GUS), SWEET5 ($P_{SWEET5}:SWEET5$ -GUS), SWEET7 ($P_{SWEET7}:SWEET7$ -GUS), and SWEET8 ($P_{SWEET8}:SWEET8$ -GUS), utilizing their native promoters within the Col-0 genetic background. Subsequently, I conducted GUS histochemical analysis.

Plant samples intended for GUS histochemical analysis were collected by harvesting above-ground tissues 48 hours following either a mock treatment (administered with a 10 mM MgCl₂ solution) or inoculation with *Pst* DC3000, which was applied as a suspension in 10 mM MgCl₂ at a concentration of 10^8 colony-forming units per milliliter. For each translational SWEET-GUS fusion, three to four independent lines were evaluated, with some lines exhibiting reduced basal levels of GUS activity (refer

to Fig. A2-5). The GUS activities associated with SWEET4-GUS, SWEET5-GUS, SWEET7-GUS, and SWEET8-GUS were detected in the cotyledons and hydathodes of both mock-treated and *Pst* DC3000-inoculated plants (see Fig. 5), indicating that the accumulation of these fusions in the cotyledons and hydathodes was independent of *Pst* DC3000. Additionally, the accumulation of SWEET4-GUS and SWEET5-GUS in the midveins was also found to be independent of *Pst* DC3000 (Fig. 5). Intriguingly, the accumulation of SWEET4-GUS in the minor veins, lateral veins, and marginal veins of the $P_{SWEET4}:SWEET4$ -GUS line 6 was contingent upon *Pst* DC3000 inoculation (Fig. 5).



Fig. 5. GUS (β -glucuronidase) fusion of the Arabidopsis plasma membrane-localized hexose uniporter SWEET4, SWEET5, SWEET7, or SWEET8 accumulates in cotyledon, vein, or hydathode. Transgenic Arabidopsis plants, specifically the $P_{SWEET4}:SWEET4$ -GUS reporter line 6 ($n=2$ biological replicates), $P_{SWEET5}:SWEET5$ -GUS reporter line 8 ($n=1$), $P_{SWEET7}:SWEET7$ -GUS reporter line 9 ($n=2$), and $P_{SWEET8}:SWEET8$ -GUS reporter line 1 ($n=2$), were subjected to spray inoculation with either 10 mM $MgCl_2$ (as depicted in the upper panel) or an inoculum of *Pst* DC3000 at a concentration of 10^8 colony-forming units per milliliter (as shown in the lower panel). A representative transgenic Arabidopsis plant exhibiting GUS activity was observed in the cotyledon, vein, or hydathode at 48 hours post-inoculation. This experiment was conducted once.

The mRNA levels of SWEET4 are not increased in leaves infected with the *Pst* DC3000 type III secretion mutant (Chen et al., 2010). To investigate whether the accumulation of SWEET4-GUS in minor veins, lateral veins, and marginal veins necessitates the presence of a virulent *Pst* DC3000 strain, I inoculated $P_{SWEET4}:SWEET4$ -GUS line 6 with either *Pst* DC3000 or a *Pst* DC3000 variant deficient in the critical transcriptional regulator of virulence functions (*Pst* DC3000 *hrpL*⁻) (Bonardi et al., 2011). The results indicated that GUS activities associated with SWEET4-GUS in the aforementioned veins were not observed in leaves inoculated with *Pst* DC3000 *hrpL*⁻ (Fig. 6). This correlation between the expression of virulence genes and the accumulation of

SWEET4-GUS implies that either the virulent *Pst* DC3000 can exploit SWEET4 to facilitate disease progression, or that the host's defense response against virulent *Pst* DC3000 is contingent upon the presence of SWEET4.



Fig. 6. GUS (β -glucuronidase) fusion of the Arabidopsis plasma membrane-localized hexose uniporter SWEET4 is induced by *Pst* DC3000 infection. Transgenic Arabidopsis plants ($P_{SWEET4}:SWEET4$ -GUS reporter line 6) were subjected to drop-inoculation with the virulent strain of *Pst* DC3000 at a concentration of 10^8 colony-forming units mL^{-1} , alongside controls consisting of autoclaved water (mock treatment) and the non-virulent *Pst* DC3000 strain (*Pst* DC3000 *hrpL*⁻) at the same concentration. At 48 hours post-inoculation with *Pst* DC3000, four representative transgenic Arabidopsis plants exhibited GUS activity in the mid vein, minor veins, lateral veins, and marginal veins (a). In contrast, GUS activity was observed solely in the mid vein at 48 hours following inoculation with either autoclaved water (b) or the non-virulent *Pst* DC3000 *hrpL*⁻ strain (c). Scale bars represent 1 cm. $n = 6$ biological replicates. This experiment was conducted once.

The results of my GUS histochemical analysis implies that glucose signaling and pathogen feeding mediated by SWEET4 predominantly occur within the vascular tissues, rather than in the epidermal or mesophyll cells. Although the mRNA levels of SWEET4 was elevated in leaves infected with *Pst* DC3000, the *sweet4* knockout mutant exhibited susceptibility to *Pst* DC3000 comparable to that of the Col-0 wild type (Chong et al., 2014; Liu et al., 2016; Fatima and Senthil-Kumar, 2021). In summary, I have elucidated the spatial distribution of hexose uniporters SWEET4, SWEET5, SWEET7, and SWEET8 in leaves infected with *Pst* DC3000, as well as the critical roles of SWEET11, SWEET12, and SWEET13 in Arabidopsis susceptibility to this pathogen.

Investigating the transcriptional regulation of STP13 in Arabidopsis leaves infected by *Pst* DC3000

The transcriptional reprogramming of defense and susceptibility genes is essential for the survival or mortality of plants in response to pathogen attacks. Phytopathogenic organisms possess the ability to exploit the host's transcriptional machinery to induce disease. Inhibiting the transcriptional reprogramming triggered by pathogens can

enhance disease resistance in crops without compromising yield (Oliva et al., 2019). Therefore, elucidating the genetic determinants and molecular mechanisms that govern the expression of defense and susceptibility genes is critical for the advancement of disease resistance breeding.

Various methodologies have been established to identify transcriptional regulators associated to particular DNA sequences in plants, such as reverse chromatin immunoprecipitation (R-ChIP) and reverse chromatin immunoprecipitation utilizing the CRISPR-dCas9 system (R-ChIP-dCas9) (Wen et al., 2020; Wang et al., 2023). Nonetheless, the purification of DNA-associated proteins in both R-ChIP and R-ChIP-dCas9 relies on chemical cross-linking, a process that may inadvertently modify the inherent chromatin context.

A viable methodology for investigating transient or weak protein-protein interactions within a relatively natural cellular context involves the fusion of the protein of interest with a promiscuous biotin ligase, which facilitates the biotinylation of nearby proteins (Roux et al., 2012). The integration of biotin proximity labeling with the CRISPR-dCas9 system may facilitate the identification of proteins that are associated with specific DNA sequences in plant systems. Given its capacity to biotinylate proteins under conditions conducive to plant growth, TurboID was selected as the enzyme for the proximity labeling process (Mair et al., 2019).

In order to conduct CRISPR/dCas9-TurboID-based proximity labeling in Arabidopsis, I developed transgenic Col-0 plants harboring the transgene $P_{AtUBQ10}:dCas9-TurboID-mVenus$. However, no transgenic plants exhibiting mVenus fluorescence were observed (data not presented). The absence of detectable levels of the fusion protein dCas9-TurboID-mVenus in the transgenic plants may be attributed to the phenomenon of transgene silencing.

To facilitate the accumulation of Cas9-TurboID-mVenus within the nucleus of transgenic Col-0 plants, modifications were made to the promoter, replacing $P_{AtUBQ10}$ with an estradiol-inducible promoter ($P_{CaMV35S}:XVE-P_{LexA}$). Additionally, the dCas9 was substituted with an intron-optimized variant, and the simian vacuolating virus 40 nuclear localization signal (SV40 NLS) peptide (PKKKRKV) was appended to both the amino-terminus and carboxyl-terminus of dCas9-TurboID-mVenus (Grützner et al.,

2021). To assess the accumulation of the dCas9-TurboID-mVenus fusion protein in Col-0 plants harboring the transgene $P_{CaMV35S}:XVE-P_{LexA}:dCas9-TurboID-mVenus$ (hereafter referred to as XVE-dCas9-Tb), leaves were infiltrated with β -estradiol and subsequently imaged using confocal microscopy 24 hours post-infiltration. Similar to the localization observed with the dCas9-eGFP (enhanced green fluorescent protein) fusion in human cells, the dCas9-TurboID-mVenus fusion was found to localize within the nucleolus of leaf epidermal cells (Fig. 7a) (Chen et al., 2013).

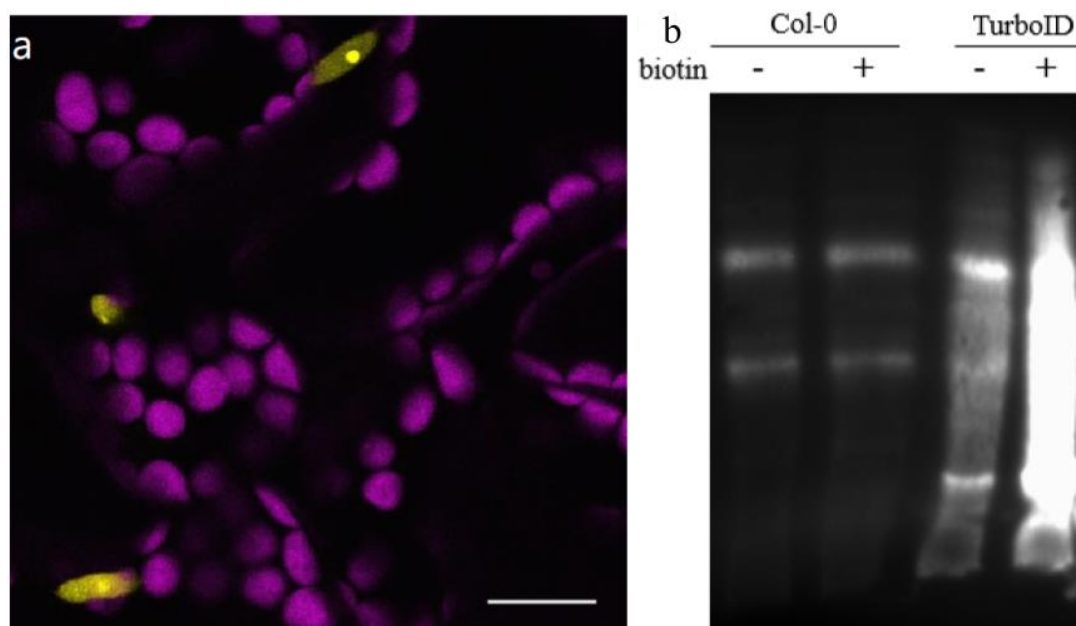


Fig. 7. dCas9-TurboID-mVenus localized in the nuclear and exhibited biotinylation activity in Arabidopsis leaf cells. (a) The leaves of transgenic Arabidopsis plants ($P_{CaMV35S}:XVE-P_{LexA}:dCas9-TurboID-mVenus$) were subjected to infiltration with a 20 μ M solution of β -estradiol utilizing a syringe. After a period of 24 hours post-infiltration, the fluorescence of mVenus (a yellow fluorescent protein) was observed, indicating localization within the nucleolus of adaxial epidermal cells. The magenta coloration represents chlorophyll autofluorescence. The scale bar measures 20 μ m. (b) Following the 24-hour period post- β -estradiol infiltration, the leaves of both Col-0 and transgenic plants (TurboID) underwent incubation in either water (-) or a 50 μ M biotin solution (+) for one hour at a temperature of 22°C. Total protein was then extracted from the leaves and utilized for streptavidin immunoblot analysis. $n = 1$. These experiments were conducted once.

To evaluate the biotin ligase activity of dCas9-TurboID-mVenus in the context of XVE-dCas9-Tb, I conducted a Western blot analysis utilizing total protein extracts and horseradish peroxidase-conjugated streptavidin, as described by Mair et al. (2019). The results indicated a significantly higher concentration of biotinylated proteins in the leaf samples of XVE-dCas9-Tb compared to those from Col-0 (see Fig. 7b). Consequently,

this indicates the potential application of XVE-dCas9-Tb for the biotinylation of proteins that are associated with DNA.

Hexose/proton symporters, such as STP13, play a crucial role in the defense mechanisms of plants against *Pst* DC3000 (Yamada et al., 2016; Yamada and Mine, 2024). The observed increase in mRNA levels of STP13 during the invasion by *Pst* DC3000 may be attributed to heightened gene expression, potentially facilitated by the binding of transcription factors or the presence of open chromatin configurations (Nobori et al., 2025). In order to utilize the recently developed CRISPR/dCas9-TurboID-based proximity labeling technique for the identification of transcription factors and chromatin remodelers associated with the STP13 promoter in response to *Pst* DC3000 infection, I constructed a tobacco rattle virus (TRV) RNA2 genome-derived vector (TRV2-*P_{pea early browning virus}:gRNA^{PSTP13}-tRNA^{Atlleu}*) to facilitate the delivery of mobile guide RNA (gRNA) (Nagalakshmi et al., 2022). The gRNA was specifically designed to target the promoter region of STP13, located on chromosome 5 at positions 9312835-9312854.

The TRV was reconstituted in the XVE-dCas9-Tb system through the agroflooding technique, utilizing a combination of *Agrobacterium* cultures that contained the TRV RNA1 genome vector (pYL192) and the TRV2-*P_{pea early browning virus}:gRNA^{PSTP13}-tRNA^{Atlleu}*. The XVE-dCas9-Tb plants were subsequently inoculated with *Agrobacterium* to facilitate the biotinylation of proteins associated with the STP13 promoter (refer to Fig. 8). Biotinylated proteins were enriched from the leaves of both mock-inoculated and *Pst* DC3000-infected XVE-dCas9-Tb plants and the peptide samples were analyzed at the Molecular Proteomics Laboratory at Heinrich Heine University Düsseldorf. With the exception of the trypsin digestion step, all LC-MS sample preparation was performed at 4 °C to prevent TurboID-mediated protein biotinylation, as outlined by Branon et al. (2018).

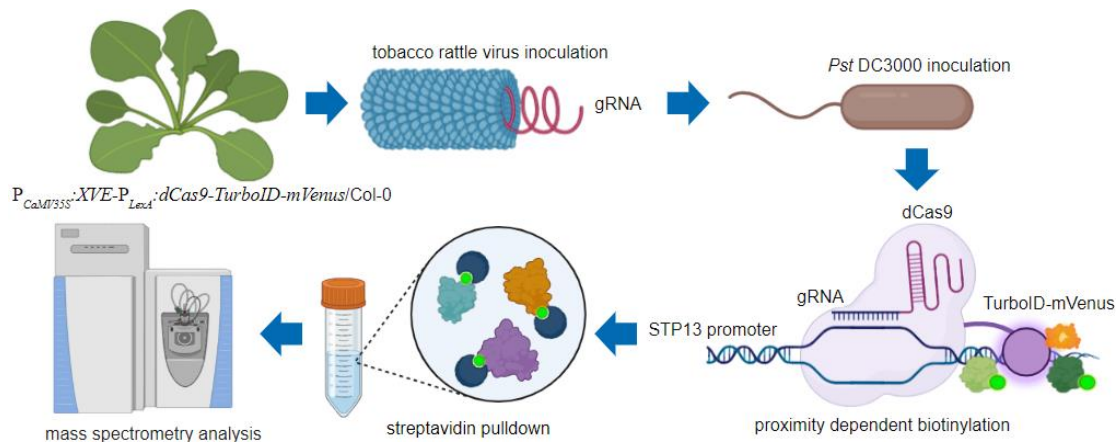


Fig. 8. Experimental workflow of CRISPR/dCas9-TurboID-based proximity labeling method for discovering proteins associated with the STP13 promoter upon *Pst* DC3000 challenge. Transgenic plants ($P_{CaMV35S}:XVE-P_{LexA}:dCas9-TurboID-mVenus$, designated as XVE-dCas9-Tb) were inoculated with *Agrobacterium tumefaciens* (*A. tumefaciens*) strains containing vectors derived from the tobacco rattle virus (TRV), specifically the pYL192 vector derived from the TRV RNA1 genome and the $P_{pea\ early\ browning\ virus}:gRNA^{PSTP13}-tRNA^{Atlleu}$ vector derived from the TRV RNA2 genome. Three weeks following the inoculation with *A. tumefaciens*, the XVE-dCas9-Tb plants were subsequently inoculated with *Pst* DC3000. The expression of dCas9-TurboID-mVenus was induced two days after the *Pst* DC3000 inoculation by applying a β -estradiol spray to the XVE-dCas9-Tb plants. The CRISPR/dCas9-TurboID-mVenus ribonucleoprotein complex binds to the guide RNA target site and facilitates biotinylation of proteins associated with the STP13 promoter. Total protein was extracted from the leaves three days post-inoculation with *Pst* DC3000. Biotinylated proteins were isolated using streptavidin-conjugated agarose beads, and following on-bead trypsin digestion, the resulting supernatants were analyzed via mass spectrometry. Created with BioRender.com.

The levels of biotinylated dCas9-TurboID-mVenus in samples infected with *Pst* DC3000 were comparable to those detected in mock (10 mM MgCl₂) samples (see Fig. 9a). This finding indicates that the cis-biotinylation functionality of dCas9-TurboID-mVenus was preserved in the samples subjected to infection with *Pst* DC3000. A total of 674 proteins were identified through LC-MS, with 217 of these proteins exhibiting significant enrichment in the mock samples (refer to Table A4). Although dCas9-TurboID-mVenus was observed to localize within the nucleus, as indicated by mVenus fluorescence, only approximately 16% of the identified proteins were predicted to be nuclear-localized (see Fig. 9b). The sole protein that showed enrichment in the *Pst* DC3000-infected samples was the biotin carboxyl carrier protein associated with acetyl-CoA carboxylase (*accB*, PSPTO_4860) from *Pst* DC3000, which may be attributed to its capacity for biotin binding (see Fig. 9c).

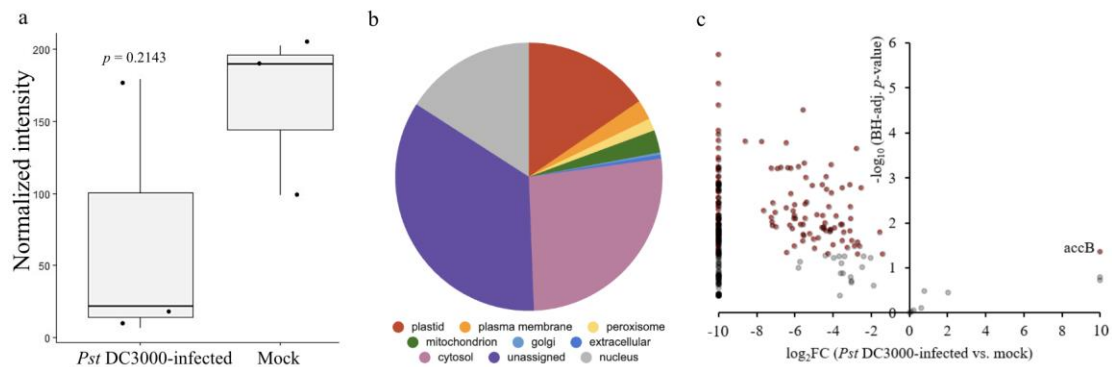


Fig. 9. Identification of proteins associated with the STP13 promoter upon *Pst* DC3000 challenge. (a) The protein levels of the biotinylated dCas9-TurboID-mVenus fusion protein in transgenic plants (*P_{CaMV35S}:XVE-P_{LexA}:dCas9-TurboID-mVenus*) were evaluated three days post-inoculation with either 10 mM MgCl₂ or inoculum of *Pst* DC3000 at a concentration of 10⁶ colony-forming units per milliliter. The boxplot illustrates the minimum (indicated by the lower end of the whisker), first quartile (lower edge), median (central line), third quartile (upper edge), and maximum (upper end of the whisker) of the normalized peptide intensity ratio (dCas9-TurboID-mVenus/Actin-8). Each data point corresponds to an individual biological replicate, with three biological replicates per treatment, each comprising three plants. (b) The relative distribution (%) of proteins identified through mass spectrometry analysis across nine distinct plant cellular compartments is presented. The multiple marker abundance profiling (MMAP) tool from the subcellular localization database for Arabidopsis proteins version 5 (SUBA5) was employed to predict the subcellular localization of the identified proteins. (c) A volcano plot depicting the proteins quantified in samples infected with *Pst* DC3000 (*n* = 3) in comparison to the mock samples (*n* = 3) treated with 10 mM MgCl₂ is provided. Each data point represents a protein that was identified, with proteins exhibiting a Benjamini-Hochberg (BH) adjusted *p*-value of less than 0.05 highlighted in red. This experiment was conducted once.

It is conceivable that the gRNA target site under investigation was not accessible to the dCas9-TurboID-mVenus during the infection by *Pst* DC3000, or that the biotinylated transcription factors and chromatin remodelers underwent degradation prior to the designated sampling time. By directing dCas9-TurboID-mVenus to alternative regions of the STP13 promoter or by collecting samples from *Pst* DC3000-infected leaves at various time intervals, it may be possible to identify the transcription factors and chromatin remodelers that are associated with the STP13 promoter in response to *Pst* DC3000 infection.

Hexose/proton symporters STP3 and STP4 are dispensable for Arabidopsis susceptibility to *B. cinerea* infection

Sugars function as virulence-inducing ligands and nutritional metabolites for the necrotrophic fungal pathogen *B. cinerea* (Doehlemann et al., 2005; Dulermo et al., 2009). *B. cinerea* causes cell death in leaf tissues and then feeds on the glucose that is released from these dying or dead cells (Veillet et al., 2016). The *stp13* mutant, which is deficient in the hexose/proton symporter, exhibits increased susceptibility to *B.*

cinerea, implying that the retrieval of hexoses mediated by STP13 enhances Arabidopsis resistance to this pathogen (Lemonnier et al., 2014). Alternatively, the influx of hexoses facilitated by STP13 may bolster antifungal immune responses (Yamada and Mine, 2024).

The genes *STP1*, *STP3*, *STP4*, and *STP13* exhibit increased mRNA levels in response to the invasion of *B. cinerea* (Lemonnier et al., 2014; Sham et al., 2014; Sham et al., 2017). It is plausible that these proteins accumulate within leaf cells, such as epidermal and mesophyll cells, in proximity to the fungal hyphae. To investigate the accumulation of STP1, STP3, STP4, and STP13 at the protein level in Arabidopsis leaves during *B. cinerea* infection, I constructed translational reporters utilizing eGFP-GUS for each gene: *STP1* ($P_{STP1}:STP1$ -P2A-eGFP-GUS), *STP3* ($P_{STP3}:STP3$ -P2A-eGFP-GUS), *STP4* ($P_{STP4}:STP4$ -P2A-eGFP-GUS), and *STP13* ($P_{STP13}:STP13$ -P2A-eGFP-GUS), all within the Col-0 genetic background. The inclusion of the P2A sequence facilitates the independent translation of STP and eGFP-GUS through ribosomal skipping, thereby enabling the documentation of all translation events. Confocal microscopy was then used to observe translation events at the cellular level.

Leaves from translational reporter Arabidopsis lines were subjected to drop-inoculation with *B. cinerea* B05.10 conidia on their adaxial surface. To visualize the GFP fluorescence resulting from eGFP-GUS accumulation in the vascular tissue, the inoculated leaves were imaged from the abaxial surface following the removal of the epidermal layer (Kim et al., 2021b). At 24 hours post-inoculation with *B. cinerea*, GFP fluorescence was observed in the adaxial epidermal cells, bundle sheath cells, xylem parenchyma cells, and spongy mesophyll cells of the $P_{STP1}:STP1$ -P2A-eGFP-GUS line 1 (Fig. 10a-d). In the $P_{STP3}:STP3$ -P2A-eGFP-GUS line 1, GFP fluorescence was detected in the adaxial epidermal cells and palisade mesophyll cells at 72 hours post-inoculation (Fig. 10e, f). At 72 hours post-inoculation, GFP fluorescence was observed in the adaxial epidermal cells, palisade mesophyll cells, and spongy mesophyll cells of the $P_{STP4}:STP4$ -P2A-eGFP-GUS line 1 (Fig. 10g, h). In the case of $P_{STP13}:STP13$ -P2A-eGFP-GUS line 2, GFP fluorescence was emitted from adaxial epidermal cells, palisade mesophyll cells, bundle sheath cells, xylem parenchyma cells, spongy mesophyll cells, and phloem cells at 24 hours post-inoculation with *B. cinerea* (Fig. 10i-l).

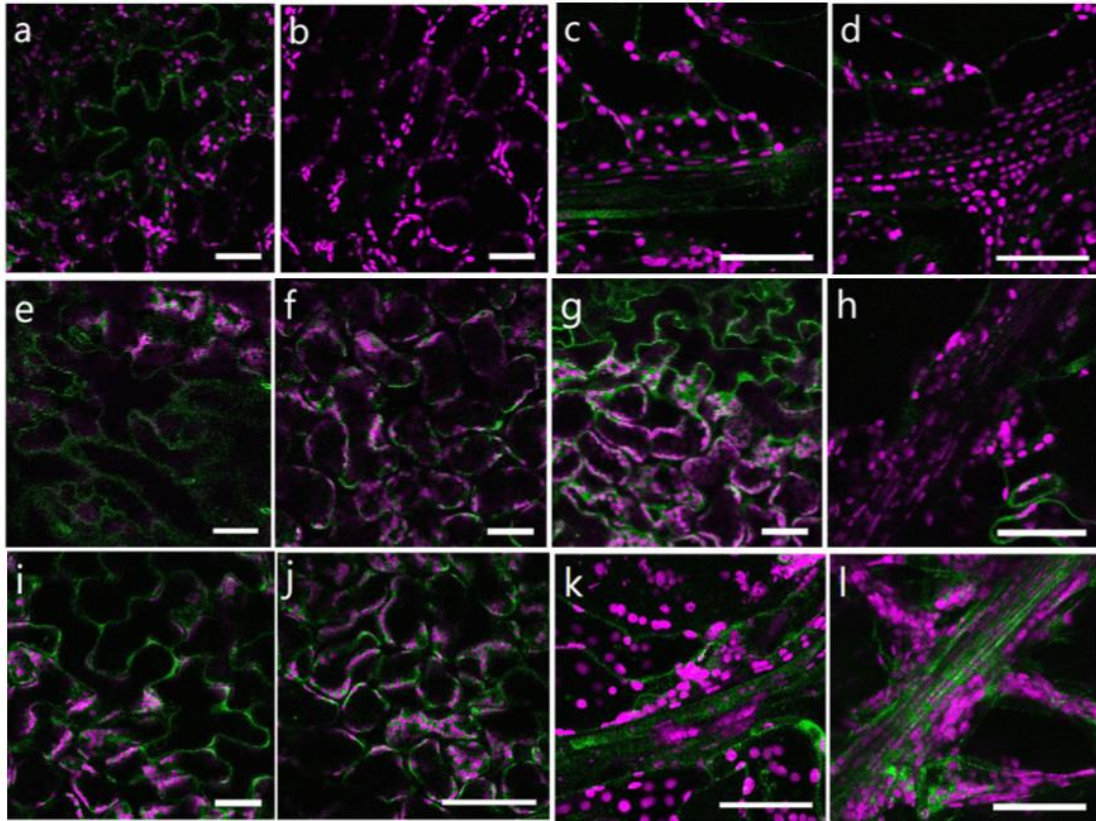


Fig. 10. Fluorescent reporter genes analysis of *B. cinerea*-infected $P_{STP1}:STP1$ -P2A-eGFP-GUS, $P_{STP3}:STP3$ -P2A-eGFP-GUS, $P_{STP4}:STP4$ -P2A-eGFP-GUS, and $P_{STP13}:STP13$ -P2A-eGFP-GUS plants. The plants underwent drop inoculation with a conidial suspension at a concentration of 2.5×10^5 conidia mL^{-1} , utilizing 2 μL for STP3 and STP4, and 4 μL for STP1 and STP13. Leaf regions adjacent to the lesion were examined using a confocal laser scanning microscope 24 hours (STP1 and STP13) or 72 hours (STP3 and STP4) post-inoculation. The fluorescence of green fluorescent protein (GFP) was observed in adaxial epidermal cells (a), bundle sheath cells (c), xylem parenchyma cells (c), and spongy mesophyll cells (c, d) in the $P_{STP1}:STP1$ -P2A-eGFP-GUS line 1, while it was absent in palisade mesophyll cells (b) and phloem cells (d). In the $P_{STP3}:STP3$ -P2A-eGFP-GUS line 1, GFP fluorescence was detected in adaxial epidermal cells (e) and palisade mesophyll cells (f). The GFP fluorescence was observed in adaxial epidermal cells (g), palisade mesophyll cells (g), and spongy mesophyll cells (h) in the $P_{STP4}:STP4$ -P2A-eGFP-GUS line 1, while it was absent in bundle sheath cells (h), xylem parenchyma cells (h), and phloem cells (h). In the $P_{STP13}:STP13$ -P2A-eGFP-GUS line 2, GFP fluorescence was detected in adaxial epidermal cells (i), palisade mesophyll cells (j), bundle sheath cells (k, l), xylem parenchyma cells (k), phloem cells (l), and spongy mesophyll cells (k, l). Chlorophyll autofluorescence is indicated in magenta. Scale bar: 50 μm . $n = 3$ biological replicates. These experiments were conducted once.

The findings from confocal imaging imply that STP1, STP3, and STP4 may play a role in enhancing Arabidopsis resistance to *B. cinerea*. Previous research has established that STP1 is not essential for Arabidopsis resistance to this pathogen (Veillet, 2016). To investigate the potential contributions of STP3 and STP4 to Arabidopsis resistance against *B. cinerea*, I created a double knockout mutant in the Col-0 genetic background, designated *stp3;4^{cr}*, utilizing CRISPR/Cas9-mediated mutagenesis (refer to Fig. A6). Subsequently, I performed three independent infection trials with *B. cinerea*. The sizes

of disease lesions were measured as a metric for assessing the susceptibility of Arabidopsis to *B. cinerea* infection two days following inoculation. The disease lesions observed in the *stp3;4^{cr}* were statistically comparable to those in the Col-0 in two of the trials, as indicated by an unpaired two-tailed Student's *t*-test ($p = 0.443, 0.24$) (see Fig. 11). However, in one trial, the disease lesions in the *stp3;4^{cr}* were significantly larger than those in the Col-0, with a p -value of 0.0004 according to the unpaired two-tailed Student's *t*-test. These findings indicate that the *stp3;4^{cr}* exhibits a susceptibility to *B. cinerea* infection that is similar to that of the Col-0.

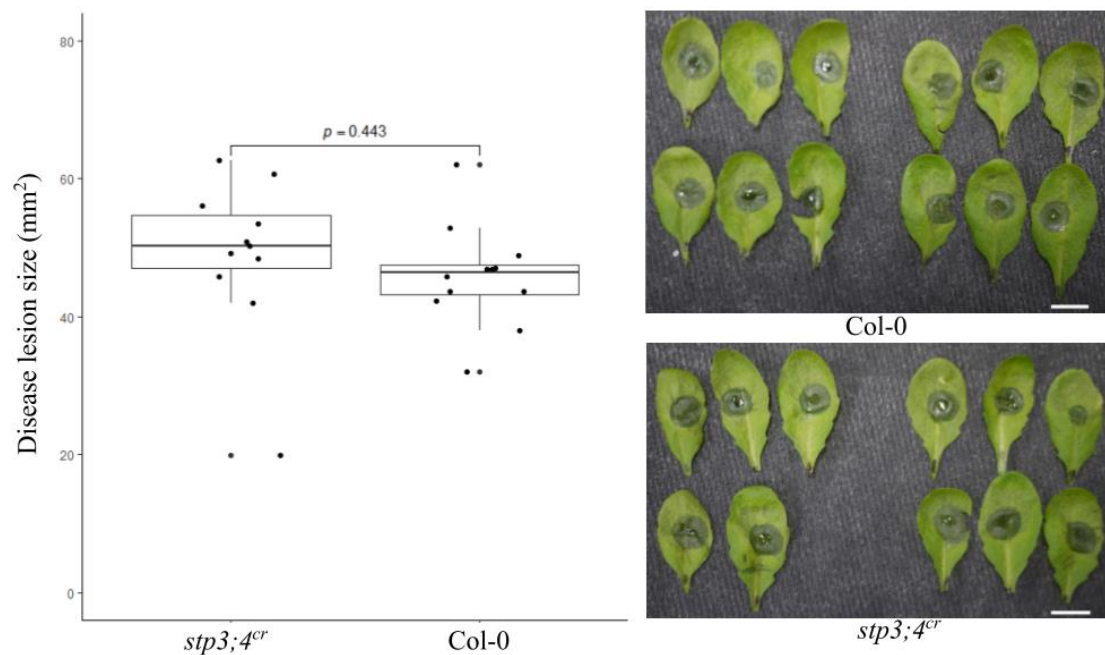


Fig. 11. The lesion area resulting from infection by the *B. cinerea* strain B05.10 was assessed in both the Col-0 genotype and the sugar transport protein 3 and 4 double knockout mutant (*stp3;4^{cr}*). The plants were inoculated via drop application of 7 μ L of a conidial suspension (2×10^5 conidia mL^{-1}), and lesion areas were quantified 48 hours post-inoculation. Panel (a) presents a boxplot illustrating the minimum (indicated by the lower end of the whisker), first quartile (lower edge), median (central line), third quartile (upper edge), and maximum (upper end of the whisker) lesion sizes for both Col-0 (12 biological replicates) and *stp3;4^{cr}* (11 biological replicates). Each dot represents an individual lesion resulting from the droplet inoculation. The statistical analysis was performed using unpaired two-tailed Student's *t*-test. Panel (b) displays images of the infected leaves from both genotypes at the 46-hour post-inoculation. Scale bars: 1 cm. This experiment was conducted once.

The predominant role of STP13 in the Arabidopsis resistance against *B. cinerea* may be ascribed to its specific accumulation within phloem cells (Fig. 10l). Increased activity of cell wall invertase has been observed in Arabidopsis leaves infected by *B. cinerea* (Veillet et al., 2016). It is conceivable that the hydrolysis of sucrose mediated by CWINV1 facilitates the influx of hexose through STP13 in the phloem. To investigate whether CWINV1 accumulates in phloem cells during the invasion of *B.*

cinerea, I constructed a translational reporter $P_{CWINV1}:CWINV1\text{-P2A-eGFP-GUS}$ and conducted confocal microscopy analysis. GFP fluorescence was identified in the adaxial epidermal cells, palisade mesophyll cells, and spongy mesophyll cells of $P_{CWINV1}:CWINV1\text{-P2A-eGFP-GUS}$ line 1 at 24 hours following *B. cinerea* inoculation (Fig. 12). Although CWINV1 was not detected in phloem cells during the challenge with *B. cinerea*, it remains plausible that the hydrosis process allows hexose produced by CWINV1 to be absorbed by STP13 localized in the phloem.

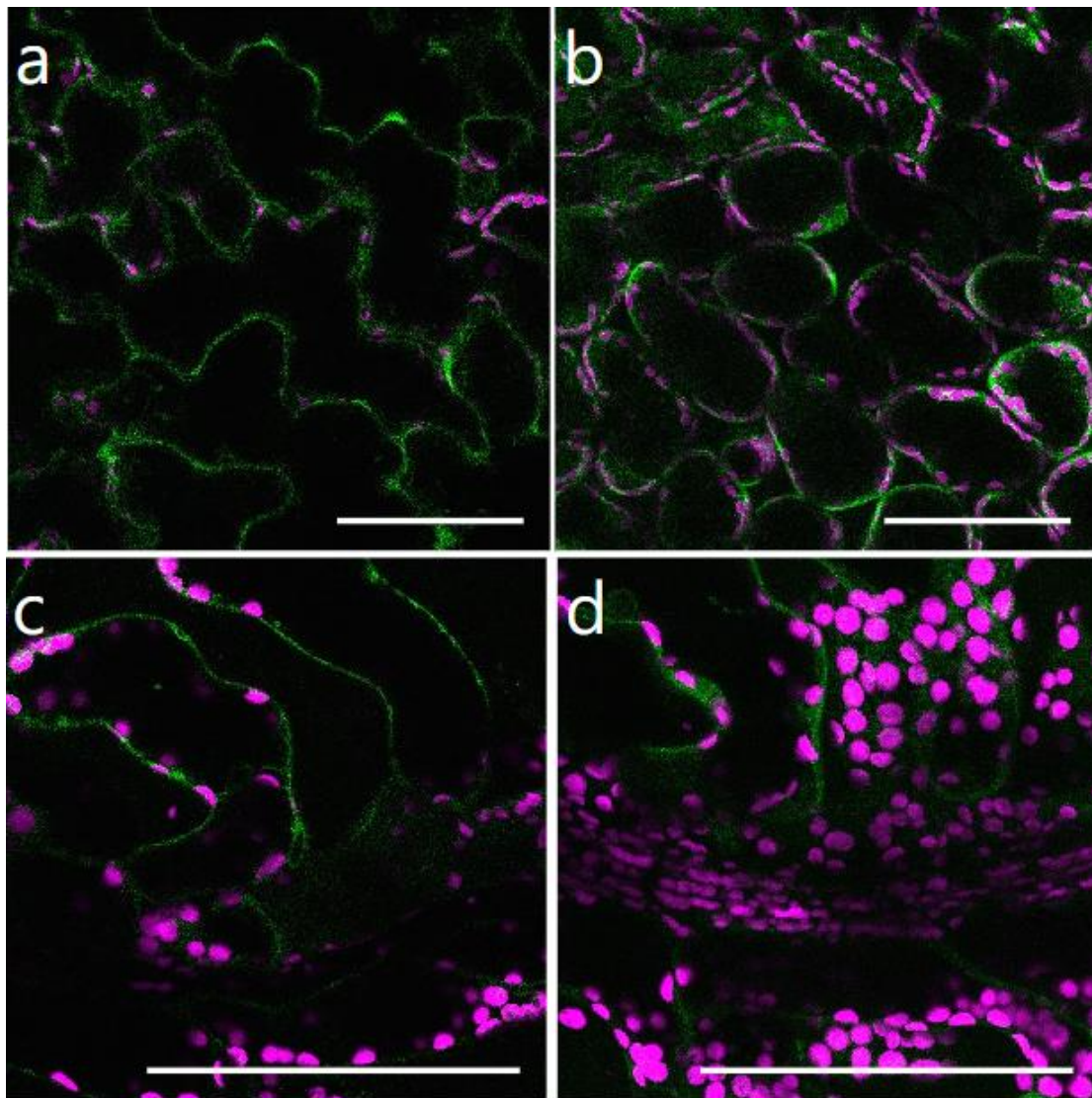


Fig. 12. Fluorescent reporter gene analysis of *B. cinerea*-infected $P_{CWINV1}:CWINV1\text{-P2A-eGFP-GUS}$ plants. The plants were subjected to drop inoculation using 4 μL of a conidial suspension at a concentration of 2.5×10^5 conidia mL^{-1} . Leaf regions adjacent to the lesion were examined using a confocal laser scanning microscope 24 hours post-inoculation. The fluorescence of green fluorescent protein (GFP) was observed in adaxial epidermal cells (a), palisade mesophyll cells (b), spongy mesophyll cells (c, d) in the $P_{CWINV1}:CWINV1\text{-P2A-eGFP-GUS}$ line 1, while it was absent in bundle sheath cells (c, d), xylem parenchyma cells (c), and phloem cells (d). Chlorophyll autofluorescence is indicated in magenta. Scale bar: 100 μm . $n = 3$ biological replicates. This experiment was conducted once.

SWEET4 has been identified as a contributor to Arabidopsis susceptibility to *B. cinerea* infection (Chong et al., 2014). To investigate the accumulation of SWEET4 at the protein level in leaves during *B. cinerea* infection, I inoculated the translational GUS reporter line $P_{SWEET4}:SWEET4$ -GUS line 6 with *B. cinerea* and conducted GUS histochemical analysis. The GUS activity associated with SWEET4-GUS was predominantly observed in the veins of leaves infected with *B. cinerea* two days post-inoculation (Fig. 13a). To further elucidate the specific leaf cell types that accumulate SWEET4 during the invasion of *B. cinerea*, I developed translational GFP reporters for SWEET4 ($P_{SWEET4}:SWEET4$ -GFP) in the Col-0 genetic background and performed confocal microscopy. Three days after *B. cinerea* inoculation, GFP fluorescence was detected in the companion cells of the $P_{SWEET4}:SWEET4$ -GFP line 1 (Fig. 13b). It is plausible that the hexose influx mediated by STP13 counteracts the hexose efflux facilitated by SWEET4 in the phloem. Collectively, these findings imply that the phloem serves as a major site for both *B. cinerea* feeding and sugar signaling.

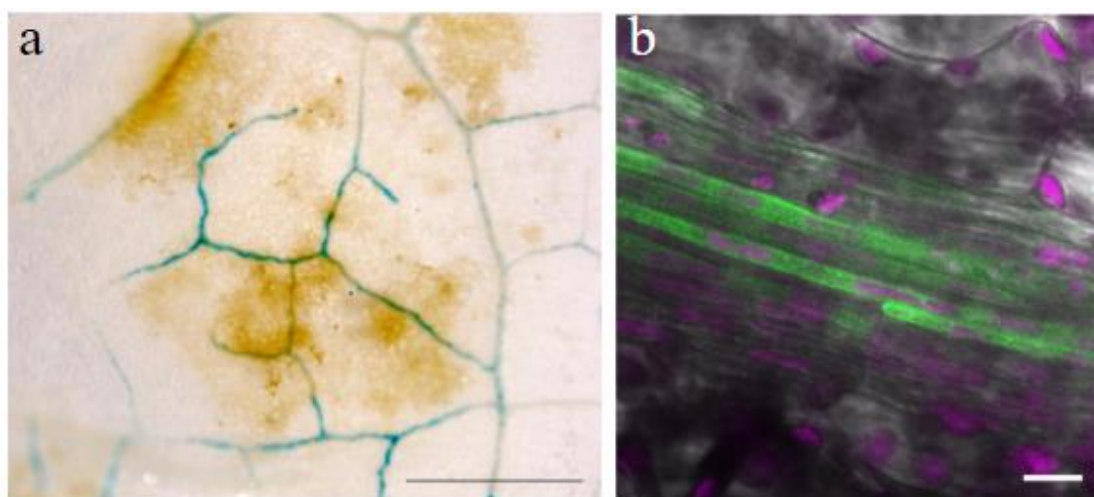


Fig. 13. Reporter gene analysis of *B. cinerea*-infected $P_{SWEET4}:SWEET4$ -GUS and $P_{SWEET4}:SWEET4$ -GFP plants. (a) Plants were subjected to drop inoculation with a 5 μ L suspension of conidia at a concentration of 5×10^5 conidia mL^{-1} . The β -glucuronidase (GUS)-stained $P_{SWEET4}:SWEET4$ -GUS reporter line 6 exhibited GUS activity localized within the leaf vasculature at 48 hours following inoculation. The scale bar represents 100 μ m. (b) In a separate experiment, plants were drop-inoculated with a 2 μ L suspension of conidia at a concentration of 2.5×10^5 conidia mL^{-1} . Leaf regions adjacent to the lesion were visualized using a confocal laser scanning microscope at 72 hours post-inoculation. The presence of green fluorescent protein (GFP) fluorescence, indicated in green, highlighted companion cells in the $P_{SWEET4}:SWEET4$ -GFP reporter line 1, while magenta coloration represented chlorophyll autofluorescence. The scale bar in this instance is 10 μ m. $n = 2$ biological replicates. These experiments were conducted once.

Vacuolar invertases VIN1 and VIN2 might contribute Arabidopsis resistance to *B. cinerea* infection

Vacuolar sucrose constitutes approximately 18% of the total cellular sucrose in the leaves of Arabidopsis (Vu et al., 2020). It is noteworthy that VIN1 and VIN2 show elevated mRNA levels and enhanced protein activity during the later stages of *B. cinerea* infection (Veillet et al., 2016). In order to examine the accumulation of VIN1 or VIN2 proteins in leaves during infection by *B. cinerea*, I developed translational reporters $P_{VIN1}:VIN1$ -P2A-eGFP-GUS and $P_{VIN2}:VIN2$ -P2A-eGFP-GUS, followed by confocal microscopy analysis. In the case of $P_{VIN1}:VIN1$ -P2A-eGFP-GUS line 5, GFP fluorescence was detected in adaxial epidermal cells, bundle sheath cells, and spongy mesophyll cells at 24 hours post-inoculation with *B. cinerea* (Fig. 14a-d). By 48 hours post-inoculation, GFP fluorescence was observed in adaxial epidermal cells, palisade mesophyll cells, bundle sheath cells, and spongy mesophyll cells in the $P_{VIN2}:VIN2$ -P2A-eGFP-GUS line 2 (Fig. 14e-h).

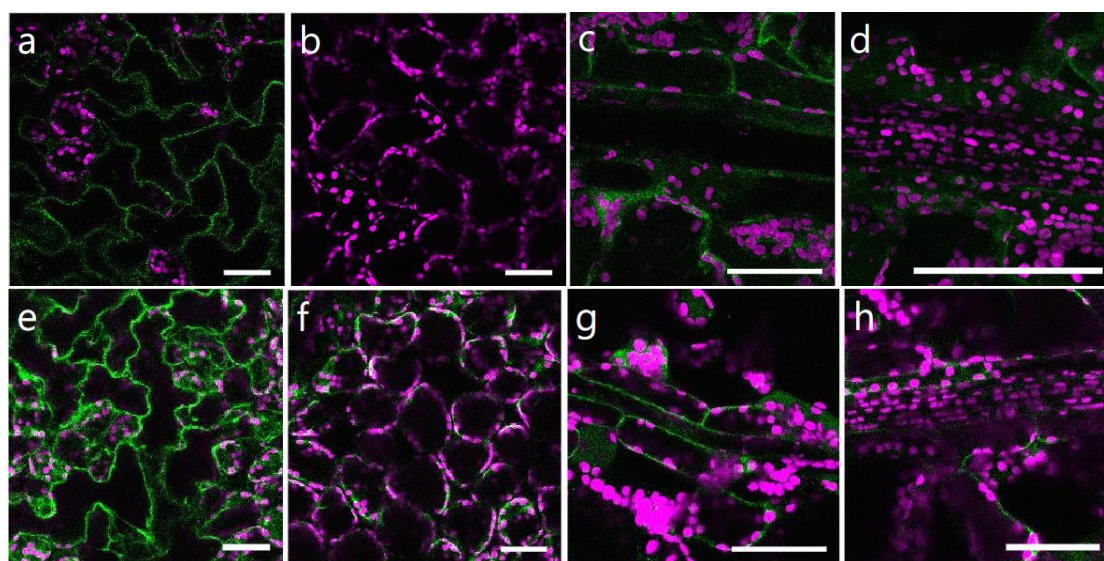


Fig. 14. Fluorescent reporter genes analysis of *B. cinerea*-infected $P_{VIN1}:VIN1$ -P2A-eGFP-GUS and $P_{VIN2}:VIN2$ -P2A-eGFP-GUS plants. The plants were subjected to drop inoculation using 4 μ L of a conidial suspension at a concentration of 2.5×10^5 conidia mL^{-1} . Leaf regions adjacent to the lesion were examined using a confocal laser scanning microscope 24 hours (VIN1) or 48 hours (VIN2) post-inoculation. The fluorescence of green fluorescent protein (GFP) was observed in adaxial epidermal cells (a), bundle sheath cells (c), xylem parenchyma cells (c), and spongy mesophyll cells (c, d) in the $P_{VIN1}:VIN1$ -P2A-eGFP-GUS line 5, while it was absent in palisade mesophyll cells (b) and phloem cells (d). In the $P_{VIN2}:VIN2$ -P2A-eGFP-GUS line 2, GFP fluorescence was detected in adaxial epidermal cells (e), palisade mesophyll cells (f), bundle sheath cells (g, h), and spongy mesophyll cells (g, h) but not in xylem parenchyma cells (g) and phloem cells (h). Chlorophyll autofluorescence is indicated in magenta. Scale bar: 50 μ m. $n = 3$ biological replicates. These experiments were conducted once.

To examine the role of vacuolar invertases in the susceptibility of Arabidopsis to *B. cinerea* infection, I developed the double knockout mutant *vin1;2^{cr}* in the Col-0 genetic background and performed eight independent infections with *B. cinerea* (see Fig. A7). The disease lesions observed in the *vin1;2^{cr}* were statistically comparable to those in the Col-0 in four of the trials (unpaired two-tailed Student's *t*-test, $p = 0.83, 0.47, 0.39, 0.07$). However, in three additional trials, the disease lesions in the *vin1;2^{cr}* were significantly larger than those in the Col-0 (unpaired two-tailed Student's *t*-test, $p = 0.048, 0.02, 0.000224$) (see Fig. 15). In one trial, the disease lesions in the *vin1;2^{cr}* were significantly smaller than those in the Col-0, with a *p*-value of 0.008 according to the unpaired two-tailed Student's *t*-test. These results show that the *vin1;2^{cr}* may exhibit increased susceptibility to *B. cinerea* infection compared to the Col-0 control.

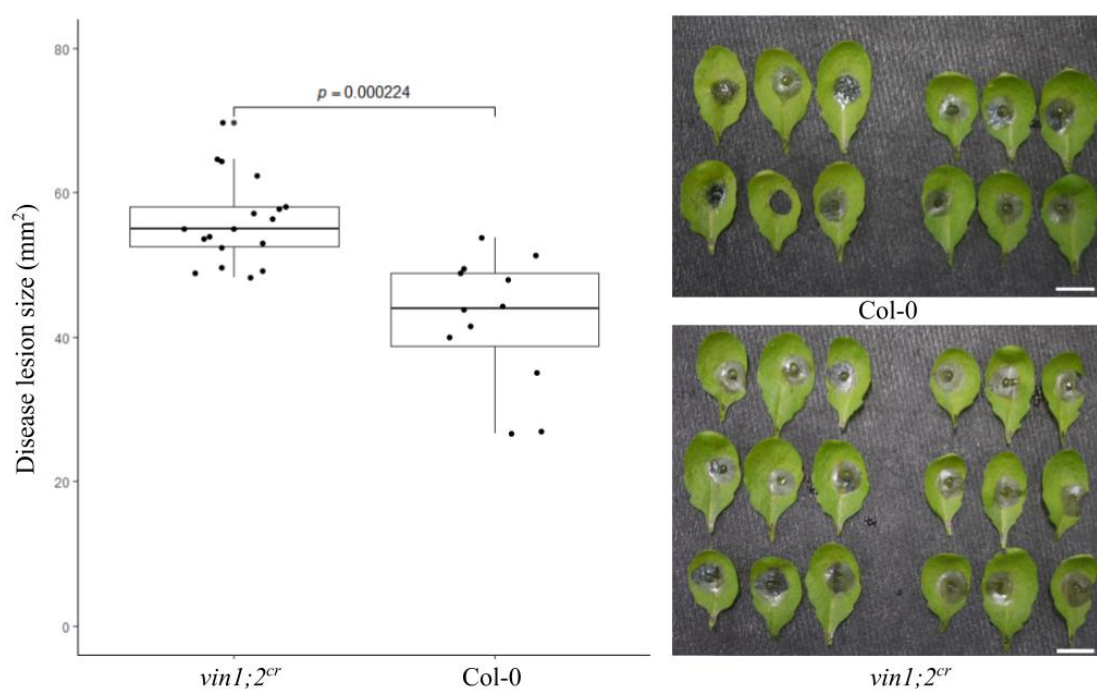


Fig. 15. The lesion area resulting from infection by the *B. cinerea* strain B05.10 was assessed in both the Col-0 genotype and the vacuolar invertase 1 and 2 double knockout mutant (*vin1;2^{cr}*). The plants were inoculated via drop application of 6 μL of a conidial suspension (10^5 conidia mL^{-1}), and lesion areas were quantified 46 hours post-inoculation. Panel (a) presents a boxplot illustrating the minimum (indicated by the lower end of the whisker), first quartile (lower edge), median (central line), third quartile (upper edge), and maximum (upper end of the whisker) lesion sizes for both Col-0 (12 biological replicates) and *vin1;2^{cr}* (19 biological replicates). Each dot represents an individual lesion resulting from the droplet inoculation. The statistical analysis was performed using unpaired two-tailed Student's *t*-test. Panel (b) displays images of the infected leaves from both genotypes at the 46-hour post-inoculation. Scale bars: 1 cm. This experiment was conducted once.

Cell wall/vacuolar inhibitor of fructosidase C/VIF1 and C/VIF2 are dispensable for Arabidopsis susceptibility to *B. cinerea* infection

The sucrose hydrolysis by acid invertases is subject to inhibition by C/VIF (Link et al., 2004). It has been suggested that CWINV1, VIN1, or VIN2 may be inhibited by C/VIF1 or C/VIF2 in Arabidopsis leaves during *B. cinerea* infection (Veillet et al., 2016). To investigate whether C/VIF1 and C/VIF2 are present in the same cell types as acid invertases, I constructed translational reporters $P_{C/VIF1}:C/VIF1$ -P2A-eGFP-GUS and $P_{C/VIF2}:C/VIF2$ -P2A-eGFP-GUS, followed by confocal microscopy analysis. The results indicated that GFP fluorescence was detected in phloem cells and spongy mesophyll cells of $P_{C/VIF1}:C/VIF1$ -P2A-eGFP-GUS line 4 72 hours after inoculation with *B. cinerea* (Fig. 16a, b). Similarly, in $P_{C/VIF2}:C/VIF2$ -P2A-eGFP-GUS line 5, GFP fluorescence was also observed in phloem cells and spongy mesophyll cells at the same time point post-inoculation (Fig. 16c, d).

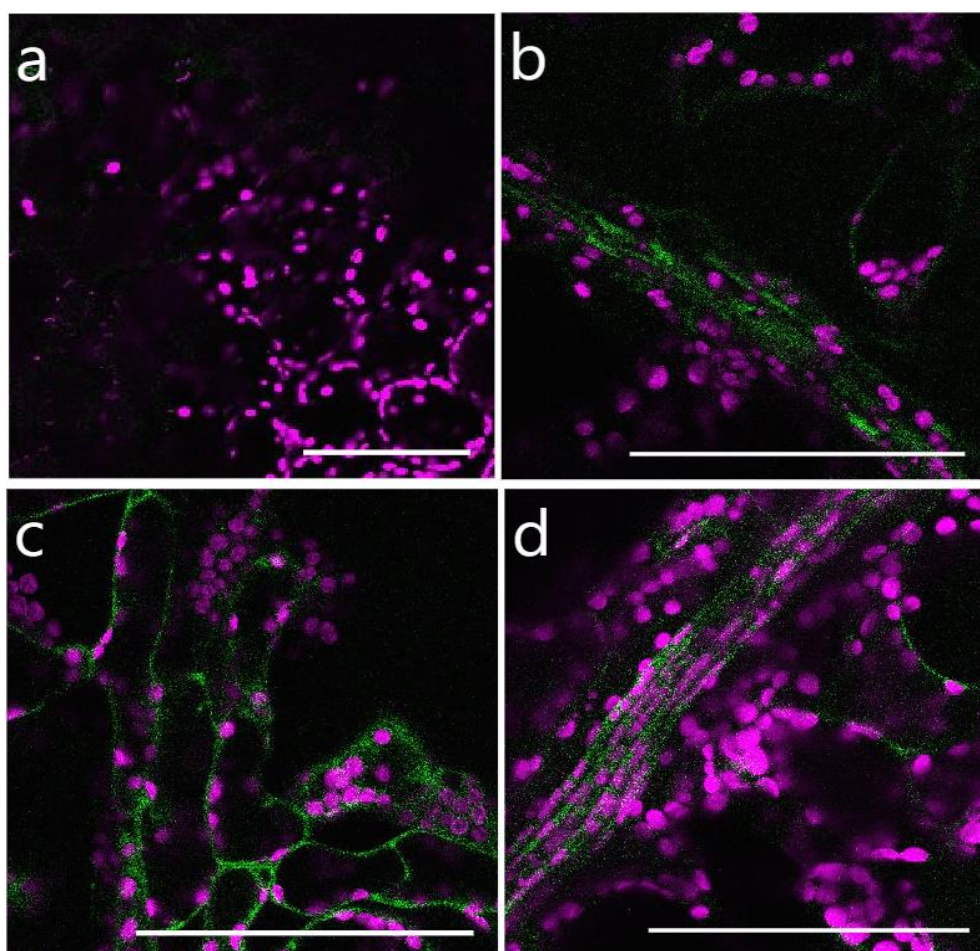


Fig. 16. Fluorescent reporter genes analysis of *B. cinerea*-infected $P_{C/VIF1}:C/VIF1$ -P2A-eGFP-GUS and $P_{C/VIF2}:C/VIF2$ -P2A-eGFP-GUS plants. The plants were subjected to drop inoculation using 2 μ L of a conidial suspension at a concentration of 2×10^5 conidia mL^{-1} . Leaf regions adjacent to the lesion were examined using a confocal laser scanning microscope 72

hours post-inoculation. The fluorescence of green fluorescent protein (GFP) was observed in phloem cells (b) and spongy mesophyll cells (b) in the $P_{C/VIF1}:C/VIF1$ -P2A-eGFP-GUS line 4, while it was absent in adaxial epidermal cells (a), palisade mesophyll cells (a), bundle sheath cells (b), and xylem parenchyma cells (b). In the $P_{C/VIF2}:C/VIF2$ -P2A-eGFP-GUS line 5, GFP fluorescence was detected in spongy mesophyll cells (c, d) or phloem cells (d) but not in xylem parenchyma cells (c) and bundle sheath cells (c, d). Chlorophyll autofluorescence is indicated in magenta. Scale bar: 100 μ m. $n = 3$ biological replicates. These experiments were conducted once.

It is plausible to hypothesize that C/VIF1 and C/VIF2 may play a role in the inhibition of acid invertase activities within spongy mesophyll cells, thereby affecting the susceptibility of Arabidopsis to infection by *B. cinerea*. To investigate the potential involvement of C/VIF1 and C/VIF2 in Arabidopsis susceptibility to *B. cinerea*, I created a double knockout mutant in the Col-0 genetic background, designated $c/vif1;2^{cr}$, and conducted three independent infection trials with *B. cinerea* (refer to Fig. A8). The disease lesions observed in the $c/vif1;2^{cr}$ were statistically comparable to those in the Col-0 in two of the trials, as indicated by an unpaired two-tailed Student's *t*-test ($p = 0.07, 0.053$) (see Fig. 17). However, in one trial, the disease lesions in the $c/vif1;2^{cr}$ were significantly larger than those in the Col-0, with a p -value of 0.0001 according to the unpaired two-tailed Student's *t*-test. These findings show that the $c/vif1;2^{cr}$ exhibits a susceptibility to *B. cinerea* infection that is similar to that of the Col-0.

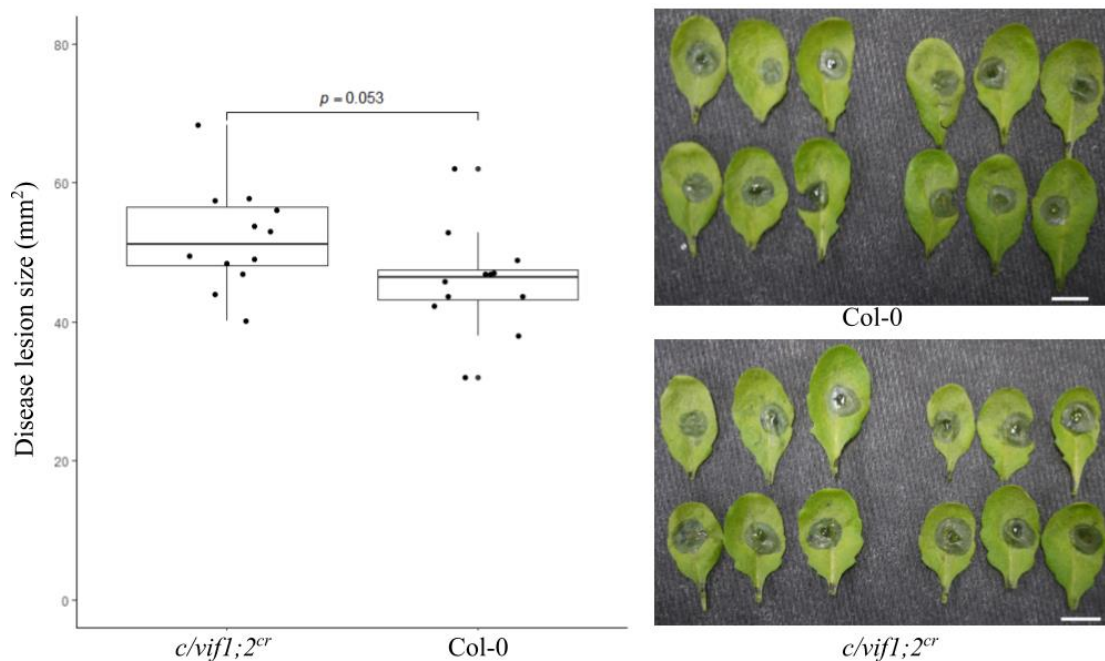


Fig. 17. The lesion area resulting from infection by the *B. cinerea* strain B05.10 was assessed in both the Col-0 genotype and the cell wall/vacuolar inhibitor of fructosidase 1 and 2 double knockout mutant ($c/vif1;2^{cr}$). The plants were inoculated via drop application of 7 μ L of a conidial suspension (2×10^5 conidia mL^{-1}), and lesion areas were quantified 48 hours post-inoculation. Panel (a) presents a boxplot illustrating the minimum (indicated by the

lower end of the whisker), first quartile (lower edge), median (central line), third quartile (upper edge), and maximum (upper end of the whisker) lesion sizes for both Col-0 (12 biological replicates) and *c/vif1;2^{cr}* (12 biological replicates). Each dot represents an individual lesion resulting from the droplet inoculation. The statistical analysis was performed using unpaired two-tailed Student's *t*-test. Panel (b) displays images of the infected leaves from both genotypes at the 48-hour post-inoculation. Scale bars: 1 cm. This experiment was conducted once.

Tonoplast-localized hexose uniporter SWEET2 and SWEET17 are dispensable for Arabidopsis susceptibility to *B. cinerea* infection

The hypersusceptible phenotype observed in *vin1;2^{cr}* implies that the levels of vacuolar hexose may play a significant role in determining Arabidopsis susceptibility to infection by *B. cinerea*. SWEET2 and SWEET17 may be involved in either the efflux of hexose from the vacuole or the sequestration of hexose within the vacuole, both of which could potentially affect the Arabidopsis susceptibility to *B. cinerea* infection. To investigate whether SWEET2 and SWEET17 accumulate at the margins of disease lesions, I conducted GUS histochemical analysis utilizing translational reporters $P_{SWEET2}:SWEET2$ -GUS and $P_{SWEET17}:SWEET17$ -GUS (Chen et al., 2015a; Guo et al., 2014). The GUS activity of both SWEET2-GUS and SWEET17-GUS was detected at the periphery of the disease lesions (Fig. 18).

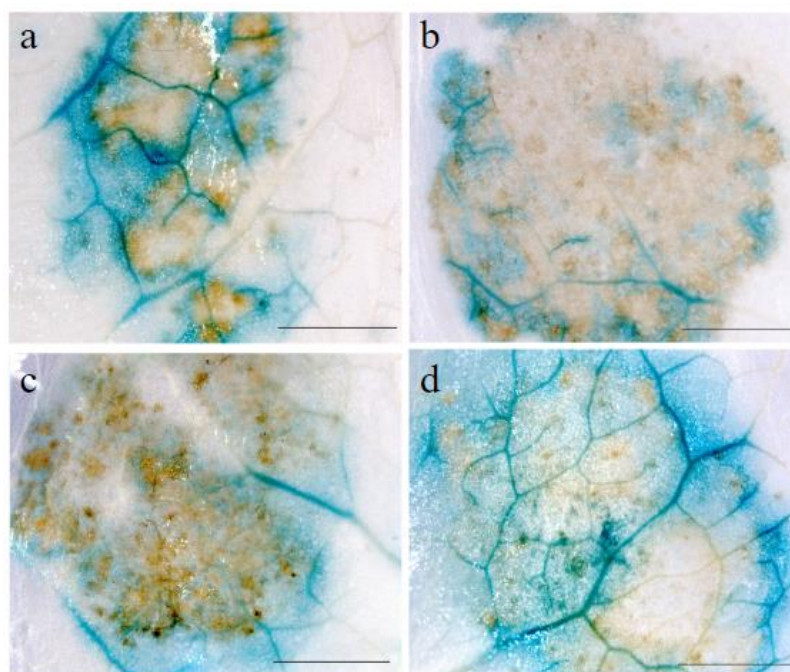


Fig. 18. Reporter genes analysis of $P_{SWEET2}:SWEET2$ -GUS and $P_{SWEET17}:SWEET17$ -GUS plants. Plants were inoculated via drop application with 5 μ L of a conidial suspension at a concentration of 5×10^5 conidia per mL. Light microscopy images were obtained to assess β -glucuronidase (GUS) activity in the $P_{SWEET2}:SWEET2$ -GUS reporter lines 2 (a) and 8 (b), as well as in the $P_{SWEET17}:SWEET17$ -GUS reporter lines 5 (c) and 9 (d). These images illustrate

GUS activity within disease lesions observed 48 hours following inoculation with *B. cinerea*. Scale bar: 100 μm . $n = 2$ biological replicates. These experiments were conducted once.

To investigate the potential involvement of SWEET2 and SWEET17 in the susceptibility of Arabidopsis to *B. cinerea* infection, I developed a double knockout mutant in the Col-0 genetic background, designated *sweet2;17^{cr}*, and conducted six independent infection trials with *B. cinerea* (refer to Fig. A9). The disease lesions observed in the *sweet2;17^{cr}* were statistically comparable to those in the Col-0 in five of the trials, as indicated by an unpaired two-tailed Student's *t*-test ($p = 0.852, 0.76, 0.7, 0.17, 0.07$) (see Fig. 19). However, in one trial, the disease lesions in the *sweet2;17^{cr}* were significantly larger than those in the Col-0, with a p -value of 0.01 according to the unpaired two-tailed Student's *t*-test. These findings show that the *sweet2;17^{cr}* exhibits a susceptibility to *B. cinerea* infection that is similar to that of the Col-0.

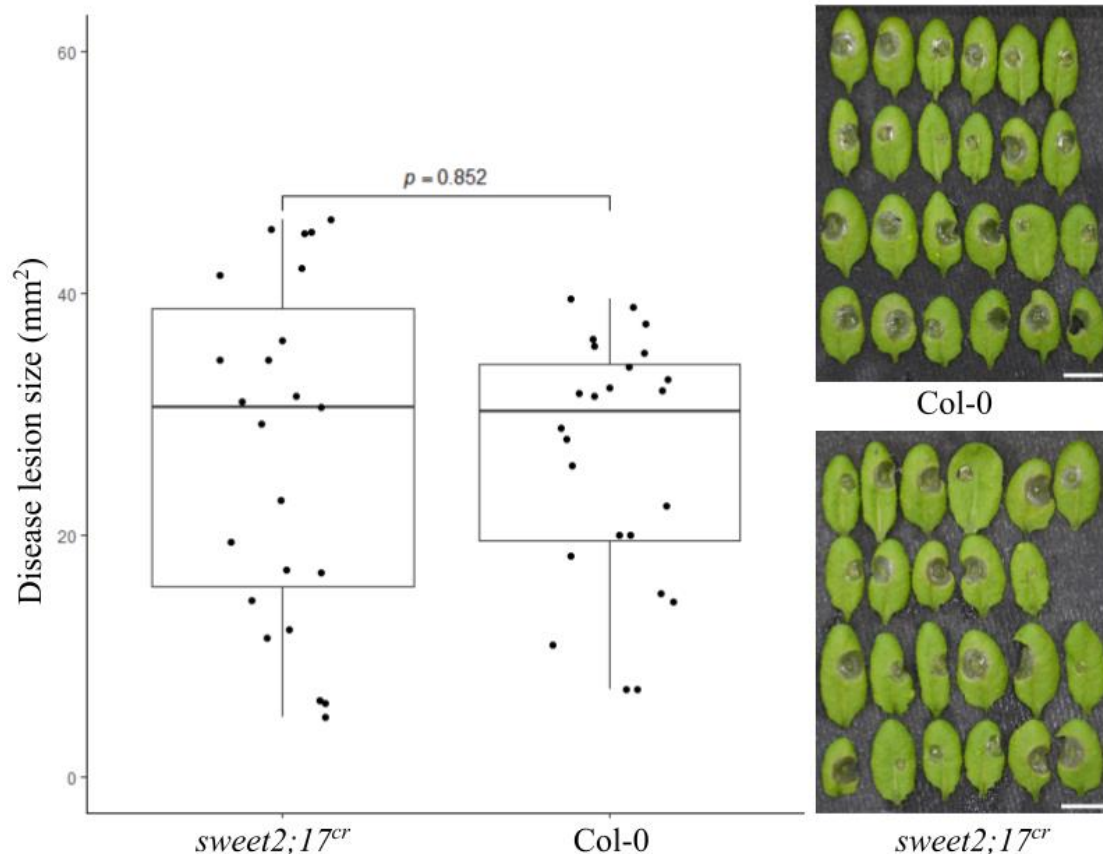


Fig. 19. The lesion area resulting from infection by the *B. cinerea* strain B05.10 was assessed in both the Col-0 genotype and the tonoplast-localized hexose uniporters SWEET2 and 17 double knockout mutant (*sweet2;17^{cr}*). The plants were inoculated via drop application of 4 μL of a conidial suspension (2×10^5 conidia mL^{-1}), and lesion areas were quantified 72 hours post-inoculation. Panel (a) presents a boxplot illustrating the minimum (indicated by the lower end of the whisker), first quartile (lower edge), median (central line), third quartile (upper edge), and maximum (upper end of the whisker) lesion sizes for both Col-0 (24 biological replicates) and *sweet2;17^{cr}* (23 biological replicates). Each dot represents an individual lesion resulting from the droplet inoculation. The statistical analysis was performed

using unpaired two-tailed Student's *t*-test. Panel (b) displays images of the infected leaves from both genotypes at the 72-hour post-inoculation. Scale bars: 1 cm. This experiment was conducted once.

Cytosolic invertase 1 contributes Arabidopsis susceptibility to *B. cinerea* infection

In the leaves of Arabidopsis, the cytosol serves as the predominant reservoir for cellular sucrose, accounting for approximately 53% of the total (Vu et al., 2020). Similar to vacuolar invertases, the activity of cytosolic invertases is observed to increase during the later stages of *B. cinerea* invasion (Veillet et al., 2016). To elucidate the spatial distribution of cytosolic invertases in leaves infected by *B. cinerea*, I developed translational reporters $P_{CINV1}:CINV1$ -P2A-eGFP-GUS and $P_{CINV2}:CINV2$ -P2A-eGFP-GUS, followed by confocal microscopy analysis. In the case of $P_{CINV1}:CINV1$ -P2A-eGFP-GUS line 2, GFP fluorescence was detected in adaxial epidermal cells, palisade mesophyll cells, bundle sheath cells, phloem cells, and spongy mesophyll cells at 48 hours post-inoculation with *B. cinerea* (Fig. 20a-d). At 24 hours post-inoculation, GFP fluorescence was observed in adaxial epidermal cells and xylem parenchyma cells of the $P_{CINV2}:CINV2$ -P2A-eGFP-GUS line 10 (Fig. 20e-h).

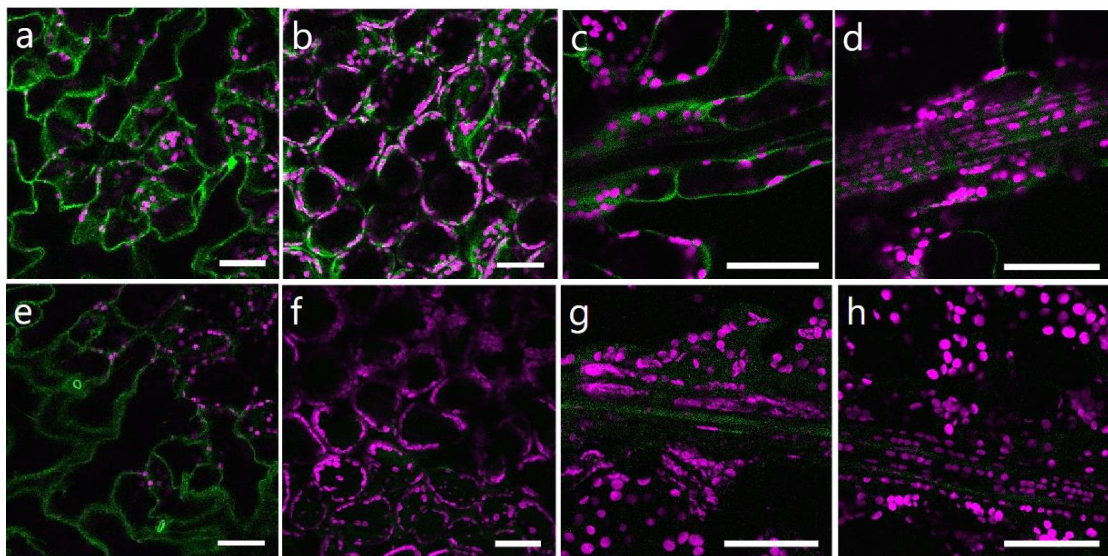


Fig. 20. Fluorescent reporter genes analysis of *B. cinerea*-infected $P_{CINV1}:CINV1$ -P2A-eGFP-GUS and $P_{CINV2}:CINV2$ -P2A-eGFP-GUS plants. The plants were subjected to drop inoculation using 2 μ L of a conidial suspension at a concentration of 2×10^5 conidia mL^{-1} . Leaf regions adjacent to the lesion were examined using a confocal laser scanning microscope 48 hours post-inoculation. The fluorescence of green fluorescent protein (GFP) was observed in adaxial epidermal cells (a), palisade mesophyll cells (b), bundle sheath cells (c, d), phloem cells (d), and spongy mesophyll cells (c, d) in the $P_{CINV1}:CINV1$ -P2A-eGFP-GUS line 2, while it was absent in xylem parenchyma cells (c). In the $P_{CINV2}:CINV2$ -P2A-eGFP-GUS line 10, GFP fluorescence was detected in adaxial epidermal cells (e) and xylem parenchyma cells (g) but not in palisade mesophyll cells (f), bundle sheath cells (g, h), phloem cells (h), and spongy mesophyll cells (g, h). Chlorophyll autofluorescence is indicated in magenta. Scale bar: 50 μ m.

$n = 3$ biological replicates. These experiments were conducted once.

Due to the significantly diminished growth rates observed in the double mutant *cinvl*;2, the single mutant *cinvl* was chosen for the purpose of conducting nine independent infection trials with *B. cinerea* (Barratt et al., 2009). The disease lesions observed in the *cinvl* were statistically comparable to those in the Col-0 in two of the trials (unpaired two-tailed Student's *t*-test, $p = 0.46, 0.28$). However, in seven additional trials, the disease lesions in the *cinvl* were significantly smaller than those in the Col-0 (unpaired two-tailed Student's *t*-test, $p = 0.005, 0.003, 0.001, 0.0003, 0.0001, 6.4E-05, 3.6E-06$) (see Fig. 21). These results show that the *cinvl* exhibits a reduced susceptibility to *B. cinerea* infection.

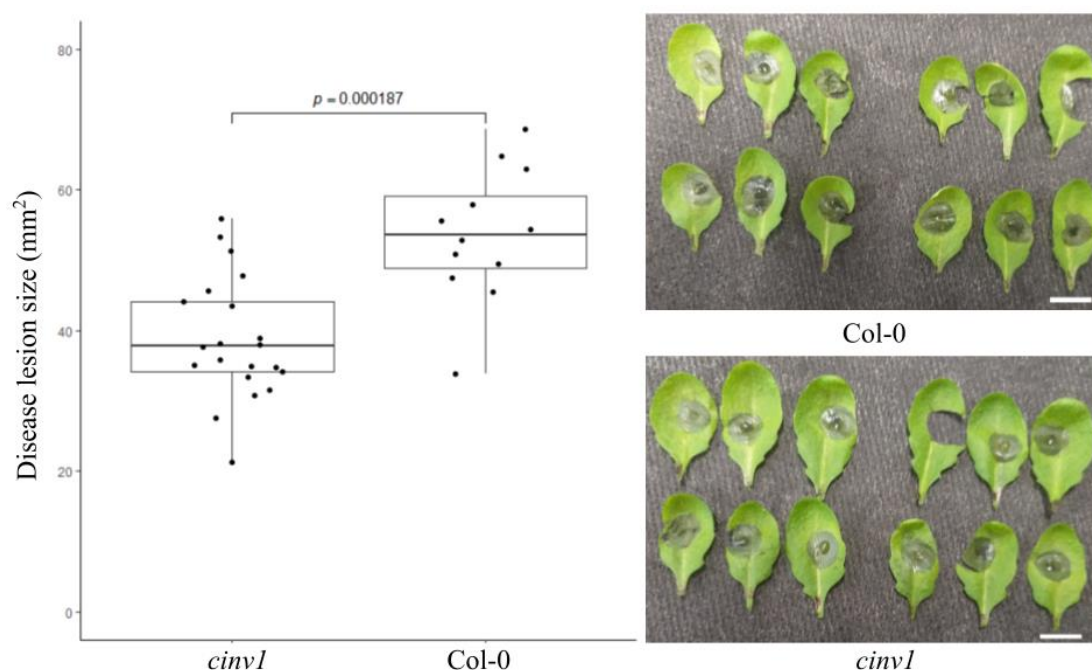


Fig. 21. The lesion area resulting from infection by the *B. cinerea* strain B05.10 was assessed in both the Col-0 genotype and the cytosolic invertase 1 knockout mutant (*cinvl*). The plants were inoculated via drop application of 6 μL of a conidial suspension (1.5×10^5 conidia mL^{-1}), and lesion areas were quantified 47 hours post-inoculation. Panel (a) presents a boxplot illustrating the minimum (indicated by the lower end of the whisker), first quartile (lower edge), median (central line), third quartile (upper edge), and maximum (upper end of the whisker) lesion sizes for both Col-0 (12 biological replicates) and *cinvl* (12 biological replicates). Each dot represents an individual lesion resulting from the droplet inoculation. The statistical analysis was performed using unpaired two-tailed Student's *t*-test. Panel (b) displays images of the infected leaves from both genotypes at the 47-hour post-inoculation. Scale bars: 1 cm. This experiment was conducted once.

Plasma membrane-localized sucrose uniporters SWEET11, SWEET12 and SWEET13 contribute Arabidopsis susceptibility to *B. cinerea* infection

In Arabidopsis leaves infected by *B. cinerea*, sucrose present in the apoplasm may be

hydrolyzed by cell wall invertases or potential fungal invertases, thereby contributing to antifungal defense mechanisms and facilitating the feeding of *B. cinerea* (Veillet et al., 2016). In addition to being released from necrotic leaf cells, sucrose may also be exported from viable leaf cells via the plasma membrane-localized sucrose uniporter. At the mRNA level, SWEET11, SWEET12, and SWEET13 represent the most prevalent plasma membrane-localized sucrose uniporters in leaves during the course of *B. cinerea* infection (Veillet, 2016).

To examine the accumulation of SWEET12 in Arabidopsis leaves during infection by *B. cinerea*, I conducted a histochemical analysis utilizing the translational reporter $P_{SWEET12}:SWEET12$ -GUS line 14 (Chen et al., 2012). The GUS activity associated with SWEET12-GUS was predominantly observed in the vascular tissue surrounding the disease lesion (Fig. 22a). Additionally, confocal imaging employing the translational reporter $P_{SWEET12}:SWEET12$ -GFP line 3 further demonstrated the presence of SWEET12-GFP in phloem parenchyma cells (Fig. 22b) (Chen et al., 2012).

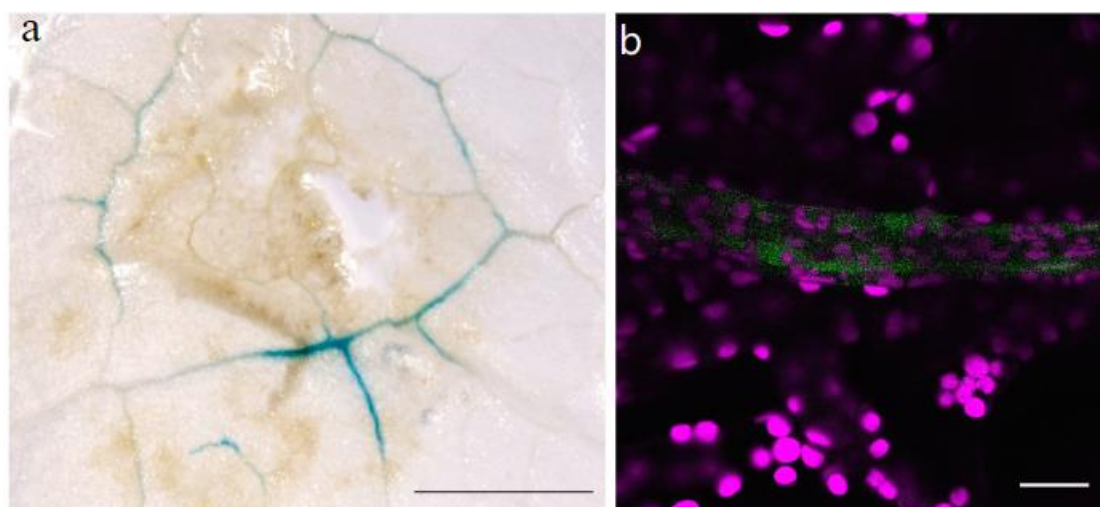


Fig. 22. Reporter gene analysis of *B. cinerea*-infected $P_{SWEET12}:SWEET12$ -GUS and $P_{SWEET12}:SWEET12$ -GFP plants. (a) The plants were subjected to drop-inoculation with 5 μ L of a conidial suspension at a concentration of 5×10^5 conidia mL^{-1} . The β -glucuronidase (GUS)-stained $P_{SWEET12}:SWEET12$ -GUS reporter line 14 exhibited GUS activity within the leaf vasculature 48 hours following inoculation with *B. cinerea*. Scale bar: 100 μ m. $n = 2$ biological replicates. (b) In a separate experiment, plants were drop-inoculated with 2 μ L of a conidial suspension at a concentration of 2.5×10^5 conidia mL^{-1} . The leaf regions surrounding the lesion were imaged using a confocal laser scanning microscope 48 hours post-inoculation with *B. cinerea*. The green fluorescent protein (GFP) fluorescence, indicated in green, highlighted the phloem parenchyma cells in $P_{SWEET12}:SWEET12$ -GFP reporter line 3, while magenta represents chlorophyll autofluorescence. Scale bar: 10 μ m. $n = 2$ biological replicates. These experiments were conducted once.

To assess the involvement of SWEET11, SWEET12, and SWEET13 in the

susceptibility of Arabidopsis to *B. cinerea* infection, I performed five independent infection trials using the Col-0 and the T-DNA triple mutant *sweet11;12;13*. The disease lesions observed in the *sweet11;12;13* were statistically smaller to those in the Col-0 in four of the trials (unpaired two-tailed Student's *t*-test, $p = 0.006, 0.002, 5.24\text{E-}06, 1.25\text{E-}19$) (see Fig. 23). However, in one of the trials, the disease lesions in the *sweet11;12;13* were comparable to those in the Col-0 (unpaired two-tailed Student's *t*-test, $p = 0.25$). These results show that the *sweet11;12;13* exhibits a reduced susceptibility to *B. cinerea* infection.

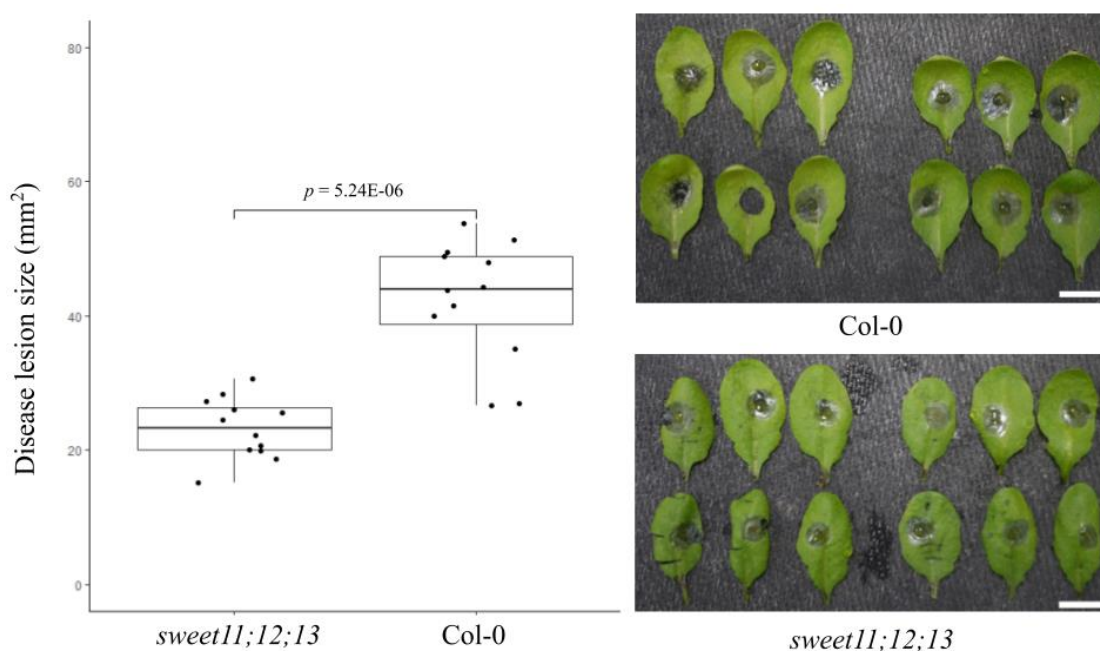


Fig. 23. The lesion area resulting from infection by the *B. cinerea* strain B05.10 was assessed in both the Col-0 genotype and the plasma membrane-localized sucrose uniporters SWEET11, SWEET12, and SWEET13 triple mutant (*sweet11;12;13*). The plants were inoculated via drop application of 6 μL of a conidial suspension (10^5 conidia mL^{-1}), and lesion areas were quantified 46 hours post-inoculation. Panel (a) presents a boxplot illustrating the minimum (indicated by the lower end of the whisker), first quartile (lower edge), median (central line), third quartile (upper edge), and maximum (upper end of the whisker) lesion sizes for both Col-0 (12 biological replicates) and *sweet11;12;13* (12 biological replicates). Each dot represents an individual lesion resulting from the droplet inoculation. The statistical analysis was performed using unpaired two-tailed Student's *t*-test. Panel (b) displays images of the infected leaves from both genotypes at the 46-hour post-inoculation. Scale bars: 1 cm. This experiment was conducted once.

Sucrose/proton symporters SUC1 and SUC3 are dispensable for Arabidopsis susceptibility to *B. cinerea* infection

The resistant phenotype exhibited by *sweet11;12;13* in response to *B. cinerea* implies that the retrieval of sucrose plays a significant role in enhancing Arabidopsis resistance against this pathogen. SUC1 and SUC3 may be involved in this sucrose retrieval

process, as evidenced by the increased mRNA levels of these transporters in *Arabidopsis* leaves infected with *B. cinerea* (Veillet et al., 2016). To further explore the accumulation of SUC1 and SUC3 in *Arabidopsis* leaves during infection by *B. cinerea*, I constructed $P_{SUC1}:SUC1$ -P2A-eGFP-GUS and $P_{SUC3}:SUC3$ -P2A-eGFP-GUS reporter lines and conducted confocal microscopy analyses. At 24 hours following inoculation with *B. cinerea*, GFP fluorescence was detected in both the adaxial epidermal cells and xylem parenchyma cells of the $P_{SUC3}:SUC3$ -P2A-eGFP-GUS line 2, while GFP fluorescence was exclusively observed in the xylem parenchyma cells of the $P_{SUC1}:SUC1$ -P2A-eGFP-GUS line 1 (Fig. 24).

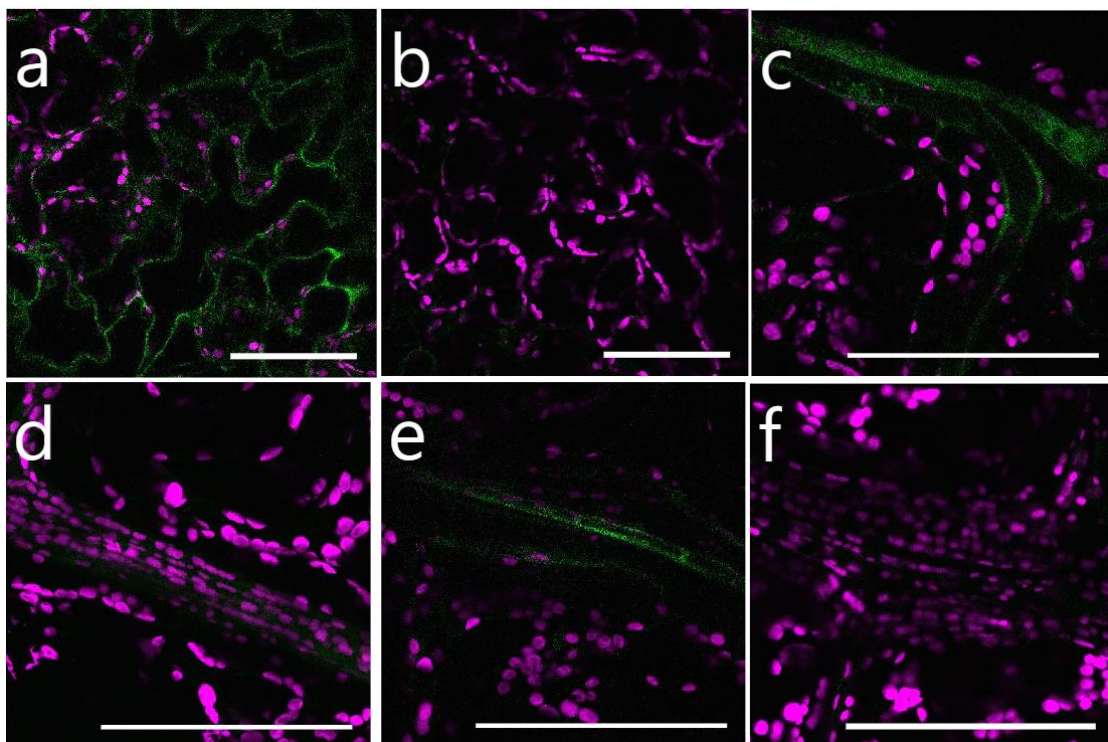


Fig. 24. Fluorescent reporter genes analysis of *B. cinerea*-infected $P_{SUC3}:SUC3$ -P2A-eGFP-GUS and $P_{SUC1}:SUC1$ -P2A-eGFP-GUS plants. The plants were subjected to drop inoculation using 4 μL of a conidial suspension at a concentration of 2.5×10^5 conidia mL^{-1} . Leaf regions adjacent to the lesion were examined using a confocal laser scanning microscope 24 hours post-inoculation. The fluorescence of green fluorescent protein (GFP) was observed in adaxial epidermal cells (a) and xylem parenchyma cells (c) in the $P_{SUC3}:SUC3$ -P2A-eGFP-GUS line 2, while it was absent in palisade mesophyll cells (b), bundle sheath cells (c, d), spongy mesophyll cells (c, d), and phloem cells (d). In the $P_{SUC1}:SUC1$ -P2A-eGFP-GUS line 1, GFP fluorescence was detected in xylem parenchyma cells (e) but not in bundle sheath cells (e, f), spongy mesophyll cells (e, f), and phloem cells (f) at the 24-hour following *B. cinerea* inoculation. Chlorophyll autofluorescence is indicated in magenta. Scale bar: 100 μm . $n = 3$ biological replicates. These experiments were conducted once.

To elucidate the roles of SUC1 and SUC3 in the susceptibility of *Arabidopsis* to *B. cinerea* infection, I developed a double knockout mutant in the Col-0 genetic

background, designated *suc1;3^{cr}*, and conducted eight independent infection trials with *B. cinerea* (see Fig. A10). The disease lesions identified in the *suc1;3^{cr}* genotype were statistically similar to those observed in the Col-0 across six of the trials conducted (unpaired two-tailed Student's *t*-test, $p = 0.85, 0.61, 0.5, 0.182, 0.14, \text{ or } 0.11$) (see Fig. 25). However, in one trial, the lesions in the *suc1;3^{cr}* were significantly larger than those in the Col-0 (unpaired two-tailed Student's *t*-test, $p = 0.02$), while in another trial, the lesions in the *suc1;3^{cr}* were significantly smaller than those in the Col-0 (unpaired two-tailed Student's *t*-test, $p = 0.006$). These findings show that the *suc1;3^{cr}* exhibits a susceptibility to *B. cinerea* infection that is similar to that of the Col-0.

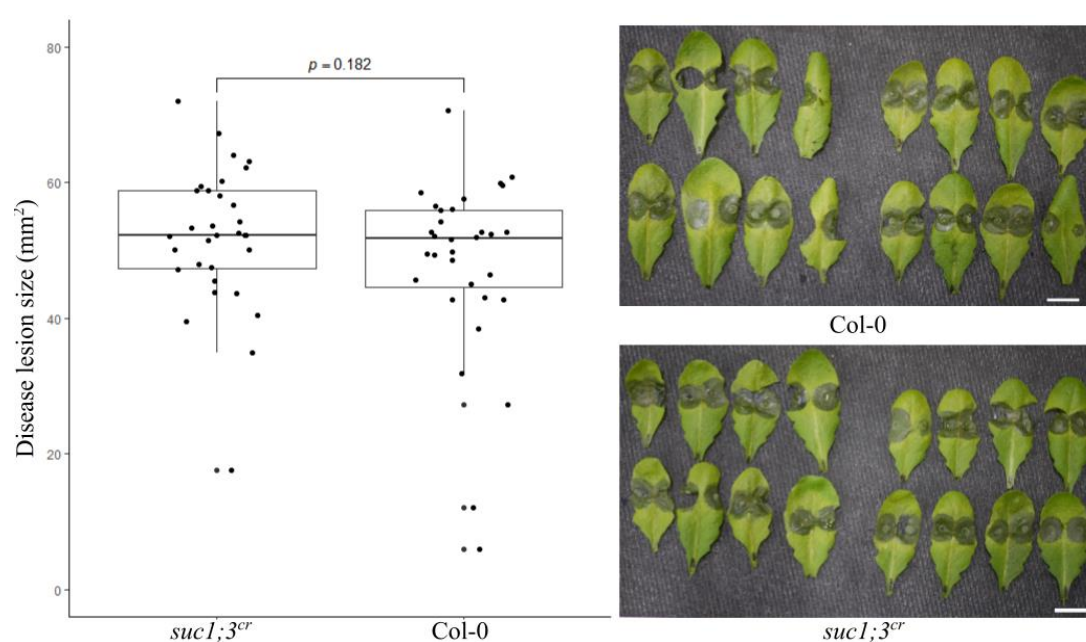


Fig. 25. The lesion area resulting from infection by the *B. cinerea* strain B05.10 was assessed in both the Col-0 genotype and the sucrose transporter 1 and 3 double mutant (*suc1;3^{cr}*). The plants were inoculated via drop application of 5 μL of a conidial suspension (2×10^5 conidia mL^{-1}), and lesion areas were quantified 53 hours post-inoculation. Panel (a) presents a boxplot illustrating the minimum (indicated by the lower end of the whisker), first quartile (lower edge), median (central line), third quartile (upper edge), and maximum (upper end of the whisker) lesion sizes for both Col-0 (32 biological replicates) and *suc1;3^{cr}* (32 biological replicates). Each dot represents an individual lesion resulting from the droplet inoculation. The statistical analysis was performed using unpaired two-tailed Student's *t*-test. Panel (b) displays images of the infected leaves from both genotypes at the 53-hour post-inoculation. Scale bars: 1 cm. This experiment was conducted once.

Discussion

Sugars influence the susceptibility of Arabidopsis to infection by *Pst* DC3000

Sucrose and glucose function as virulence-inducing ligands and nutritional metabolites for *Pst* DC3000 (McCraw et al., 2016; Stauber et al., 2012; Turner et al., 2020). The mRNA levels of levansucrase (Lsc-1), ScrY, ScrB, and the maltose-maltodextrin importer are significantly elevated during the colonization of the Arabidopsis leaf apoplast compared to growth on KB plates (Nobori et al., 2018). This observation indicates that *Pst* DC3000 activates its sucrose utilization system in response to plant infection (Kilic et al., 2007). Additionally, it has been demonstrated that the mRNA levels of Lsc-1 and ScrB are adversely influenced by pattern-triggered immunity (Nobori et al., 2018; Wang et al., 2022a). Nevertheless, the mechanisms by which *Pst* DC3000 detects, absorbs, and metabolizes sucrose during colonization of plant tissues, as well as the potential sites of release for plant-derived sugars, remain inadequately understood.

The proliferation of *Pst* DC3000 is notably slower in HDM_{Suc} when the *ScrY* gene is disrupted. This observation implies that the remaining sucrose transporters localized in the outer membrane are insufficient to facilitate the rapid growth of *Pst* DC3000 in HDM_{Suc}. Conversely, the *ScrY* gene appears to be non-essential for the proliferation of *Pst* DC3000 within the apoplast of Arabidopsis leaves, indicating that the other outer membrane-localized sucrose transporters may adequately support bacterial growth in this environment. In contrast to ScrY, the *ScrB* gene is critical for the proliferation of *Pst* DC3000 in the Arabidopsis leaf apoplast, yet it is not required for sucrose utilization in HDM_{Suc}. This discrepancy implies that other sucrose metabolism enzymes may compensate for the loss of ScrB, allowing for rapid proliferation of *Pst* DC3000 in HDM_{Suc} despite the disruption of ScrB. However, it is plausible that ScrB-mediated sucrose utilization is more efficient than that of the alternative sucrose metabolism enzymes during the colonization of the Arabidopsis leaf apoplast. Additionally, the disruption of ScrB may lead to sucrose-phosphate stress, potentially diminishing the virulence of *Pst* DC3000 (Wadler and Vanderpool, 2007). Notably, ScrB is also essential for the fitness of *Pseudomonas syringae* pv. *syringae* B728a during its colonization of the leaf apoplast (Helmann et al., 2019).

If sucrose derived from Arabidopsis is recognized and utilized by *Pst* DC3000, it is probable that the plasma membrane-localized sugar efflux carriers known as SWEETs contribute to the susceptibility of Arabidopsis to *Pst* DC3000 infection. In comparison to the Col-0 wild type, hexose uniporter mutants *sweet5*, *sweet7*, and the sucrose uniporter mutant *sweet12* exhibit increased susceptibility to *Pst* DC3000 infection, whereas sucrose uniporter mutants *sweet11* and *sweet11;12* show reduced susceptibility to this pathogen (Fatima and Senthil-Kumar, 2021). Furthermore, the triple mutant *sweet11;12;13* also shows decreased susceptibility to *Pst* DC3000 infection.

mRNA levels of SWEET4, SWEET5, SWEET7, and SWEET8 are increased in Arabidopsis leaves during *Pst* DC3000 infection (Chen et al., 2010). However, through GUS histochemical analysis, I was unable to ascertain a significant increase in the protein levels of SWEET5, SWEET7, and SWEET8 in plants inoculated with *Pst* DC3000. This observation may be attributed to two potential factors that could account for the inconsistency between my GUS histochemistry findings and the quantitative reverse transcription PCR results reported in the literature (Chen et al., 2010). First, it is possible that the mRNA levels of SWEET5, SWEET7, and SWEET8 do not exhibit a positive correlation with their respective protein levels. For instance, a similar discrepancy has been noted in the case of SWEET15 in senescent leaves (Chen et al., 2015b). Second, the observed discrepancy may stem from the absence of regulatory elements within my GUS reporter constructs.

SWEET12 is transcriptionally activated 24 hours following infection with *Pst* DC3000 and may contribute to a reduction in Arabidopsis susceptibility to this pathogen by inhibiting the sucrose transport function of SWEET11 in phloem parenchyma cells (Fatima and Senthil-Kumar, 2021; Nobori et al., 2025). SWEET5 may exert an inhibitory effect on SWEET11 due to their concurrent accumulation in the midvein and their demonstrated interaction in yeast cells (Xuan et al., 2013). In contrast, while SWEET7 has been shown to interact with SWEET11 in yeast, it does not accumulate in the midvein following challenge with *Pst* DC3000, implying that it is unlikely to inhibit SWEET11. A recent investigation indicates that SWEET5, SWEET7, and SWEET8 exhibit hydrogen peroxide (H₂O₂) transport capabilities in yeast cells (Selvam et al., 2024). It is plausible that SWEET5 and SWEET7 play a role in

enhancing Arabidopsis resistance to *Pst* DC3000 by coordinating H₂O₂ signaling within the hydathode and midvein.

Notably, SWEET4, SWEET11, and SWEET12 exhibit accumulation in the veins of Arabidopsis leaves infected with *Pst* DC3000 at the protein level (Fatima and Senthil-Kumar, 2021). Analysis of single-cell RNA sequencing data shows that SWEET4 may localize in companion cells and phloem parenchyma cells within the leaves inoculated by *Pst* DC3000 (Zhu et al., 2023). The pathogen *Pst* DC3000 is known to manipulate the plant ABA signaling pathway and introduce the water- and solute-permeable channel AvrE into Arabidopsis leaf cells, thereby inducing hydrosis (Nomura et al., 2023; Roussin-Léveillé et al., 2024). It is plausible that the hydrosis induced by *Pst* DC3000 may facilitate SWEET-mediated sugar efflux while concurrently inhibiting SUC and STP-mediated sugar influx (Roussin-Léveillé et al., 2024). This implies that sugars designated for phloem loading may be recognized and utilized by the invading *Pst* DC3000.

The sucrose concentrations measured in the leaf apoplasm of the *sweet11* mutant are approximately 50% lower than those found in the Col-0 and *sweet12* genotypes. However, the *in vitro* proliferation of *Pst* DC3000 within the *sweet11* apoplasm extract is comparable to that observed in the extracts from Col-0 and *sweet12* apoplasm (Fatima and Senthil-Kumar, 2021). Notably, the transcriptomic, phosphoproteomic, and metabolomic data from the *sweet11;12* mutant indicate enhanced antibacterial defense responses (Gebauer et al., 2017; Stefan et al., 2022). These findings imply that the susceptibility of Arabidopsis to *Pst* DC3000 infection is not solely dependent on the sucrose levels present in the leaf apoplasm. The development of *Pst* DC3000 mutants that are completely deficient in sucrose utilization could provide valuable insights into the functions of SWEET11, SWEET12, and SWEET13 in modulating Arabidopsis susceptibility to *Pst* DC3000 infection. In conclusion, the findings of this study show that phloem-derived sugars are critical determinants of Arabidopsis susceptibility to *Pst* DC3000 infection.

Identifying proteins associated with the Arabidopsis STP13 promoter through proximity labeling continues to present significant challenges

The identification of proteins associated with low-copy genomic loci presents a significant challenge for biologists (Gauchier et al., 2020). The utilization of

CRISPR/dCas9-mediated DNA targeting in conjunction with proximity labeling serves as an effective methodology for the identification of DNA-associated proteins within their native chromatin context (Myers et al., 2018; Lin et al., 2023; Sun et al., 2023; Cenik et al., 2024). In this study, I integrated CRISPR/dCas9-TurboID-based proximity labeling with TRV-mediated gRNA expression to elucidate the proteins associated with the STP13 promoter in Arabidopsis leaves infected with *Pst* DC3000.

The dCas9-TurboID-mVenus fusion showed biotin ligase activity in Arabidopsis; however, no transcription factors or chromatin remodelers were found to be enriched in samples infected with *Pst* DC3000. Although selecting appropriate gRNA target sites and sampling time points may facilitate the identification of transcription factors or chromatin remodelers, the current version of the CRISPR/dCas9-TurboID-based proximity labeling technique necessitates further optimization. It is important to note that transcription factors and chromatin remodelers are typically low-abundance proteins. In animal cells, the dCas9-TurboID fusion has been shown to enrich biotinylated nuclear proteins (Lin et al., 2023; Sun et al., 2023; Yheskel et al., 2023). However, biotinylated nuclear proteins were not enriched in the samples analyzed in this study. To improve the chances of identifying transcription factors and chromatin remodelers through mass spectrometry, it may be essential to incorporate a chromatin enrichment step prior to conducting streptavidin pull-down assays (Vélez-Bermúdez and Schmidt, 2021).

The biotin ligase activity associated with the dCas9-TurboID fusion protein is not limited to the specific gRNA target sites, which implies that any approach aimed at minimizing background labeling could facilitate the identification of transcription factors and chromatin remodelers. Recent advancements have seen the integration of a Tat peptide-derived degron domain (tDeg) and a Pepper aptamer with CRISPR/dCas9 technology to diminish the background fluorescence in dCas9-mediated genomic DNA imaging (Zhang et al., 2024). It would be worthwhile to investigate whether this strategy could render TurboID-tDeg unstable in the absence of the dCas9-gRNA-Pepper aptamer complex within plant systems.

Naturally biotinylated proteins present in living plant cells contribute to elevated background levels in proximity labeling utilizing TurboID. In contrast, pupylation-based interaction tagging (PUP-IT) represents a novel proximity tagging technique that

exhibits reduced background labeling in plant systems (Ye et al., 2022). In the PUP-IT methodology, a bacterial Pup ligase (PafA) is fused to a bait protein, and in the presence of adenosine triphosphate, it facilitates the conjugation of a tagged Pup (comprising 64 amino acids) to a lysine residue within the target protein. It would be beneficial to investigate whether the dCas9-PafA system demonstrates lower background labeling compared to the dCas9-TurboID system in plant models. Overall, my research has laid the groundwork for the advancement of single-copy locus proteomics in Arabidopsis.

Sugar modulates the susceptibility of Arabidopsis to infection by *B. cinerea*

B. cinerea induces cell death in leaf tissues to obtain nutrients from the necrotic cells and to evade plant-derived antifungal compounds (Bi et al., 2023). In response to the proliferation of *B. cinerea*, Arabidopsis may utilize hexose/proton symporters to retrieve hexose from the apoplast of infected tissues. Through the application of translational fusions of hexose/proton symporters STP1, STP3, STP4, and STP13, along with confocal microscopy, I have identified that these symporters are present in various leaf cell types, including adaxial epidermal cells, palisade mesophyll cells, bundle sheath cells, spongy mesophyll cells, xylem parenchyma cells, and phloem cells.

According to their protein accumulation profiles, STP1, STP3, STP4, and STP13 appear to contribute, at least in part, to the enhancement of Arabidopsis resistance against *B. cinerea*. Nevertheless, the *stp1* single knockout mutant and the *stp3,4^{cr}* double knockout mutant exhibit susceptibility to *B. cinerea* infection comparable to that of the Col-0 (Veillet, 2016). In contrast to STP1, STP3, and STP4, STP13 is localized within phloem cells, where it functions to counteract the hexose efflux facilitated by SWEET4. It is plausible to hypothesize that the influx of hexose into phloem cells may inhibit the colonization of *B. cinerea*, potentially through mechanisms such as hexose retrieval or the production of antifungal compounds, including camalexin (Yamada and Mine, 2024). Conducting cell-type specific knockout and complementation studies could provide further evidence that STP13-mediated hexose influx into phloem cells is essential for Arabidopsis resistance to *B. cinerea*.

It is plausible that *B. cinerea* exhibits accelerated growth in response to the increased release of sugars from necrotic leaf cells. A recent investigation involving transgenic Arabidopsis plants, which possess enhanced plasmodesmal closure and sugar

accumulation, may provide evidence to support this hypothesis (Tee et al., 2024). It can be anticipated that heightened invertase activity during the later stages of *B. cinerea* infection results in the accumulation of hexoses within the vacuole and cytosol, thereby augmenting the susceptibility of Arabidopsis to *B. cinerea* infection.

The vacuolar invertase double knockout mutant *vin1;2^{cr}* demonstrates heightened vulnerability to *B. cinerea* infection. Importantly, the cellular sucrose concentration in the VIN1 and VIN2 double knockdown mutant *amiR vil-2* is approximately 200% greater than that observed in the Col-0, with a substantial portion of this sucrose (around 58%) sequestered within the vacuole (Vu et al., 2020). Conversely, the cytosolic glucose levels in *amiR vil-2* are approximately 22% of those found in Col-0 (Vu et al., 2020). Glucose has been shown to enhance the production of the antimicrobial compound camalexin, potentially through the activation of the CPK5-WRKY DNA-BINDING PROTEIN 33 (WRKY33)-PHYTOALEXIN DEFICIENT 3 (PAD3) signaling pathway (Yamada and Mine, 2024). Thus, the hypersusceptible phenotype identified in *vin1;2^{cr}* may be ascribed to an excessive accumulation of sucrose in conjunction with a compromised antifungal defense response. It is reasonable to propose that Arabidopsis may enhance the activity of VIN to decrease sucrose availability and facilitate the antifungal defense response during the later stages of *B. cinerea* infection (Veillet et al., 2016).

While VIN1 and VIN2 plays a role in conferring resistance to *B. cinerea* in Arabidopsis, the double knockout mutant *c/vif1;2^{cr}* exhibits susceptibility to *B. cinerea* infection comparable to that of the Col-0. This observation implies that C/VIF1 and C/VIF2 are not the sole acid invertase inhibitors that affect VIN1 and VIN2 within spongy mesophyll cells. Alternatively, it is possible that the VIN-mediated resistance of Arabidopsis to *B. cinerea* infection may occur in other cell types, such as adaxial epidermal cells, palisade mesophyll cells, or bundle sheath cells.

The tonoplast-localized hexose uniporter single knockout mutant *sweet2* exhibits reduced levels of glucose, fructose, and sucrose, whereas the single knockout mutant *sweet17* demonstrates elevated fructose levels (Guo et al., 2014; Chardon et al., 2013; Chen et al., 2015a). However, the double knockout mutant *sweet2;17^{cr}* shows a susceptibility to *B. cinerea* infection that is comparable to that of the Col-0. It is possible that the tonoplast-localized hexose uniporter SWEET16 may compensate for the roles

of SWEET2 and SWEET17 during the invasion by *B. cinerea* (Guo et al., 2014; Chardon et al., 2013).

The *cinvl* mutant demonstrates a diminished susceptibility to infection by *B. cinerea*. Specifically, the mRNA levels of PAD3 and the cellular glucose concentrations in the roots of the double mutant *cinvl;2* are approximately eight and ten times greater, respectively, than those observed in the Col-0 (Pignocchi et al., 2021). Conversely, the levels of hexose phosphates and glycolytic intermediates in the roots of *cinvl;2* is significantly lower. This decrease in glycolytic intermediates in the roots of *cinvl;2* correlates with an increase in autophagy, which is likely due to the hypoactive state of the target of rapamycin (TOR) kinase pathway (Xiong et al., 2013; Marshall and Vierstra, 2018; Pignocchi et al., 2021). The resistance of plants to necrotrophic fungal pathogens is contingent upon TOR signaling and autophagy (Lai et al., 2011; Lenz et al., 2011; Marash et al., 2022). Additionally, elevated cellular glucose levels and reduced glycolytic intermediates are also observed in the shoots of *cinvl;2* at the end of the day (Pignocchi et al., 2021). Consequently, the hyposusceptible phenotype exhibited by the *cinvl* mutant may be linked to an enhanced antifungal immune response and a suppression of host cell death.

In addition to invertases, I have identified that the Arabidopsis triple mutant of the plasma membrane-localized sucrose uniporter, designated *sweet11;12;13*, exhibits reduced susceptibility to infection by *B. cinerea*. It is hypothesized that *B. cinerea* may derive sugars from both necrotic leaf cells and living leaf cells. Within leaves infected by *B. cinerea*, the phloem is likely a primary site for sugar efflux from living cells, as both SWEET4 and SWEET12 are known to accumulate in phloem cells. Therefore, it is plausible that the sucrose efflux mediated by SWEET11, SWEET12, and SWEET13 from phloem cells plays a role in facilitating the feeding of *B. cinerea*.

The disruption of SWEET11 and SWEET12-mediated phloem loading may result in increased intracellular concentrations of sucrose, glucose, and fructose (Chen et al., 2012; Le Hir et al., 2015; Gebauer et al., 2017; Aubry et al., 2024). These elevated sugar levels could potentially enhance the antifungal immune response in *sweet11;12* (Gebauer et al., 2017). For instance, the mRNA levels of WALL-ASSOCIATED KINASE 1 and LEUCINE-RICH REPEAT RECEPTOR PROTEIN 23, both of which play a role in Arabidopsis resistance to *B. cinerea* infection, are increased in the

sweet11;12 (Brutus et al., 2010; Gebauer et al., 2017; Ono et al., 2020). Additionally, there is an increase in the phosphorylation of proteins that are critical for Arabidopsis resistance to *B. cinerea*, including the camalexin transporter PENETRATION3, LYSM-CONTAINING RECEPTOR-LIKE KINASE 4, and RESPIRATORY BURST OXIDASE HOMOLOG PROTEIN D (Wan et al., 2012; He et al., 2019; Stefan et al., 2022; Zhang et al., 2021). Consequently, similar to the response noted during *Pst* DC3000 infection, the diminished susceptibility of *sweet11;12;13* to *B. cinerea* infection may be attributed to an enhanced antimicrobial immune response.

The hyposusceptible phenotype observed in *sweet11;12;13* implies that elevated sucrose concentrations in the apoplasm facilitate the colonization of *B. cinerea*. Research indicates that sucrose/proton symporters activated in leaves infected by *B. cinerea* may inhibit the pathogen's growth (Veillet et al., 2016). Nevertheless, the double knockout mutant *suc1;3^{cr}* exhibits susceptibility to *B. cinerea* infection comparable to that of the Col-0. Among the sucrose/proton symporters, SUC2 is identified as the most prevalent at the mRNA level in leaves infected by *B. cinerea* (Veillet et al., 2016). It appears that the uptake of sucrose into phloem cells via SUC2 is of greater significance than the retrieval of sucrose mediated by SUC1 or SUC3 in the adaxial epidermal cells or xylem parenchyma cells during the invasion of *B. cinerea*.

The findings of my research indicate potential relationships between sugar availability, sugar signaling, and Arabidopsis susceptibility to *B. cinerea* infection. This investigation employed genetic approaches, translational reporter lines, and confocal imaging techniques. However, two significant limitations persist. The first limitation pertains to the pleiotropic effects associated with the sugar transporter and invertase knockout mutants, such as the hyperaccumulation of sugars, which complicates functional analyses. To mitigate these confounding effects, the application of chemical genetics and inducible gene knockout or protein inhibition strategies in a cell-type-specific manner may prove beneficial. The second limitation arises from the reliance on transgenic methods to examine protein accumulation patterns; employing immunofluorescence staining may provide a more accurate assessment of native protein distribution. Despite these limitations, I propose a model elucidating the mechanisms of sugar allocation and signaling in Arabidopsis leaves during the invasion of *B. cinerea*, as illustrated in Figures 26-27. In conclusion, I have identified several plant genetic

components (VIN1, VIN2, CINV1, SWEET11, SWEET12, and SWEET13) that may play critical roles in *B. cinerea* feeding, antifungal defense mechanisms, and the survival of Arabidopsis cells.

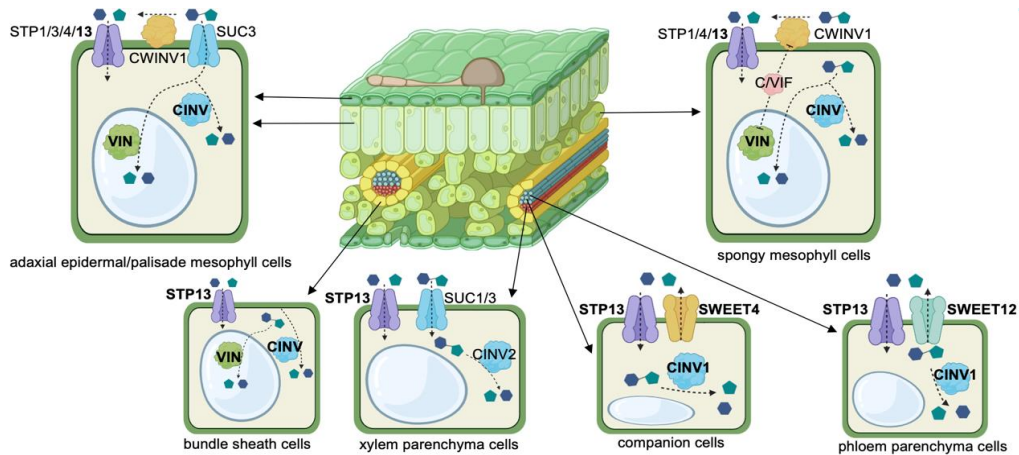


Fig. 26. Hypothetical model of sugar allocation in *B. cinerea*-infected Arabidopsis leaves. *B. cinerea* induces the death of leaf cells and promotes leaf hydrosis. Plasma membrane-localized hexose/proton symporters STP1, STP3, STP4, STP13, and cell wall invertase CWINV1 play a crucial role in inhibiting fungal growth by decreasing hexose concentrations in the apoplasm and elevating hexose concentrations in the cytosol. The presence of water within disease lesions facilitates the efflux of sucrose from phloem parenchyma cells through the action of sucrose uniporter SWEET12, as well as the efflux of hexose from companion cells via hexose uniporter SWEET4. Simultaneously, this condition restricts the entry of sucrose into adaxial epidermal cells or xylem parenchyma cells, a process facilitated by sucrose/proton symporters SUC1 or SUC3 that are localized in the plasma membrane. Cytosolic invertase (CINV) and vacuolar invertase (VIN) catalyze the hydrolysis of sucrose within the cytosol and the vacuole, respectively, resulting in the production of glucose and fructose. Acid invertases are subject to inhibition by the cell wall/vacuolar inhibitor of fructosidases (C/VIF) within the spongy mesophyll cells. Created with BioRender.com.

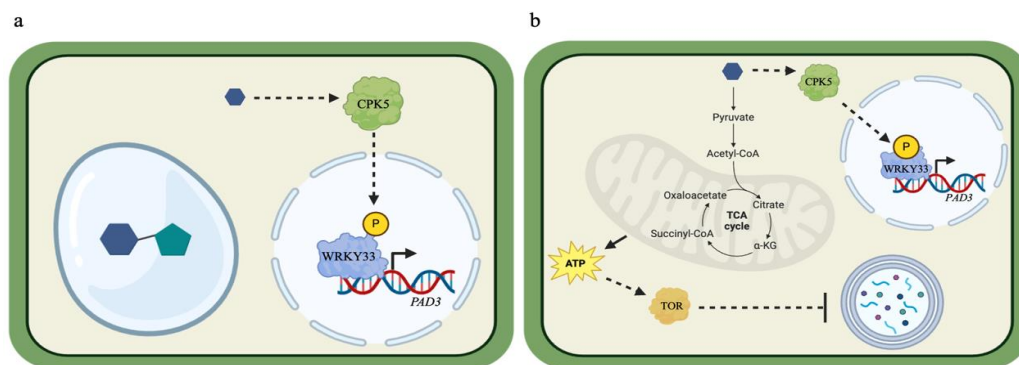


Fig. 27. Hypothetical models of sugar signaling in *B. cinerea*-infected invertase knockout mutants. (a) The trans-phosphorylation activity of CALMODULIN-DOMAIN PROTEIN KINASE 5 (CPK5) on the WRKY DNA-BINDING PROTEIN 33 (WRKY33) wbox1 fragment is diminished in the vacuolar invertase double knockout mutant *vin1;2^{cr}*, which exhibits reduced cytosolic glucose concentrations alongside increased vacuolar sucrose levels. Consequently, the DNA binding affinity of WRKY33 for the promoter of PHYTOALEXIN DEFICIENT 3 (PAD3) is compromised, leading to a decrease in camalexin production. (b) In contrast, the

cytosolic invertase knockout mutant *cinvl* displays elevated cellular glucose levels but reduced levels of glycolytic intermediates. The activation of CPK5 in this context results in the phosphorylation of WRKY33, thereby enhancing the expression of PAD3 and facilitating camalexin biosynthesis. Furthermore, a reduction in the activity of the target of rapamycin (TOR) pathway promotes autophagy, which in turn inhibits host cell death. Created with BioRender.com.

Conclusion

Sugars function as virulence-inducing ligands and nutritional metabolites for phytopathogenic microorganisms exhibiting diverse lifestyles. Both *Pst* DC3000 and *B. cinerea* are capable of inducing water soaking in the leaves of Arabidopsis. The availability of water within the leaf apoplast may enhance the uptake of sucrose by these phytopathogenic microorganisms. This process is critically dependent on the sucrose uniporters SWEET11, SWEET12, and SWEET13, which are specifically localized in phloem parenchyma cells and are vital for Arabidopsis susceptibility to both *Pst* DC3000 and *B. cinerea*. Additionally, during the colonization of Arabidopsis leaves, these pathogens may utilize hexose that are effluxed by the hexose uniporter SWEET4.

Sugar/proton symporters, including STP1, STP3, STP4, STP13, SUC1, and SUC3, which are localized in adaxial epidermal cells, mesophyll cells, bundle sheath cells, phloem cells, or xylem parenchyma cells, may inhibit the growth of *B. cinerea* by either lowering sugar concentrations in the leaf apoplast or by enhancing antifungal immune responses. Vacuolar invertases (VIN1 and VIN2), which are localized in the adaxial epidermal cells, mesophyll cells, or bundle sheath cells, have the potential to inhibit the growth of *B. cinerea* by reducing vacuolar sucrose concentrations and bolstering antifungal defense mechanisms. In contrast, the presence of cytosolic invertase CINV1 in adaxial epidermal cells, mesophyll cells, bundle sheath cells, or phloem cells may play a role in the susceptibility of Arabidopsis to infection by *B. cinerea*, likely due to its critical role in cytosolic sucrose metabolism, which in turn influences antifungal immunity, TOR kinase activity, and autophagy.

Pst DC3000 relies on the bacterial sucrose porin precursor ScrY for the rapid utilization of sucrose in vitro, as well as the bacterial S6P hydrolase ScrB for its proliferation within Arabidopsis leaves. An attempt to identify transcriptional activators of the hexose/proton symporter STP13 in Arabidopsis leaves infected with *Pst* DC3000, utilizing the recently developed CRISPR/dCas9-TurboID-based proximity labeling method, was unsuccessful; however, it lays the groundwork for future investigations into single locus proteomics in plant systems. In conclusion, this study elucidates potential genetic components implicated in sugar-dependent pathogenesis, plant defense mechanisms, and host cell survival within the Arabidopsis-*Pst* DC3000/*B. cinerea* pathosystem.

References

- Alberto, F., Bignon, C., Sulzenbacher, G., Henrissat, B. and Czjzek, M. (2004) The three-dimensional structure of invertase (beta-fructosidase) from *Thermotoga maritima* reveals a bimodular arrangement and an evolutionary relationship between retaining and inverting glycosidases. *J Biol Chem*, **279**, 18903-18910.
- Alonso, J. M., Stepanova, A. N., Leisse, T. J., Kim, C. J., Chen, H., Shinn, P., *et al.* (2003) Genome-wide insertional mutagenesis of *Arabidopsis thaliana*. *Science*, **301**, 653-657.
- An, J., Zeng, T., Ji, C., de Graaf, S., Zheng, Z., Xiao, T. T., *et al.* (2019) A *Medicago truncatula* SWEET transporter implicated in arbuscule maintenance during arbuscular mycorrhizal symbiosis. *New Phytologist*, **224**, 396-408.
- Anderson, J. C. (2023) Ill communication: host metabolites as virulence-regulating signals for plant-pathogenic bacteria. *Annu Rev Phytopathol*, **61**, 49-71.
- Aubry, E., Clément, G., Gilbault, E., Dinant, S. and Le Hir, R. (2024) Changes in SWEET-mediated sugar partitioning affect photosynthesis performance and plant response to drought. *Physiologia Plantarum*, **176**, e14623.
- Barratt, D. H., Derbyshire, P., Findlay, K., Pike, M., Wellner, N., Lunn, J., *et al.* (2009) Normal growth of *Arabidopsis* requires cytosolic invertase but not sucrose synthase. *Proceedings of the National Academy of Sciences*, **106**, 13124-13129.
- Bavnhøj, L., Driller, J. H., Zuzic, L., Stange, A. D., Schiøtt, B. and Pedersen, B. P. (2023) Structure and sucrose binding mechanism of the plant SUC1 sucrose transporter. *Nature Plants*, **9**, 938-950.
- Bavnhøj, L., Paulsen, P. A., Flores-Canales, J. C., Schiøtt, B. and Pedersen, B. P. (2021) Molecular mechanism of sugar transport in plants unveiled by structures of glucose/H⁺ symporter STP10. *Nature Plants*, **7**, 1409-1419.
- Bever, J. D., Richardson, S. C., Lawrence, B. M., Holmes, J. and Watson, M. (2009) Preferential allocation to beneficial symbiont with spatial structure maintains mycorrhizal mutualism. *Ecology Letters*, **12**, 13-21.
- Bi, G., Su, M., Li, N., Liang, Y., Dang, S., Xu, J., *et al.* (2021) The ZAR1 resistosome is a calcium-permeable channel triggering plant immune signaling. *Cell*, **184**, 3528-3541.e12.
- Bi, K., Liang, Y., Mengiste, T. and Sharon, A. (2023) Killing softly: a roadmap of *Botrytis cinerea* pathogenicity. *Trends Plant Sci*, **28**, 211-222.
- Birkenbihl, R. P., Kracher, B., Roccaro, M. and Somssich, I. E. (2017) Induced genome-wide binding of three *Arabidopsis* WRKY transcription factors during early MAMP-triggered immunity. *The Plant Cell*, **29**, 20-38.
- Bonardi, V., Tang, S., Stallmann, A., Roberts, M., Cherkis, K. and Dangl, J. L. (2011) Expanded functions for a family of plant intracellular immune receptors beyond specific recognition of pathogen effectors. *Proceedings of the National Academy of Sciences*, **108**, 16463-16468.
- Branon, T. C., Bosch, J. A., Sanchez, A. D., Udeshi, N. D., Svinkina, T., Carr, S. A., *et al.* (2018) Efficient proximity labeling in living cells and organisms with TurboID. *Nat Biotechnol*, **36**, 880-887.
- Brutus, A., Sicilia, F., Macone, A., Cervone, F. and De Lorenzo, G. (2010) A domain swap approach reveals a role of the plant wall-associated kinase 1 (WAK1) as a receptor of oligogalacturonides. *Proceedings of the National Academy of Sciences*, **107**, 9452-9457.
- Cenik, B. K., Aoi, Y., Iwanaszko, M., Howard, B. C., Morgan, M. A., Andersen, G. D., *et al.* (2024) TurboCas: A method for locus-specific labeling of genomic regions

- and isolating their associated protein interactome. *Molecular Cell*, **84**, 4929-4944.e8.
- Chardon, F., Bedu, M., Calenge, F., Klemens, P. A., Spinner, L., Clement, G., *et al.* (2013) Leaf fructose content is controlled by the vacuolar transporter SWEET17 in *Arabidopsis*. *Curr Biol*, **23**, 697-702.
- Chassy, B. M. and Porter, E. V. (1979) Initial characterization of sucrose-6-phosphate hydrolase from *Streptococcus mutans* and its apparent identity with intracellular invertase. *Biochem Biophys Res Commun*, **89**, 307-314.
- Chen, B., Gilbert, L. A., Cimini, B. A., Schnitzbauer, J., Zhang, W., Li, G. W., *et al.* (2013) Dynamic imaging of genomic loci in living human cells by an optimized CRISPR/Cas system. *Cell*, **155**, 1479-1491.
- Chen, H. Y., Huh, J. H., Yu, Y. C., Ho, L. H., Chen, L. Q., Tholl, D., *et al.* (2015a) The *Arabidopsis* vacuolar sugar transporter SWEET2 limits carbon sequestration from roots and restricts *Pythium* infection. *Plant J*, **83**, 1046-1058.
- Chen, L. Q., Hou, B. H., Lalonde, S., Takanaga, H., Hartung, M. L., Qu, X. Q., *et al.* (2010) Sugar transporters for intercellular exchange and nutrition of pathogens. *Nature*, **468**, 527-532.
- Chen, L. Q., Lin, I. W., Qu, X. Q., Sosso, D., McFarlane, H. E., Londoño, A., *et al.* (2015b) A cascade of sequentially expressed sucrose transporters in the seed coat and endosperm provides nutrition for the *Arabidopsis* embryo. *Plant Cell*, **27**, 607-619.
- Chen, L. Q., Qu, X. Q., Hou, B. H., Sosso, D., Osorio, S., Fernie, A. R., *et al.* (2012) Sucrose efflux mediated by SWEET proteins as a key step for phloem transport. *Science*, **335**, 207-211.
- Chen, W., Zhang, Y., Zhang, Y., Pi, Y., Gu, T., Song, L., *et al.* (2018) CRISPR/Cas9-based genome editing in *Pseudomonas aeruginosa* and cytidine deaminase-mediated base editing in *Pseudomonas* species. *iScience*, **6**, 222-231.
- Chong, J., Piron, M. C., Meyer, S., Merdinoglu, D., Bertsch, C. and Mestre, P. (2014) The SWEET family of sugar transporters in grapevine: *VvSWEET4* is involved in the interaction with *Botrytis cinerea*. *J Exp Bot*, **65**, 6589-6601.
- Clough, S. J. and Bent, A. F. (1998) Floral dip: a simplified method for *Agrobacterium*-mediated transformation of *Arabidopsis thaliana*. *Plant J*, **16**, 735-743.
- Cohn, M., Bart, R. S., Shybut, M., Dahlbeck, D., Gomez, M., Morbitzer, R., *et al.* (2014) *Xanthomonas axonopodis* virulence is promoted by a transcription activator-like effector-mediated induction of a SWEET sugar transporter in cassava. *Molecular Plant-Microbe Interactions*, **27**, 1186-1198.
- Conrath, U. (2011) Molecular aspects of defence priming. *Trends Plant Sci*, **16**, 524-531.
- Denay, G., Schultz, P., Hänsch, S., Weidtkamp-Peters, S. and Simon, R. (2019) Over the rainbow: A practical guide for fluorescent protein selection in plant FRET experiments. *Plant Direct*, **3**, e00189.
- Doehlemann, G., Molitor, F. and Hahn, M. (2005) Molecular and functional characterization of a fructose specific transporter from the gray mold fungus *Botrytis cinerea*. *Fungal Genet Biol*, **42**, 601-610.
- Duan, S., Feng, G., Limpens, E., Bonfante, P., Xie, X. and Zhang, L. (2024) Cross-kingdom nutrient exchange in the plant-arbuscular mycorrhizal fungus-bacterium continuum. *Nature Reviews Microbiology*, **22**, 773-790.
- Dulermo, T., Rasle, C., Chinnici, G., Gout, E., Bligny, R. and Cotton, P. (2009) Dynamic carbon transfer during pathogenesis of sunflower by the necrotrophic

- fungus *Botrytis cinerea*: from plant hexoses to mannitol. *New Phytologist*, **183**, 1149-1162.
- Ellison, E. E., Nagalakshmi, U., Gamo, M. E., Huang, P. J., Dinesh-Kumar, S. and Voytas, D. F. (2020) Multiplexed heritable gene editing using RNA viruses and mobile single guide RNAs. *Nat Plants*, **6**, 620-624.
- Eom, J.-S., Luo, D., Atienza-Grande, G., Yang, J., Ji, C., Thi Luu, V., *et al.* (2019) Diagnostic kit for rice blight resistance. *Nature Biotechnology*, **37**, 1372-1379.
- Fatima, U. and Senthil-Kumar, M. (2021) Sweet revenge: *AtSWEET12* in plant defense against bacterial pathogens by apoplastic sucrose limitation. *bioRxiv*, 2021.2010.2004.463061.
- Forst, D., Welte, W., Wacker, T. and Diederichs, K. (1998) Structure of the sucrose-specific porin ScrY from *Salmonella typhimurium* and its complex with sucrose. *Nat Struct Biol*, **5**, 37-46.
- Freeman, B. C. and Beattie, G. A. (2009) Bacterial growth restriction during host resistance to *Pseudomonas syringae* is associated with leaf water loss and localized cessation of vascular activity in *Arabidopsis thaliana*. *Molecular Plant-Microbe Interactions*, **22**, 857-867.
- Gauchier, M., van Mierlo, G., Vermeulen, M. and Déjardin, J. (2020) Purification and enrichment of specific chromatin loci. *Nat Methods*, **17**, 380-389.
- Gebauer, P., Korn, M., Engelsdorf, T., Sonnewald, U., Koch, C. and Voll, L. M. (2017) Sugar accumulation in leaves of *Arabidopsis sweet11/sweet12* double mutants enhances priming of the salicylic acid-mediated defense response. *Front Plant Sci*, **8**, 1378.
- Gentzel, I., Giese, L., Ekanayake, G., Mikhail, K., Zhao, W., Cocuron, J. C., *et al.* (2022) Dynamic nutrient acquisition from a hydrated apoplast supports biotrophic proliferation of a bacterial pathogen of maize. *Cell Host Microbe*, **30**, 502-517.e504.
- Grützner, R., Martin, P., Horn, C., Mortensen, S., Cram, E. J., Lee-Parsons, C. W. T., *et al.* (2021) High-efficiency genome editing in plants mediated by a Cas9 gene containing multiple introns. *Plant Communications*, **2**, 100135.
- Guo, W.-J., Nagy, R., Chen, H.-Y., Pfrunder, S., Yu, Y.-C., Santelia, D., *et al.* (2014) SWEET17, a facilitative transporter, mediates fructose transport across the tonoplast of *Arabidopsis* roots and leaves. *Plant Physiology*, **164**, 777-789.
- Gupta, P. K., Balyan, H. S. and Gautam, T. (2021) SWEET genes and TAL effectors for disease resistance in plants: Present status and future prospects. *Mol Plant Pathol*, **22**, 1014-1026.
- Hacker, J. and Carniel, E. (2001) Ecological fitness, genomic islands and bacterial pathogenicity. A Darwinian view of the evolution of microbes. *EMBO Rep*, **2**, 376-381.
- Han, L., Zhu, Y., Liu, M., Zhou, Y., Lu, G., Lan, L., *et al.* (2017) Molecular mechanism of substrate recognition and transport by the *AtSWEET13* sugar transporter. *Proceedings of the National Academy of Sciences*, **114**, 10089-10094.
- He, Y., Xu, J., Wang, X., He, X., Wang, Y., Zhou, J., *et al.* (2019) The *Arabidopsis* pleiotropic drug resistance transporters PEN3 and PDR12 mediate camalexin secretion for resistance to *Botrytis cinerea*. *Plant Cell*, **31**, 2206-2222.
- Helber, N., Wippel, K., Sauer, N., Schaarschmidt, S., Hause, B. and Requena, N. (2011) A versatile monosaccharide transporter that operates in the arbuscular mycorrhizal fungus *glomus* sp is crucial for the symbiotic relationship with plants. *The Plant Cell*, **23**, 3812-3823.

- Helmann, T. C., Deutschbauer, A. M. and Lindow, S. E. (2019) Genome-wide identification of *Pseudomonas syringae* genes required for fitness during colonization of the leaf surface and apoplast. *Proc Natl Acad Sci U S A*, **116**, 18900-18910.
- Herbers, K., Meuwly, P., Frommer, W. B., Metraux, J. P. and Sonnewald, U. (1996) Systemic acquired resistance mediated by the ectopic expression of invertase: possible hexose sensing in the secretory pathway. *Plant Cell*, **8**, 793-803.
- Hothorn, M., Van den Ende, W., Lammens, W., Rybin, V. and Scheffzek, K. (2010) Structural insights into the pH-controlled targeting of plant cell-wall invertase by a specific inhibitor protein. *Proceedings of the National Academy of Sciences*, **107**, 17427-17432.
- Hothorn, M., Wolf, S., Aloy, P., Greiner, S. and Scheffzek, K. (2004) Structural insights into the target specificity of plant invertase and pectin methylesterase inhibitory proteins. *The Plant Cell*, **16**, 3437-3447.
- Hu, Y., Ding, Y., Cai, B., Qin, X., Wu, J., Yuan, M., *et al.* (2022) Bacterial effectors manipulate plant abscisic acid signaling for creation of an aqueous apoplast. *Cell Host & Microbe*, **30**, 518-529.e516.
- Huynh, T. V., Dahlbeck, D. and Staskawicz, B. J. (1989) Bacterial blight of soybean: regulation of a pathogen gene determining host cultivar specificity. *Science*, **245**, 1374-1377.
- Jing, W., Uddin, S., Chakraborty, R., Van Anh, D. T., Macoy, D. M., Park, S. O., *et al.* (2020) Molecular characterization of HEXOKINASE1 in plant innate immunity. *Applied Biological Chemistry*, **63**, 76.
- Joardar, V., Lindeberg, M., Schneider, D. J., Collmer, A. and Buell, C. R. (2005) Lineage-specific regions in *Pseudomonas syringae* pv tomato DC3000. *Mol Plant Pathol*, **6**, 53-64.
- Karimi, M., Inzé, D. and Depicker, A. (2002) GATEWAY vectors for *Agrobacterium*-mediated plant transformation. *Trends Plant Sci*, **7**, 193-195.
- Khare, D., Choi, H., Huh, S. U., Bassin, B., Kim, J., Martinoia, E., *et al.* (2017) Arabidopsis ABCG34 contributes to defense against necrotrophic pathogens by mediating the secretion of camalexin. *Proceedings of the National Academy of Sciences*, **114**, E5712-E5720.
- Kilic, A. O., Honeyman, A. L. and Tao, L. (2007) Overlapping substrate specificity for sucrose and maltose of two binding protein-dependent sugar uptake systems in *Streptococcus mutans*. *FEMS Microbiol Lett*, **266**, 218-223.
- Kim, J.-Y., Loo, E. P. I., Pang, T. Y., Lercher, M., Frommer, W. B. and Wudick, M. M. (2021a) Cellular export of sugars and amino acids: role in feeding other cells and organisms. *Plant Physiology*, **187**, 1893-1914.
- Kim, J.-Y., Symeonidi, E., Pang, T. Y., Denyer, T., Weidauer, D., Bezruczyk, M., *et al.* (2021b) Distinct identities of leaf phloem cells revealed by single cell transcriptomics. *The Plant Cell*, **33**, 511-530.
- Labun, K., Montague, T. G., Krause, M., Torres Cleuren, Y. N., Tjeldnes, H. and Valen, E. (2019) CHOPCHOP v3: expanding the CRISPR web toolbox beyond genome editing. *Nucleic Acids Res*, **47**, W171-W174.
- Lai, Z., Wang, F., Zheng, Z., Fan, B. and Chen, Z. (2011) A critical role of autophagy in plant resistance to necrotrophic fungal pathogens. *Plant J*, **66**, 953-968.
- Lajeunesse, G., Roussin-Léveillé, C., Boutin, S., Fortin, É., Laforest-Lapointe, I. and Moffett, P. (2023) Light prevents pathogen-induced aqueous microenvironments via potentiation of salicylic acid signaling. *Nature Communications*, **14**, 713.

- Lampropoulos, A., Sutikovic, Z., Wenzl, C., Maegele, I., Lohmann, J. U. and Forner, J. (2013) GreenGate-a novel, versatile, and efficient cloning system for plant transgenesis. *PLoS One*, **8**, e83043.
- Latorraca, N. R., Fastman, N. M., Venkatakrishnan, A. J., Frommer, W. B., Dror, R. O. and Feng, L. (2017) Mechanism of substrate translocation in an alternating access transporter. *Cell*, **169**, 96-107.e112.
- Laue, H., Schenk, A., Li, H., Lambertsen, L., Neu, T. R., Molin, S., *et al.* (2006) Contribution of alginate and levan production to biofilm formation by *Pseudomonas syringae*. *Microbiology (Reading)*, **152**, 2909-2918.
- Le Hir, R., Spinner, L., Klemens, P. A., Chakraborti, D., de Marco, F., Vilaine, F., *et al.* (2015) Disruption of the sugar transporters *AtSWEET11* and *AtSWEET12* affects vascular development and freezing tolerance in Arabidopsis. *Mol Plant*, **8**, 1687-1690.
- Lee, H. G. and Seo, P. J. (2021) Transcriptional activation of SUGAR TRANSPORT PROTEIN 13 mediates biotic and abiotic stress signaling. *Plant Signal Behav*, **16**, 1920759.
- Lemonnier, P., Gaillard, C., Veillet, F., Verbeke, J., Lemoine, R., Coutos-Thévenot, P., *et al.* (2014) Expression of Arabidopsis sugar transport protein STP13 differentially affects glucose transport activity and basal resistance to *Botrytis cinerea*. *Plant Mol Biol*, **85**, 473-484.
- Lenz, H. D., Haller, E., Melzer, E., Kober, K., Wurster, K., Stahl, M., *et al.* (2011) Autophagy differentially controls plant basal immunity to biotrophic and necrotrophic pathogens. *The Plant Journal*, **66**, 818-830.
- Li, Z., Liu, S.-L., Montes-Serey, C., Walley, J. W. and Aung, K. (2024) PLASMODESMATA-LOCATED PROTEIN 6 regulates plasmodesmal function in Arabidopsis vasculature. *The Plant Cell*, **36**, 3543-3561.
- Lin, Y.-J., Yeh, A.-H., Chen, H.-I., Liu, C.-F. and Yu, M.-J. (2023) Identification of protein machineries involved in aquaporin-2 gene transcription with genomic locus proteomics (GLOPro). *Physiology*, **38**, 5732110.
- Lindow Steven, E. and Brandl Maria, T. (2003) Microbiology of the phyllosphere. *Applied and Environmental Microbiology*, **69**, 1875-1883.
- Link, M., Rausch, T. and Greiner, S. (2004) In Arabidopsis *thaliana*, the invertase inhibitors *AtC/VIF1* and 2 exhibit distinct target enzyme specificities and expression profiles. *FEBS Lett*, **573**, 105-109.
- Liu, X., Zhang, Y., Yang, C., Tian, Z. and Li, J. (2016) *AtSWEET4*, a hexose facilitator, mediates sugar transport to axial sinks and affects plant development. *Sci Rep*, **6**, 24563.
- Liu, Y., Schiff, M., Marathe, R. and Dinesh-Kumar, S. P. (2002) Tobacco Rar1, EDS1 and NPR1/NIM1 like genes are required for N-mediated resistance to tobacco mosaic virus. *Plant J*, **30**, 415-429.
- Liu, Z., Hou, S., Rodrigues, O., Wang, P., Luo, D., Munemasa, S., *et al.* (2022) Phytocytokine signalling reopens stomata in plant immunity and water loss. *Nature*, **605**, 332-339.
- Loo, E. P. I., Durán, P., Pang, T. Y., Westhoff, P., Deng, C., Durán, C., *et al.* (2024) Sugar transporters spatially organize microbiota colonization along the longitudinal root axis of Arabidopsis. *Cell Host & Microbe*, **32**, 543-556.e546.
- Lowder, L. G., Zhang, D., Baltes, N. J., Paul, J. W., 3rd, Tang, X., Zheng, X., *et al.* (2015) A CRISPR/Cas9 toolbox for multiplexed plant genome editing and transcriptional regulation. *Plant Physiol*, **169**, 971-985.

- Lowder, L. G., Zhou, J., Zhang, Y., Malzahn, A., Zhong, Z., Hsieh, T. F., *et al.* (2018) Robust transcriptional activation in plants using multiplexed CRISPR-Act2.0 and mTALE-Act systems. *Mol Plant*, **11**, 245-256.
- Mair, A., Xu, S. L., Branon, T. C., Ting, A. Y. and Bergmann, D. C. (2019) Proximity labeling of protein complexes and cell-type-specific organellar proteomes in Arabidopsis enabled by TurboID. *Elife*, **8**, e47864.
- Marash, I., Leibman-Markus, M., Gupta, R., Avni, A. and Bar, M. (2022) TOR inhibition primes immunity and pathogen resistance in tomato in a salicylic acid-dependent manner. *Molecular Plant Pathology*, **23**, 1035-1047.
- Marshall, R. S. and Vierstra, R. D. (2018) Autophagy: the master of bulk and selective recycling. *Annual Review of Plant Biology*, **69**, 173-208.
- McCraw, S. L., Park, D. H., Jones, R., Bentley, M. A., Rico, A., Ratcliffe, R. G., *et al.* (2016) GABA (γ -aminobutyric acid) uptake via the GABA permease GabP represses virulence gene expression in *Pseudomonas syringae* pv. tomato DC3000. *Mol Plant Microbe Interact*, **29**, 938-949.
- Myers, S. A., Wright, J., Peckner, R., Kalish, B. T., Zhang, F. and Carr, S. A. (2018) Discovery of proteins associated with a predefined genomic locus via dCas9–APEX-mediated proximity labeling. *Nature Methods*, **15**, 437-439.
- Nagalakshmi, U., Meier, N., Liu, J. Y., Voytas, D. F. and Dinesh-Kumar, S. P. (2022) High-efficiency multiplex biallelic heritable editing in Arabidopsis using an RNA virus. *Plant Physiol*, **189**, 1241-1245.
- Nester, E. W. (2014) Agrobacterium: nature's genetic engineer. *Front Plant Sci*, **5**, 730.
- Ngou, B. P. M., Ahn, H.-K., Ding, P. and Jones, J. D. G. (2021) Mutual potentiation of plant immunity by cell-surface and intracellular receptors. *Nature*, **592**, 110-115.
- Nobori, T., Monell, A., Lee, T. A., Sakata, Y., Shirahama, S., Zhou, J., *et al.* (2025) A rare PRIMER cell state in plant immunity. *Nature*, **638**, 197-205.
- Nobori, T., Velásquez, A. C., Wu, J., Kvitko, B. H., Kremer, J. M., Wang, Y., *et al.* (2018) Transcriptome landscape of a bacterial pathogen under plant immunity. *Proceedings of the National Academy of Sciences*, **115**, E3055-e3064.
- Nomura, K., Andrezza, F., Cheng, J., Dong, K., Zhou, P. and He, S. Y. (2023) Bacterial pathogens deliver water- and solute-permeable channels to plant cells. *Nature*, **621**, 586-591.
- Oh, H. S., Park, D. H. and Collmer, A. (2010) Components of the *Pseudomonas syringae* type III secretion system can suppress and may elicit plant innate immunity. *Mol Plant Microbe Interact*, **23**, 727-739.
- Oliva, R., Ji, C., Atienza-Grande, G., Huguet-Tapia, J. C., Perez-Quintero, A., Li, T., *et al.* (2019) Broad-spectrum resistance to bacterial blight in rice using genome editing. *Nat Biotechnol*, **37**, 1344-1350.
- Ono, E., Mise, K. and Takano, Y. (2020) RLP23 is required for Arabidopsis immunity against the grey mould pathogen *Botrytis cinerea*. *Scientific Reports*, **10**, 13798.
- Paulsen, P. A., Custódio, T. F. and Pedersen, B. P. (2019) Crystal structure of the plant symporter STP10 illuminates sugar uptake mechanism in monosaccharide transporter superfamily. *Nature Communications*, **10**, 407.
- Pignocchi, C., Ivakov, A., Feil, R., Trick, M., Pike, M., Wang, T. L., *et al.* (2021) Restriction of cytosolic sucrose hydrolysis profoundly alters development, metabolism, and gene expression in Arabidopsis roots. *Journal of Experimental Botany*, **72**, 1850-1863.

- Pini, F., East, A. K., Appia-Ayme, C., Tomek, J., Karunakaran, R., Mendoza-Suárez, M., *et al.* (2017) Bacterial biosensors for in vivo spatiotemporal mapping of root secretion. *Plant Physiology*, **174**, 1289-1306.
- Platt, T. G., Bever, J. D. and Fuqua, C. (2012) A cooperative virulence plasmid imposes a high fitness cost under conditions that induce pathogenesis. *Proc Biol Sci*, **279**, 1691-1699.
- Pruitt, R. N., Locci, F., Wanke, F., Zhang, L., Saile, S. C., Joe, A., *et al.* (2021) The EDS1–PAD4–ADR1 node mediates Arabidopsis pattern-triggered immunity. *Nature*, **598**, 495-499.
- Rico, A. and Preston, G. M. (2008) *Pseudomonas syringae* pv. tomato DC3000 uses constitutive and apoplast-induced nutrient assimilation pathways to catabolize nutrients that are abundant in the tomato apoplast. *Molecular Plant-Microbe Interactions*, **21**, 269-282.
- Riesmeier, J. W., Willmitzer, L. and Frommer, W. B. (1992) Isolation and characterization of a sucrose carrier cDNA from spinach by functional expression in yeast. *Embo j*, **11**, 4705-4713.
- Rossmann, S., Richter, R., Sun, H., Schneeberger, K., Töpfer, R., Zyprian, E., *et al.* (2020) Mutations in the miR396 binding site of the growth-regulating factor gene *VvGFR4* modulate inflorescence architecture in grapevine. *Plant J*, **101**, 1234-1248.
- Roussin-Léveillé, C., Lajeunesse, G., St-Amand, M., Veerapen, V. P., Silva-Martins, G., Nomura, K., *et al.* (2022) Evolutionarily conserved bacterial effectors hijack abscisic acid signaling to induce an aqueous environment in the apoplast. *Cell Host & Microbe*, **30**, 489-501.e484.
- Roussin-Léveillé, C., Mackey, D., Ekanayake, G., Gohmann, R. and Moffett, P. (2024) Extracellular niche establishment by plant pathogens. *Nature Reviews Microbiology*, **22**, 360-372.
- Roux, K. J., Kim, D. I., Raida, M. and Burke, B. (2012) A promiscuous biotin ligase fusion protein identifies proximal and interacting proteins in mammalian cells. *J Cell Biol*, **196**, 801-810.
- Ruan, Y. L. (2014) Sucrose metabolism: gateway to diverse carbon use and sugar signaling. *Annu Rev Plant Biol*, **65**, 33-67.
- Ryffel, F., Helfrich, E. J. N., Kiefer, P., Peyriga, L., Portais, J.-C., Piel, J., *et al.* (2016) Metabolic footprint of epiphytic bacteria on *Arabidopsis thaliana* leaves. *The ISME Journal*, **10**, 632-643.
- Sauer, N., Friedländer, K. and Gräml-Wicke, U. (1990) Primary structure, genomic organization and heterologous expression of a glucose transporter from *Arabidopsis thaliana*. *Embo j*, **9**, 3045-3050.
- Sauer, N. and Stolz, J. (1994) SUC1 and SUC2: two sucrose transporters from *Arabidopsis thaliana*; expression and characterization in baker's yeast and identification of the histidine-tagged protein. *Plant J*, **6**, 67-77.
- Schäfer, M., Pacheco, A. R., Künzler, R., Bortfeld-Miller, M., Field, C. M., Vayena, E., *et al.* (2023) Metabolic interaction models recapitulate leaf microbiota ecology. *Science*, **381**, eadf5121.
- Schenstnyi, K., Strauß, A., Dressel, A., Morbitzer, R., Wunderlich, M., Andrade, A. G., *et al.* (2022) The tomato resistance gene *Bs4* suppresses leaf watersoaking phenotypes induced by AvrHah1, a transcription activator-like effector from tomato-pathogenic xanthomonads. *New Phytol*, **236**, 1856-1870.

- Schuler, D., Wahl, R., Wippel, K., Vranes, M., Münsterkötter, M., Sauer, N., *et al.* (2015) Hxt1, a monosaccharide transporter and sensor required for virulence of the maize pathogen *Ustilago maydis*. *New Phytol*, **206**, 1086-1100.
- Schulz, A., Beyhl, D., Marten, I., Wormit, A., Neuhaus, E., Poschet, G., *et al.* (2011) Proton-driven sucrose symport and antiport are provided by the vacuolar transporters SUC4 and TMT1/2. *Plant J*, **68**, 129-136.
- Schwartz, A. R., Morbitzer, R., Lahaye, T. and Staskawicz, B. J. (2017) TALE-induced bHLH transcription factors that activate a pectate lyase contribute to water soaking in bacterial spot of tomato. *Proceedings of the National Academy of Sciences*, **114**, E897-E903.
- Selvam, B., Paul, A., Yu, Y.-C., Chen, L.-Q. and Shukla, D. (2024) SWEET family transporters act as water conducting carrier proteins in plants. *bioRxiv*, 2024.2006.2023.600272.
- Sham, A., Al-Azzawi, A., Al-Ameri, S., Al-Mahmoud, B., Awwad, F., Al-Rawashdeh, A., *et al.* (2014) Transcriptome analysis reveals genes commonly induced by *Botrytis cinerea* infection, cold, drought and oxidative stresses in Arabidopsis. *PLoS One*, **9**, e113718.
- Sham, A., Moustafa, K., Al-Shamisi, S., Alyan, S., Iratni, R. and AbuQamar, S. (2017) Microarray analysis of Arabidopsis WRKY33 mutants in response to the necrotrophic fungus *Botrytis cinerea*. *PLoS One*, **12**, e0172343.
- Sinatra, L., Yang, J., Schliehe-Diecks, J., Dienstbier, N., Vogt, M., Gebing, P., *et al.* (2022) Solid-phase synthesis of cereblon-recruiting selective histone deacetylase 6 degraders (HDAC6 PROTACs) with antileukemic activity. *J Med Chem*, **65**, 16860-16878.
- Stadler, R. and Sauer, N. (1996) The Arabidopsis *thaliana* AtSUC2 gene is specifically expressed in companion cells. *Botanica Acta*, **109**, 299-306.
- Stauber, J. L., Loginicheva, E. and Schechter, L. M. (2012) Carbon source and cell density-dependent regulation of type III secretion system gene expression in *Pseudomonas syringae* pathovar tomato DC3000. *Res Microbiol*, **163**, 531-539.
- Stefan, T., Wu, X. N., Zhang, Y., Fernie, A. and Schulze, W. X. (2022) regulatory modules of metabolites and protein phosphorylation in Arabidopsis genotypes with altered sucrose allocation. *Front Plant Sci*, **13**, 891405.
- Stein, O. and Granot, D. (2019) An overview of sucrose synthases in plants. *Front Plant Sci*, **10**, 95.
- Sturm, A., Heinemann, M., Arnoldini, M., Benecke, A., Ackermann, M., Benz, M., *et al.* (2011) The cost of virulence: retarded growth of *Salmonella* Typhimurium cells expressing type III secretion system 1. *PLOS Pathogens*, **7**, e1002143.
- Sun, T., Xu, Y., Xiang, Y., Ou, J., Soderblom, E. J. and Diao, Y. (2023) Crosstalk between RNA m(6)A and DNA methylation regulates transposable element chromatin activation and cell fate in human pluripotent stem cells. *Nat Genet*, **55**, 1324-1335.
- Sun, Y., Li, L., Macho, A. P., Han, Z., Hu, Z., Zipfel, C., *et al.* (2013) Structural basis for flg22-induced activation of the Arabidopsis FLS2-BAK1 immune complex. *Science*, **342**, 624-628.
- Tamayo, E., Figueira-Galán, D., Manck-Götzenberger, J. and Requena, N. (2022) Overexpression of the potato monosaccharide transporter *StSWEET7a* promotes root colonization by symbiotic and pathogenic fungi by increasing root sink strength. *Front Plant Sci*, **13**, 837231.

- Tang, X., Lowder, L. G., Zhang, T., Malzahn, A. A., Zheng, X., Voytas, D. F., *et al.* (2017) A CRISPR-Cpf1 system for efficient genome editing and transcriptional repression in plants. *Nat Plants*, **3**, 17018.
- Tao, Y., Cheung, L. S., Li, S., Eom, J.-S., Chen, L.-Q., Xu, Y., *et al.* (2015) Structure of a eukaryotic SWEET transporter in a homotrimeric complex. *Nature*, **527**, 259-263.
- Tarkowski, Ł., Tsirkone, V., Osipov, E., Beelen, S., Lammens, W., Vergauwen, R., *et al.* (2020) Crystal structure of *Arabidopsis thaliana* neutral invertase 2. *Acta Crystallographica Section F*, **76**, 152-157.
- Tee, E. E., Breakspear, A., Papp, D., Thomas, H. R., Walker, C., Bellandi, A., *et al.* (2024) Plasmodesmal closure elicits stress responses. *bioRxiv*, 2024.2005.2008.593115.
- Tian, H., Wu, Z., Chen, S., Ao, K., Huang, W., Yaghmaiean, H., *et al.* (2021) Activation of TIR signalling boosts pattern-triggered immunity. *Nature*, **598**, 500-503.
- Turner, S. E., Pang, Y.-Y., O'Malley, M. R., Weisberg, A. J., Fraser, V. N., Yan, Q., *et al.* (2020) A DeoR-type transcription regulator is required for sugar-induced expression of type III secretion-encoding genes in *Pseudomonas syringae* pv. tomato DC3000. *Molecular Plant-Microbe Interactions*, **33**, 509-518.
- Van den Ende, W., Lammens, W., Van Laere, A., Schroeven, L. and Le Roy, K. (2009) Donor and acceptor substrate selectivity among plant glycoside hydrolase family 32 enzymes. *The FEBS Journal*, **276**, 5788-5798.
- Van Kan, J. A., Stassen, J. H., Mosbach, A., Van Der Lee, T. A., Faino, L., Farmer, A. D., *et al.* (2017) A gapless genome sequence of the fungus *Botrytis cinerea*. *Mol Plant Pathol*, **18**, 75-89.
- Veillet, F. (2016) Étude des mécanismes moléculaires et biochimiques du transport de sucres dans les relations source/puits et au cours de l'interaction entre *Arabidopsis thaliana* et le champignon nécrotrophe *Botrytis cinerea*.
- Veillet, F., Gaillard, C., Coutos-Thévenot, P. and La Camera, S. (2016) Targeting the *AtCWIN1* gene to explore the role of invertases in sucrose transport in roots and during *Botrytis cinerea* infection. *Front Plant Sci*, **7**, 1899.
- Vélez-Bermúdez, I. C. and Schmidt, W. (2021) Chromatin enrichment for proteomics in plants (ChEP-P) implicates the histone reader ALFIN-LIKE 6 in jasmonate signalling. *BMC Genomics*, **22**, 845.
- Verhaest, M., Lammens, W., Le Roy, K., De Coninck, B., De Ranter, C. J., Van Laere, A., *et al.* (2006) X-ray diffraction structure of a cell-wall invertase from *Arabidopsis thaliana*. *Acta Crystallogr D Biol Crystallogr*, **62**, 1555-1563.
- Von Bodman, S. B., Bauer, W. D. and Coplín, D. L. (2003) Quorum sensing in plant-pathogenic bacteria. *Annu Rev Phytopathol*, **41**, 455-482.
- Vu, D. P., Martins Rodrigues, C., Jung, B., Meissner, G., Klemens, P. A. W., Holtgräwe, D., *et al.* (2020) Vacuolar sucrose homeostasis is critical for plant development, seed properties, and night-time survival in *Arabidopsis*. *J Exp Bot*, **71**, 4930-4943.
- Wadler, C. S. and Vanderpool, C. K. (2007) A dual function for a bacterial small RNA: SgrS performs base pairing-dependent regulation and encodes a functional polypeptide. *Proceedings of the National Academy of Sciences*, **104**, 20454-20459.
- Wan, J., Tanaka, K., Zhang, X. C., Son, G. H., Brechenmacher, L., Nguyen, T. H., *et al.* (2012) LYK4, a lysin motif receptor-like kinase, is important for chitin signaling and plant innate immunity in *Arabidopsis*. *Plant Physiol*, **160**, 396-406.

- Wang, H., Smith, A., Lovelace, A. and Kvitko, B. H. (2022a) In planta transcriptomics reveals conflicts between pattern-triggered immunity and the AlgU sigma factor regulon. *PLoS One*, **17**, e0274009.
- Wang, J., Gilles, E. D., Lengeler, J. W. and Jahreis, K. (2001) Modeling of inducer exclusion and catabolite repression based on a PTS-dependent sucrose and non-PTS-dependent glycerol transport systems in *Escherichia coli* K-12 and its experimental verification. *J Biotechnol*, **92**, 133-158.
- Wang, J., Hu, M., Wang, J., Qi, J., Han, Z., Wang, G., *et al.* (2019) Reconstitution and structure of a plant NLR resistosome conferring immunity. *Science*, **364**, eaav5870.
- Wang, J., Wang, A., Luo, Q., Hu, Z., Ma, Q., Li, Y., *et al.* (2022b) Glucose sensing by regulator of G protein signaling 1 (RGS1) plays a crucial role in coordinating defense in response to environmental variation in tomato. *New Phytol*, **236**, 561-575.
- Wang, Z., He, Z., Liu, Z., Qu, M., Gao, C., Wang, C., *et al.* (2023) A reverse chromatin immunoprecipitation technique based on the CRISPR-dCas9 system. *Plant Physiol*, **191**, 1505-1519.
- Weil, M., Krausgrill, S., Schuster, A. and Rausch, T. (1994) A 17-kDa *Nicotiana tabacum* cell-wall peptide acts as an in-vitro inhibitor of the cell-wall isoform of acid invertase. *Planta*, **193**, 438-445.
- Wen, X., Wang, J., Zhang, D., Ding, Y., Ji, X., Tan, Z., *et al.* (2020) Reverse chromatin immunoprecipitation (R-ChIP) enables investigation of the upstream regulators of plant genes. *Communications Biology*, **3**, 770.
- Westhoek, A., Clark, L. J., Culbert, M., Dalchau, N., Griffiths, M., Jorin, B., *et al.* (2021) Conditional sanctioning in a legume–*Rhizobium* mutualism. *Proceedings of the National Academy of Sciences*, **118**, e2025760118.
- Wright, C. A. and Beattie, G. A. (2004) *Pseudomonas syringae* pv. tomato cells encounter inhibitory levels of water stress during the hypersensitive response of *Arabidopsis thaliana*. *Proceedings of the National Academy of Sciences*, **101**, 3269-3274.
- Xie, J., Cai, K., Hu, H. X., Jiang, Y. L., Yang, F., Hu, P. F., *et al.* (2016) structural analysis of the catalytic mechanism and substrate specificity of *Anabaena Alkaline* invertase InvA reveals a novel glucosidase. *J Biol Chem*, **291**, 25667-25677.
- Xiong, Y., McCormack, M., Li, L., Hall, Q., Xiang, C. and Sheen, J. (2013) Glucose–TOR signalling reprograms the transcriptome and activates meristems. *Nature*, **496**, 181-186.
- Xuan, Y. H., Hu, Y. B., Chen, L. Q., Sosso, D., Ducat, D. C., Hou, B. H., *et al.* (2013) Functional role of oligomerization for bacterial and plant SWEET sugar transporter family. *Proceedings of the National Academy of Sciences*, **110**, E3685-3694.
- Yamada, K., Saijo, Y., Nakagami, H. and Takano, Y. (2016) Regulation of sugar transporter activity for antibacterial defense in *Arabidopsis*. *Science*, **354**, 1427-1430.
- Yamada, K. and Mine, A. (2024) Sugar coordinates plant defense signaling. *Sci Adv*, **10**, eadk4131.
- Yang, J., Luo, D., Yang, B., Frommer, W. B. and Eom, J. S. (2018) SWEET11 and 15 as key players in seed filling in rice. *New Phytol*, **218**, 604-615.

- Yang, S., Fu, Y., Zhang, Y., Peng Yuan, D., Li, S., Kumar, V., *et al.* (2023) *Rhizoctonia solani* transcriptional activator interacts with rice WRKY53 and grassy tiller 1 to activate SWEET transporters for nutrition. *J Adv Res*, **50**, 1-12.
- Ye, R., Wang, M., Du, H., Chhajed, S., Koh, J., Liu, K. H., *et al.* (2022) Glucose-driven TOR-FIE-PRC2 signalling controls plant development. *Nature*, **609**, 986-993.
- Yheskel, M., Sidoli, S. and Secombe, J. (2023) Proximity labeling reveals a new in vivo network of interactors for the histone demethylase KDM5. *Epigenetics & Chromatin*, **16**, 8.
- Yuan, M., Jiang, Z., Bi, G., Nomura, K., Liu, M., Wang, Y., *et al.* (2021) Pattern-recognition receptors are required for NLR-mediated plant immunity. *Nature*, **592**, 105-109.
- Zhang, B., Shao, L., Wang, J., Zhang, Y., Guo, X., Peng, Y., *et al.* (2021) Phosphorylation of ATG18a by BAK1 suppresses autophagy and attenuates plant resistance against necrotrophic pathogens. *Autophagy*, **17**, 2093-2110.
- Zhang, S., Kan, J., Liu, X., Wu, Y., Zhang, M., Ou, J., *et al.* (2023) Phytopathogenic bacteria utilize host glucose as a signal to stimulate virulence through LuxR homologues. *Mol Plant Pathol*, **24**, 359-373.
- Zhang, Z., Rong, X., Xie, T., Li, Z., Song, H., Zhen, S., *et al.* (2024) Fluorogenic CRISPR for genomic DNA imaging. *Nature Communications*, **15**, 934.
- Zheng, N., Li, T., Dittman, J. D., Su, J., Li, R., Gassmann, W., *et al.* (2020) CRISPR/Cas9-based gene editing using egg cell-specific promoters in Arabidopsis and soybean. *Front Plant Sci*, **11**, 800.
- Zhou, J., Wang, X., He, Y., Sang, T., Wang, P., Dai, S., *et al.* (2020) Differential phosphorylation of the transcription factor WRKY33 by the protein kinases CPK5/CPK6 and MPK3/MPK6 cooperatively regulates camalexin biosynthesis in Arabidopsis. *Plant Cell*, **32**, 2621-2638.
- Zhu, J., Lolle, S., Tang, A., Guel, B., Kvitko, B., Cole, B., *et al.* (2023) Single-cell profiling of Arabidopsis leaves to *Pseudomonas syringae* infection. *Cell Reports*, **42**, 112676.
- Zuo, J., Niu, Q. W. and Chua, N. H. (2000) Technical advance: An estrogen receptor-based transactivator XVE mediates highly inducible gene expression in transgenic plants. *Plant J*, **24**, 265-273.

Appendix

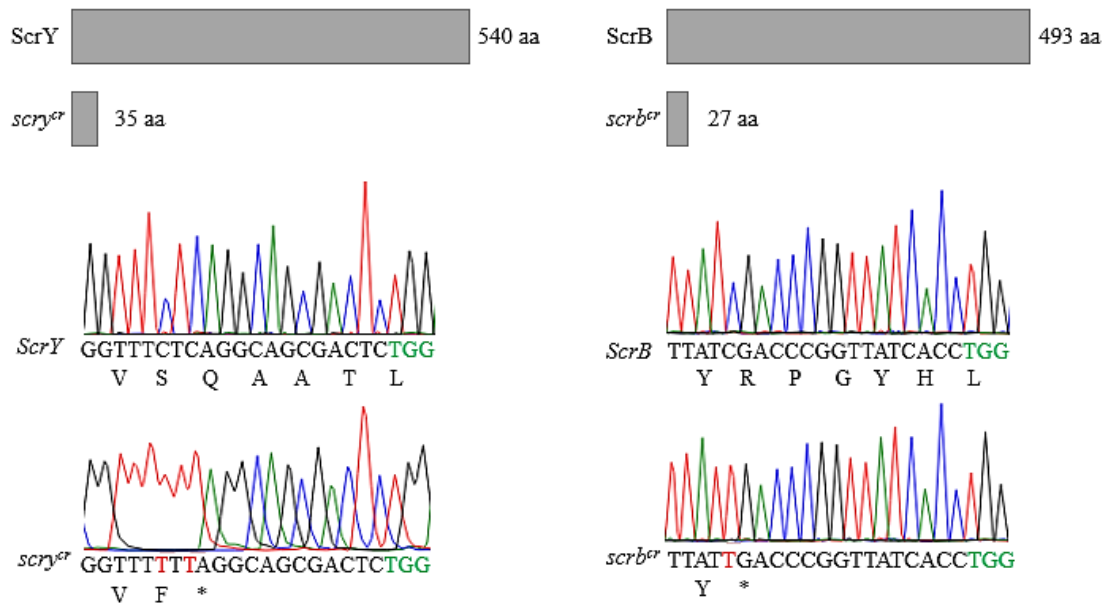


Fig. A1. Generation of the *ScrY* knockout mutant and the *ScrB* knockout mutant by the CRISPR/Cas9 genome editing tool. Protein lengths (upper panel) encoded by sucrose porin precursor gene *ScrY* (PSPTO_0890, 540 aa), sucrose-6-phosphate hydrolase gene *ScrB* (PSPTO_0885, 493 aa) in *Pst* DC3000, *scry^{cr}* (35 aa) in *Pst* DC3000 knockout strain *scry^{cr}*, and *scrbc^{cr}* (27 aa) in *Pst* DC3000 knockout strain *scrbc^{cr}*. Sanger sequencing chromatograms (lower panel) of *Pst* DC3000, *scry^{cr}*, and *scrbc^{cr}* are shown. C-to-A mutations are highlighted in red. Protospacer adjacent motifs are highlighted in green. An asterisk indicates premature stop codons. Amino acids encoded by the guide RNA protospacers are shown in abbreviation. aa, amino acid.

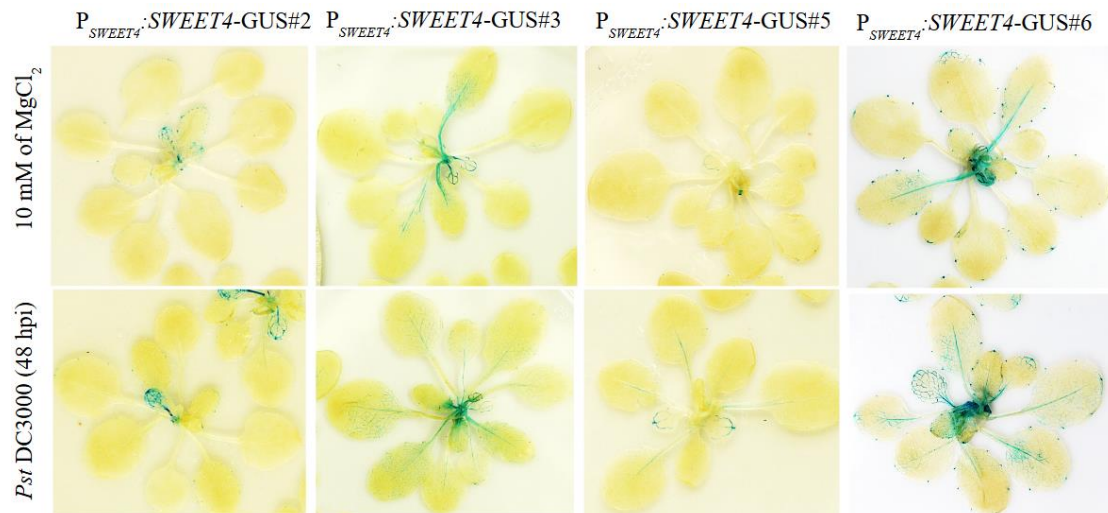


Fig. A2. GUS fusion of the Arabidopsis plasma membrane-localized hexose uniporter *SWEET4* accumulates in cotyledon, midvein, and hydathode. Transgenic Arabidopsis plants (*P_{SWEET4}:SWEET4-GUS* reporter lines 2, 3, 5, and 6) are spray-inoculated with 10 mM of $MgCl_2$ (upper panel) or *Pst* DC3000 inoculum (10^8 colony-forming units mL^{-1}) (lower panel). One representative β -glucuronidase (GUS)-stained transgenic Arabidopsis plant shows GUS activity in cotyledon, midvein, and hydathode at 48 hours post-inoculation. Scale bars: 1 cm. $n = 2-4$ biological replicates. The experiment has been performed once.

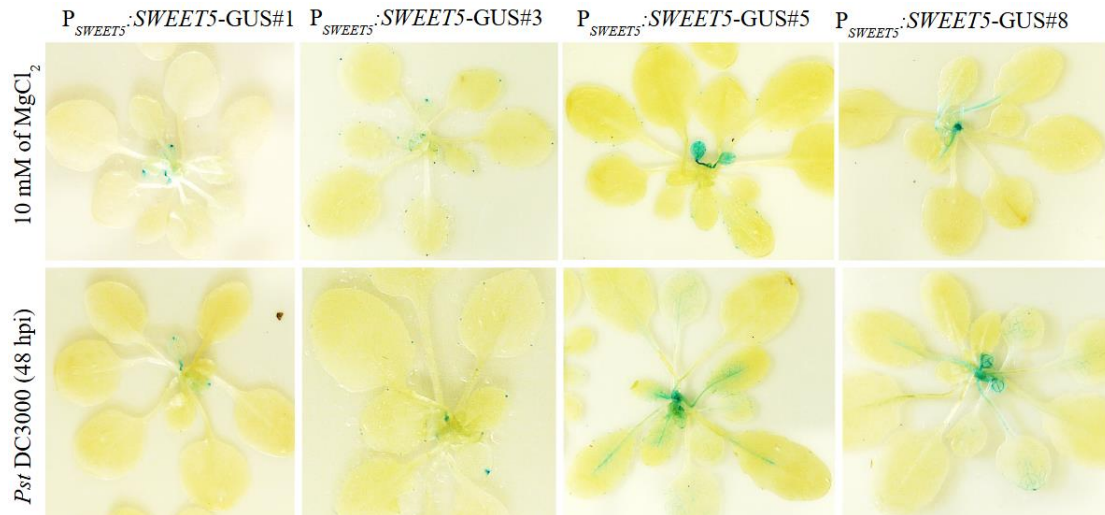


Fig. A3. GUS fusion of the Arabidopsis plasma membrane-localized hexose uniporter SWEET5 accumulates in cotyledon, midvein, and hydathode. Transgenic Arabidopsis plants ($P_{SWEET5}:SWEET5$ -GUS reporter lines 1, 3, 5, and 8) are spray-inoculated with 10 mM of $MgCl_2$ (upper panel) or *Pst* DC3000 inoculum (10^8 colony-forming units mL^{-1}) (lower panel). One representative β -glucuronidase (GUS)-stained transgenic Arabidopsis plant shows GUS activity in cotyledon, midvein, and hydathode at 48 hours post-inoculation. Scale bars: 1 cm. $n = 2$ biological replicates. The experiment has been performed once.

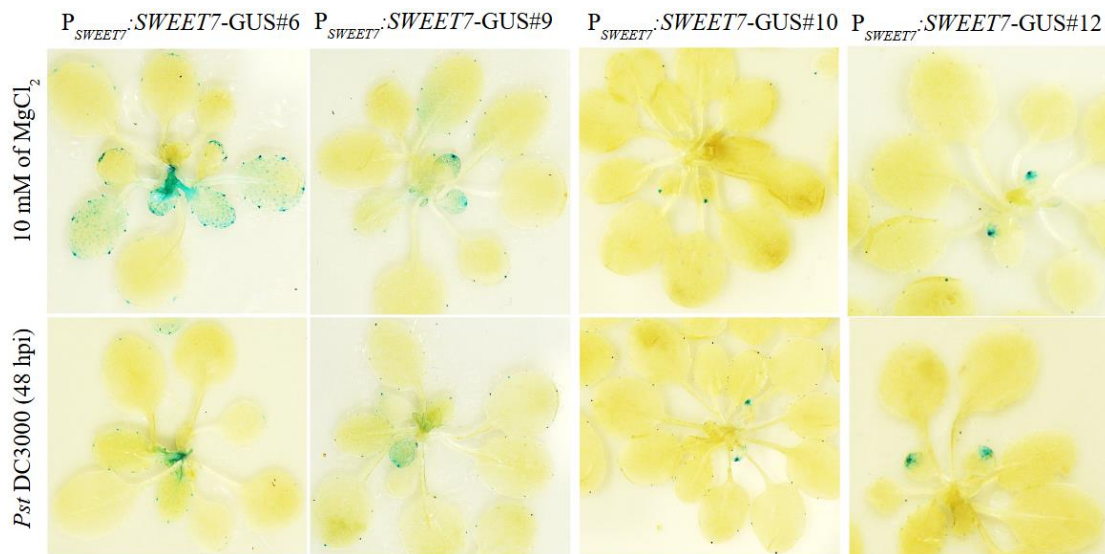


Fig. A4. GUS fusion of the Arabidopsis plasma membrane-localized hexose uniporter SWEET7 accumulates in cotyledon and hydathode. Transgenic Arabidopsis plants ($P_{SWEET7}:SWEET7$ -GUS reporter lines 6, 9, 10, and 12) are spray-inoculated with 10 mM of $MgCl_2$ (upper panel) or *Pst* DC3000 inoculum (10^8 colony-forming units mL^{-1}) (lower panel). One representative β -glucuronidase (GUS)-stained transgenic Arabidopsis plant shows GUS activity in cotyledon and hydathode at 48 hours post-inoculation. Scale bars: 1 cm. $n = 2-4$ biological replicates. The experiment has been performed once.

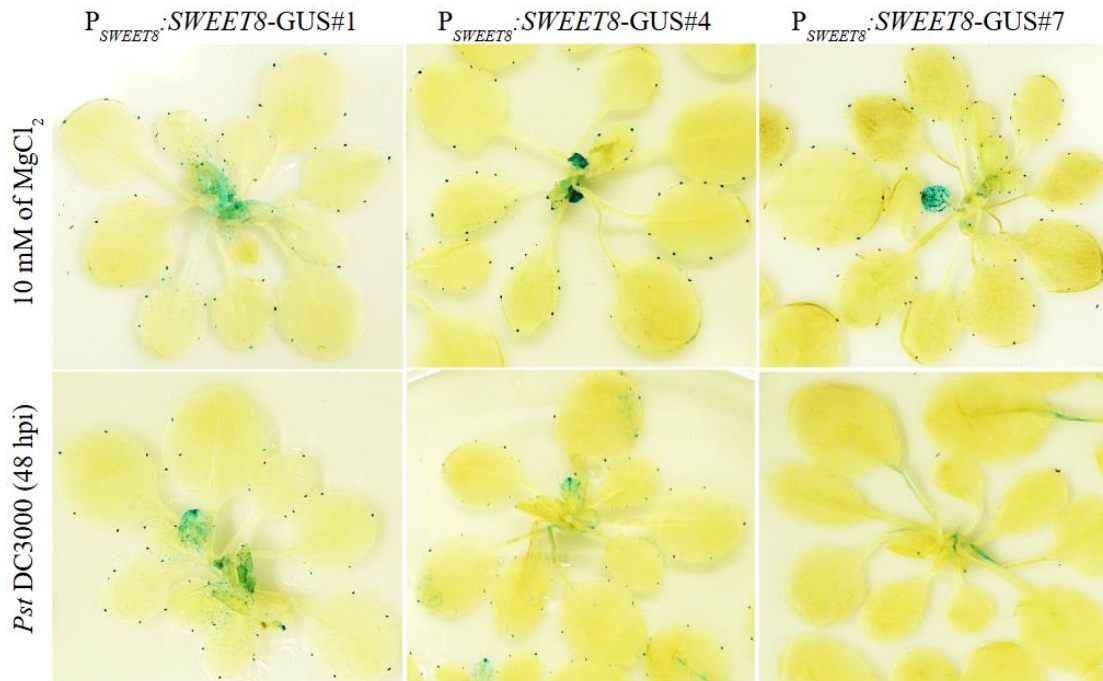


Fig. A5. GUS fusion of the Arabidopsis plasma membrane-localized hexose uniporter SWEET8 accumulates in cotyledon, midvein, and hydathode. Transgenic Arabidopsis plants ($P_{SWEET8}:SWEET8$ -GUS reporter lines 1, 4, and 7) are spray-inoculated with 10 mM of $MgCl_2$ (upper panel) or *Pst* DC3000 inoculum (10^8 colony-forming units mL^{-1}) (lower panel). One representative β -glucuronidase (GUS)-stained transgenic Arabidopsis plant shows GUS activity in cotyledon, midvein, and hydathode at 48 hours post-inoculation. Scale bars: 1 cm. $n = 2$ -4 biological replicates. The experiment has been performed once.

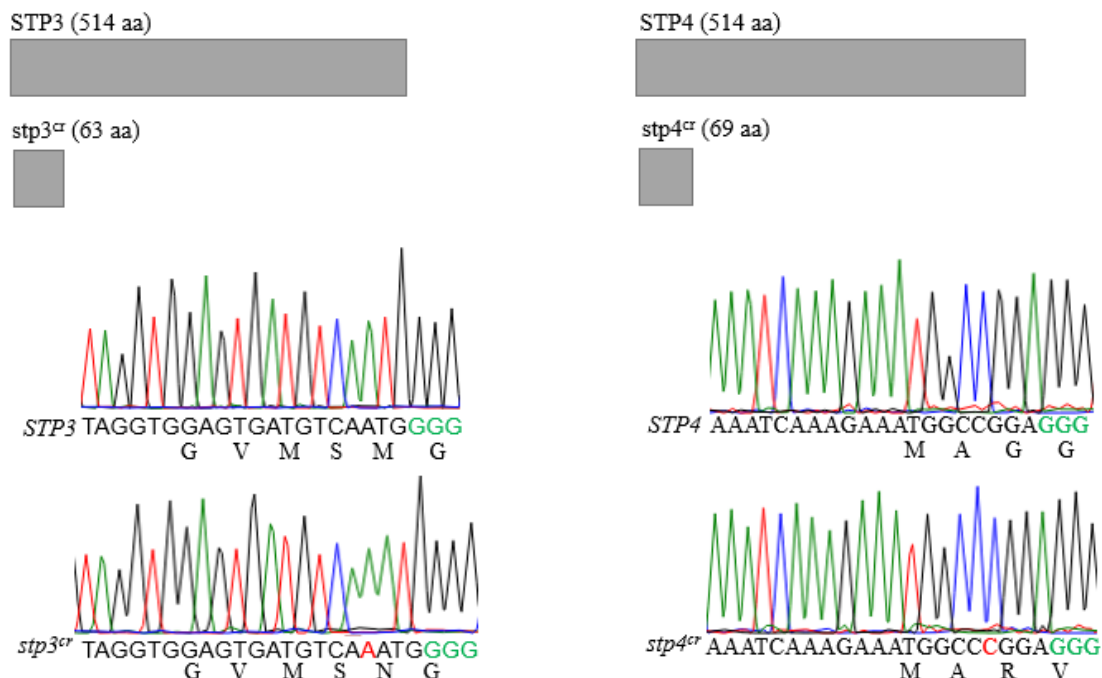


Fig. A6. Generation of the STP3 and STP4 double knockout mutant by the CRISPR/Cas9 genome editing tool. Protein lengths (upper panel) encoded by plasma membrane-localized proton/hexose symporter genes *STP3* (AT5G61520, 514 aa), *STP4* (AT3G19930, 514 aa) in Arabidopsis Col-0 and *stp3*^{cr} (63 aa), *stp4*^{cr} (69 aa) in Arabidopsis double mutant *stp3;4*^{cr}. Sanger sequencing chromatograms (lower panel) of Col-0 and *stp3;4*^{cr} are shown. Frameshift mutation is highlighted in red. Protospacer adjacent motifs are highlighted in green. Amino

acids encoded by the guide RNA protospacers are shown in abbreviation. aa, amino acid.

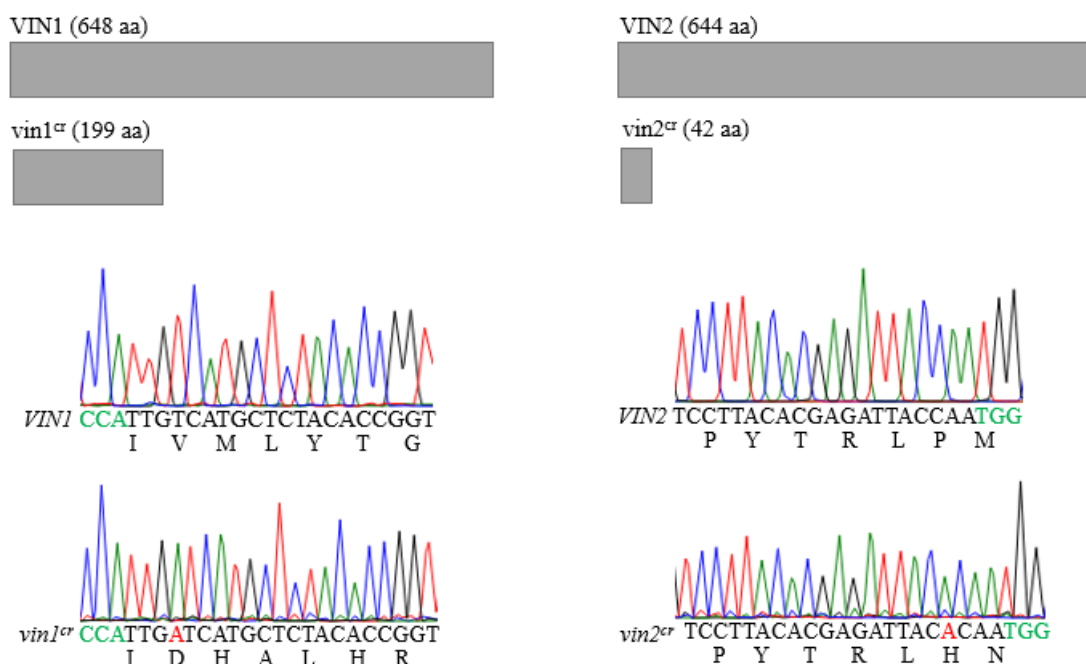


Fig. A7. Generation of the VIN1 and VIN2 double knockout mutant by the CRISPR/Cas9 genome editing tool. Protein lengths (upper panel) encoded by vacuolar invertase genes *VIN1* (AT1G62660, 648 aa), *VIN2* (AT1G12240, 644 aa) in Arabidopsis Col-0 and *vin1*^{cr} (199 aa), *vin2*^{cr} (42 aa) in Arabidopsis double mutant *vin1*;*2*^{cr}. Sanger sequencing chromatograms (lower panel) of Col-0 and *vin1*;*2*^{cr} are shown. Frameshift mutation is highlighted in red. Protospacer adjacent motifs are highlighted in green. Amino acids encoded by the guide RNA protospacers are shown in abbreviation. aa, amino acid.

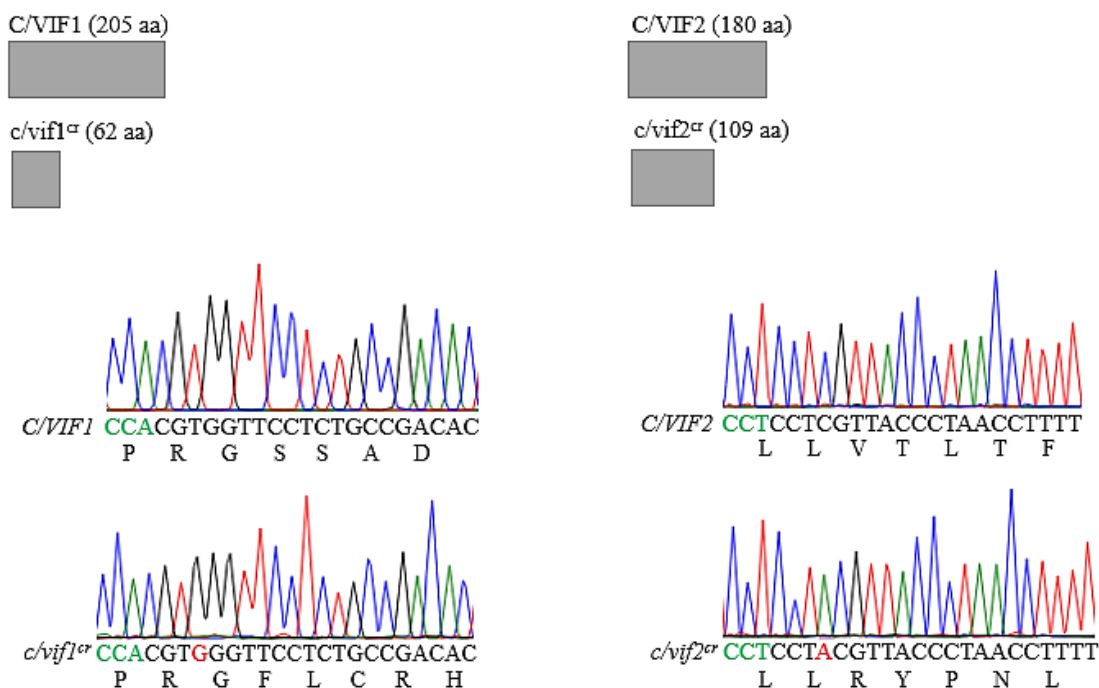


Fig. A8. Generation of the C/VIF1 and C/VIF2 double knockout mutant by the CRISPR/Cas9 genome editing tool. Protein lengths (upper panel) encoded by cell wall/vacuolar inhibitors of fructosidase genes *C/VIF1* (AT1G47960, 205 aa), *C/VIF2* (AT5G64620, 180 aa) in Arabidopsis Col-0 and *c/vif1*^{cr} (62 aa), *c/vif2*^{cr} (109 aa) in Arabidopsis

double mutant *c/vif1;2^{cr}*. Sanger sequencing chromatograms (lower panel) of Col-0 and *c/vif1;2^{cr}* are shown. Frameshift mutation is highlighted in red. Protospacer adjacent motifs are highlighted in green. Amino acids encoded by the guide RNA protospacers are shown in abbreviation. aa, amino acid.

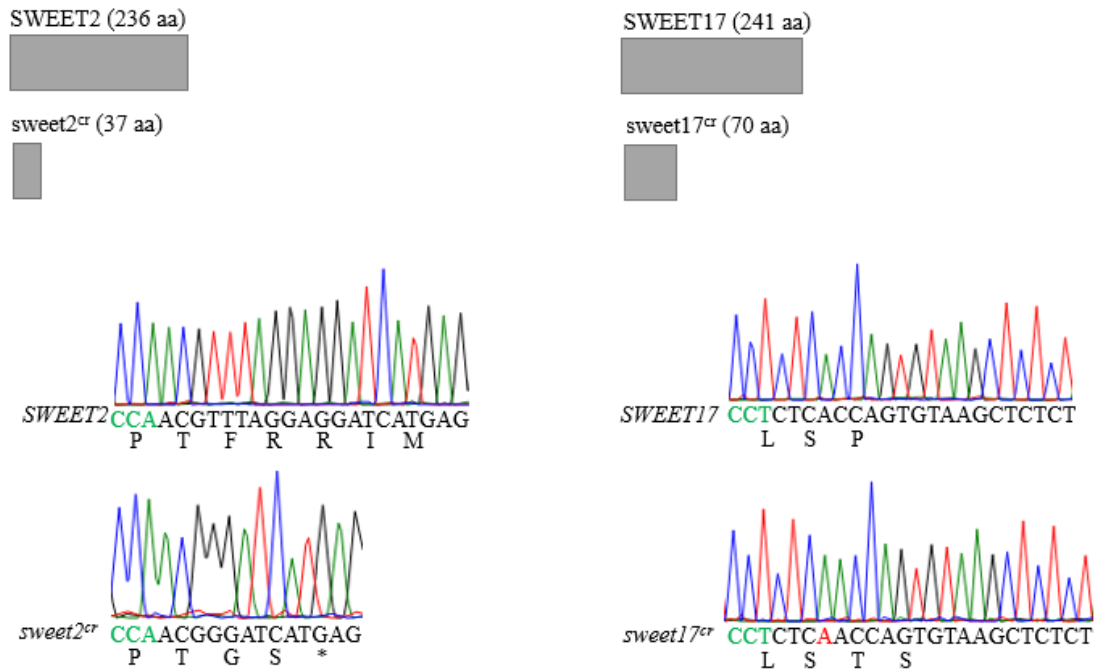


Fig. A9. Generation of the SWEET2 and SWEET17 double knockout mutant by the CRISPR/Cas9 genome editing tool. Protein lengths (upper panel) encoded by tonoplast-localized hexose uniporter genes *SWEET2* (AT3G14770, 236 aa), *SWEET17* (AT4G15920, 241 aa) in Arabidopsis Col-0 and *sweet2^{cr}* (37 aa), *sweet17^{cr}* (70 aa) in Arabidopsis double mutant *sweet2;17^{cr}*. Sanger sequencing chromatograms (lower panel) of Col-0 and *sweet2;17^{cr}* are shown. Frameshift mutation is highlighted in red. Protospacer adjacent motifs are highlighted in green. An asterisk indicates premature stop codons. Amino acids encoded by the guide RNA protospacers are shown in abbreviation. aa, amino acid.

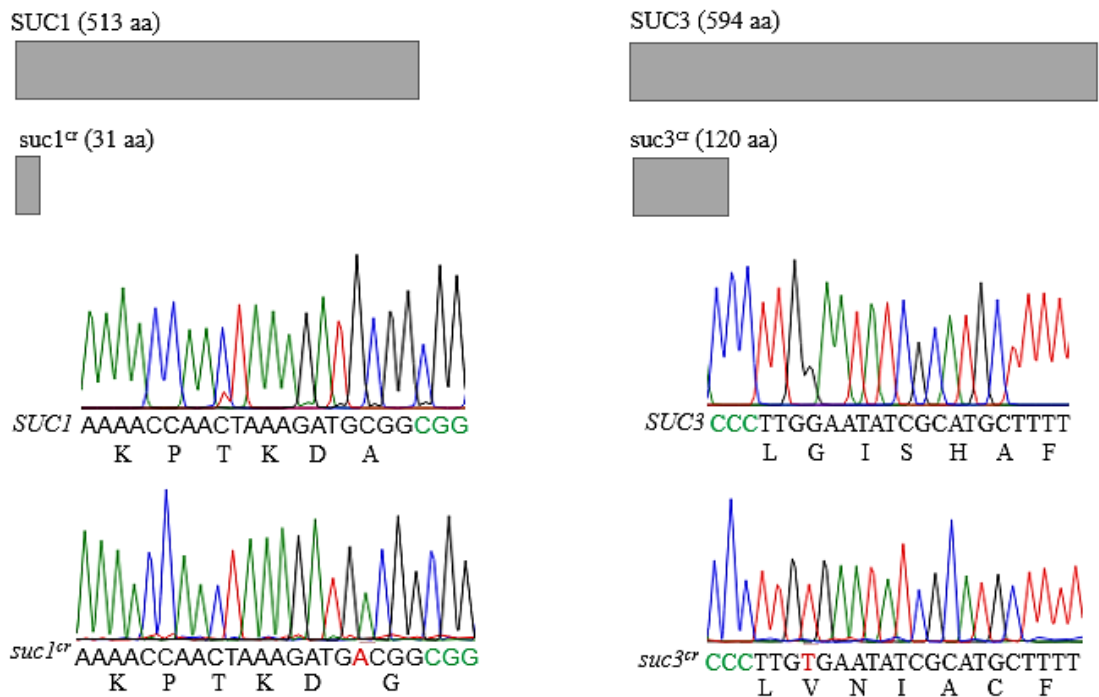


Fig. A10. Generation of the SUC1 and SUC3 double knockout mutant by the CRISPR/Cas9 genome editing tool. Protein lengths (upper panel) encoded by plasma membrane-localized proton/sucrose symporter genes *SUC1* (AT1G71880, 513 aa), *SUC3* (AT2G02860, 594 aa) in Arabidopsis Col-0 and *suc1^{cr}* (31 aa), *suc3^{cr}* (120 aa) in Arabidopsis double mutant *suc1;3^{cr}*. Sanger sequencing chromatograms (lower panel) of Col-0 and *suc1;3^{cr}* are shown. Frameshift mutation is highlighted in red. Protospacer adjacent motifs are highlighted in green. Amino acids encoded by the guide RNA protospacers are shown in abbreviation. aa, amino acid.

Table A1. DNA oligonucleotides used in this study

Name of oligonucleotides	DNA Sequence of DNA oligonucleotides (5 to 3)	Purpose of DNA oligonucleotides
SWEET4-F	GCAGGTCGACTCTAGAAGTGGTTCCA CGGAGATGACG	Used with SWEET4-R to amplify P _{SWEET4} :SWEET4
SWEET4-R	CGGTACCCGGGGATCCAGCTGAAACT CGTTAGCTTGTC	
SWEET4-ACCT-F	AGTGAAGCTTGGTCTCAACCTAGTGG TTCCACGGAGATG	Used with SWEET4-TCAG-R to amplify P _{SWEET4} :SWEET4 for GreenGate cloning
SWEET4-TCAG-R	GCGAGAATTCGGTCTCACTGAAGCTG AAACTCGTTTACG	
SWEET5-F	GCAGGTCGACTCTAGATTAGGACTGA CACCAGCGATGC	Used with SWEET5-R to amplify P _{SWEET5} :SWEET5
SWEET5-R	CGGTACCCGGGGATCCAGCCTGGCCA AGTTCGATTC	
SWEET7-F	GCAGGTCGACTCTAGAATTCAGGCTT GGCGTAACTTG	Used with SWEET7-R to amplify P _{SWEET7} :SWEET7
SWEET7-R	CGGTACCCGGGGATCCAACATTGTTA GGTTCTTGGTTGG	
SWEET8-F	GCAGGTCGACTCTAGAACCATGACAA TTTGGCTCCGAG	Used with SWEET8-R to amplify P _{SWEET8} :SWEET8
SWEET8-R	CGGTACCCGGGGATCCAACCCTCTCC GTAGCAGAAATC	
ScrY-Q36-GTGG	GTGGGGTTTCTCAGGCAGCGACTC	Used with ScrY-Q36-AAAC to create the 20 bp gRNA spacer targeting ScrY (PSPTO_0890) in pnCasPA-BEC
ScrY-Q36-AAAC	AAACGAGTCGCTGCCTGAGAAACC	
ScrB-R28-GTGG	GTGGTTATCGACCCGGTTATCACC	Used with ScrB-R28-AAAC to create the 20 bp gRNA spacer targeting ScrB (PSPTO_0885) in pnCasPA-BEC
ScrB-R28-AAAC	AAACGGTGATAACCGGGTGCATAA	
ScrY-F	CAGGAAGAAGAGATTTACAGC	Used with ScrY-R to screen pnCasPA-BEC-mediated mutagenesis
ScrY-R	CATAGCCCTTAAAGCTGAAG	
ScrB-F	ATGAGCAACCCGATGTC	Used with ScrB-R to screen pnCasPA-BEC-mediated mutagenesis
ScrB-R	CACTGCACCTGACGGATA	
CINV1-F	CAGCGATCGCACCAGTTAGTCCGCT TCTCTCTGT	Used with CINV1-R to amplified P _{CINV1} :CINV1
CINV1-R	GGGACATCGTATGGGTAGAGTTGTGG CCAAGACGC	

<i>attL2</i> -F	TACCCATACGATGTCACCCAGCTTTC TTGTACA	Used with <i>attL1</i> -R to amplified pDONR221
<i>attL1</i> -R	CTGGTGCGATCGCTGGTAGCGTTAAC CATTTCGA	
P2A- <i>attL2</i> -F	CCTGGACCTAAGGGTTCACCCAGCTT TCTTGTACA	Used with CINV1-R to amplified pDONR221- <i>P_{CINV1}:CINV1</i>
HA-F	TACCCATACGATGTCCCC	Used with P2A-R to amplified HA-P2A or with pGGZ003-R to amplified pGreenII-HA-P2A- eGFP-GUS
P2A-R	ACCCTTAGGTCCAGGAT	
<i>KpnI</i> -P2A-F	CGATCGCACCAAGTACCGACTACGCA GCAGCTACAGGATCT	Used with GUS-R to amplified P2A-eGFP-GUS
GUS-R	ACGAAAGCTTTGCAGGTCATTGTTTG CCTCCCTG	
pGGZ003-R	CTGGTGCGATCGCTGTT	
HA-P2A	ACCTACCATACGATGTCCTGACTA CGCAGCAGCTACAGGATCTG	for adding HA peptide
CINV2-F	CAGCGATCGCACCAAGACATTAGCTCG ACGAGAA	Used with CINV2-R to amplified <i>P_{CINV2}:CINV2</i>
CINV2-R	GGGACATCGTATGGGTAGCAAGTCCA TGAAGCAGA	
C/VIF1-F	CAGCGATCGCACCAAGAACAGTCA CAAATGAATCTAA	Used with C/VIF1-R to amplified <i>P_{C/VIF1}:C/VIF1</i>
C/VIF1-R	GACATCGTATGGGTAGGTCCAACAAG TTCTTCCTCTATTG	
C/VIF2-F	CAGCGATCGCACCAAGGAGTGTG GCCCAATA	Used with C/VIF2-R to amplified <i>P_{C/VIF2}:C/VIF2</i>
C/VIF2-R	GGGACATCGTATGGGTATTCAACAAG GCGATCAAGA	
VIN1-1-F	CAGCGATCGCACCAAGCCTGCCGAAT TGATTCTCG	Used with VIN1-1-R to amplified the first part of <i>P_{VIN1}:VIN1</i>
VIN1-1-R	TATCTATCAATTGTGTAGCCA	
VIN1-2-F	TGGCTACACAATTGATAG	Used with VIN1-2-R to amplified the second part of <i>P_{VIN1}:VIN1</i>
VIN1-2-R	GACATCGTATGGGTAGGTGCTGGAAG GAACACC	
VIN2-F	CAGCGATCGCACCAAGATTGTGGGTTC ATACCAATAATT	Used with VIN2-R to amplified <i>P_{VIN2}:VIN2</i>
VIN2-R	GACATCGTATGGGTAGGTACGGGAG AGAGCACG	
CWINV1-F	CAGCGATCGCACCAAGACATGGTGTGG GTCTTCT	Used with CWINV1-R to amplified <i>P_{CWINV1}:CWINV1</i>
CWINV1-R	GGGACATCGTATGGGTAAGTATTTG GGCAGAGTT	
SUC1-F	CAGCGATCGCACCAAGCAGTTAAGTTT TCGGTTCAC	Used with SUC1-R to amplified <i>P_{SUC1}:SUC1</i>
SUC1-R	GGGACATCGTATGGGTAGTGAATCC TCCCATGGT	
SUC3-1-F	CAGCGATCGCACCAAGGAGTGTG GATATAAGAGTTC	Used with SUC3-1-R to amplified the first part of <i>P_{SUC3}:SUC3</i>

SUC3-1-R	AGTAAGAAGAGAAAGTTGCA	
SUC3-2-F	TTGCAACTTTCTCTCT	Used with SUC3-2-R to amplified the first part of P _{SUC3} :SUC3
SUC3-2-R	GGGACATCGTATGGGTAGCCGATGTG GAAACCGGT	
STP1-1-F	GCCAACAGCGATCGCACCAGTGAATT CAAACCCGTGAC	Used with STP1-1-R to amplified the first part of P _{STP1} :STP1
STP1-1-R	ATAGACAGTGGGAATAGAA	
STP1-2-F	TTCTATTCCCCACTGTCT	Used with STP1-2-R to amplified the second part of P _{STP1} :STP1
STP1-2-R	TCGGGGACATCGTATGGGTAAACATG CTTCGTTCCAGC	
SapI-HA-F	GGCTACGCTCTTCCCTTAGCCATTAC CCATACGATGTCCCC	Used with SapI-RB-R to amplified pGreenII-HA-P2A-eGFP-GUS
SapI-RB-R	GGCTACGCTCTTCTACCAACAGAATA CTGGTGCGATCGCTGTTG	
STP3-SapI-F	GGCTACGCTCTTCTGGTGCCACGTGT AATAAG	Used with STP3-SapI-R to amplified P _{STP3} :STP3 with SapI site
STP3-SapI-R	GGCTACGCTCTTCCAAGAATGGTGGT TTCTTG	
STP4-F	GCCAACAGCGATCGCACCAGGCGAT ATCGAGATGTGAC	Used with STP4-R to amplified P _{STP4} :STP4
STP4-R	TCGGGGACATCGTATGGGTATACGGA CTTCTGTTGCAT	
STP13-F	CAGCGATCGCACCAGTCGTGACTTAG CAGACTC	Used with STP13-R to amplified P _{STP13} :STP13
STP13-R	GGGACATCGTATGGGTAAAGCCGTGT TGAAGGATC	
SWEET4-ATTG	ATTGGGGAGATAAGAACAAGAACA	Used with SWEET4-AAAC to create the 20 bp gRNA spacer targeting SWEET4 in pCR-gRNA
SWEET4-AAAC	AAACTGTTCTTGTCTTATCTCCC	
UMAMIT18-GTCA	GTCAAAAGGGAGCCATGACAACCG	Used with UMAMIT18-AAAC to create the 20 bp gRNA spacer targeting UMAMIT18 in pCR-gRNA
UMAMIT18-AAAC	AAACCGTTGTCATGGCTCCCTTT	
UMAMIT20-ATTG	ATTGATTATGGCCACTCTTAACCA	Used with UMAMIT20-AAAC to create the 20 bp gRNA spacer targeting AtUMAMIT20 in pCR-gRNA
UMAMIT20-AAAC	AAACTGGTTAAGAGTGGCCATAAT	
UMAMIT29-GTCA	GTCACGAGCTTGTGGATGAGAATG	Used with UMAMIT29-AAAC to create the 20 bp gRNA spacer targeting UMAMIT29 in pCR-gRNA
UMAMIT29-AAAC	AAACCATTCTCATCCACAAGCTCG	
SWEET2-BsaI-F	GGCTACGGTCTCCATTGCTCATGATC CTCCTAAACGTGTTTTAGAGCTAGAA ATAGC	Used with SWEET17-BsaI-R to amplify gRNA expression cassette
SWEET2-CR-F	CGTTTCACCAATGTGAGTTC	Used with SWEET2-CR-R to screen CRISPR-Cas9-mediated mutagenesis
SWEET2-CR-R	GCTGAAACGTAGCTCCAAC	
SWEET17-BsaI-R	GGCTACGGTCTCGAAACCTCACCAGT	

	GTAAGCTCTCTTGACCAATGTTGCTC CC	
AtSWEET17-CR-F	CAAGTGCACGATCCAATAC	Used with SWEET17-CR-R to screen CRISPR-Cas9-mediated mutagenesis
AtSWEET17-CR-R	CGATGATCCTAACAACGTG	
VIN1- <i>Bsa</i> I-F	GGCTACGGTCTCCATTGACCGGTGTA GAGCATGACAAGTTTTAGAGCTAGAA ATAGC	Used with VIN2- <i>Bsa</i> I-R to amplify gRNA expression cassette
VIN1-CR-F	TAGCCATGGTTCCTGAC	Used with VIN1-CR-R to screen CRISPR-Cas9-mediated mutagenesis
VIN1-CR-R	GGGTCTTCAGGATAGGC	
VIN2- <i>Bsa</i> I-R	GGCTACGGTCTCGAAACTTGGAATC TCGTGTAAGGATGACCAATGTTGCTC CC	
VIN2-CR-F	CCCAATTTTCTCTTCCAGC	Used with VIN2-CR-R to screen CRISPR-Cas9-mediated mutagenesis
VIN2-CR-R	TCGTGTGTGGCGATGAG	
SUC1- <i>Bsa</i> I-F	GGCTACGGTCTCCATTGAAAACCAAC TAAAGATGCGGGTTTTAGAGCTAGAA ATAGC	Used with SUC3- <i>Bsa</i> I-R to amplify gRNA expression cassette
SUC1-CR-F	ATGGGAGCCTATGAAACA	Used with SUC1-CR-R to screen CRISPR-Cas9-mediated mutagenesis
SUC1-CR-R	ATAACCGAAATCCGCAG	
SUC3- <i>Bsa</i> I-R	GGCTACGGTCTCGAAACTTGGAATAT CGCATGCTTTTTGACCAATGTTGCTCC C	
SUC3-CR-F	GGTGGGTAGTTATGGTGG	Used with SUC3-CR-R to screen CRISPR-Cas9-mediated mutagenesis
SUC3-CR-R	GCTGGACCTAAAACCCA	
C/VIF1- <i>Bsa</i> I-F	GGCTACGGTCTCCATTGGTGTGGCA GAGGAACCACGGTTTTAGAGCTAGA AATAGC	Used with C/VIF2- <i>Bsa</i> I-R to amplify gRNA expression cassette
C/VIF1-CR-F	AACATGTAAAGAGACACCA	Used with C/VIF1-CR-R to screen CRISPR-Cas9-mediated mutagenesis
C/VIF2-CR-R	AACTACTCATGTCCCACA	
C/VIF2- <i>Bsa</i> I-R	GGCTACGGTCTCGAAACCCTCGTTAC CCTAACCTTTTTGACCAATGTTGCTCC C	
C/VIF2-CR-F	TCCGTAAACAGTTGCTCA	Used with C/VIF2-CR-R to screen CRISPR-Cas9-mediated mutagenesis
C/VIF2-CR-R	TCGGAGCAATCTTGTAAAG	
STP3- <i>Bsa</i> I-F	GGCTACGGTCTCCATTGTAGGTGGAG TGATGTCAATGGTTTTAGAGCTAGAA ATAGC	Used with STP4- <i>Bsa</i> I-R to amplify gRNA expression cassette
STP3-CR-F	GCGTTTGCAAAAAGAATA	Used with STP3-CR-R to screen CRISPR-Cas9-mediated mutagenesis
AtSTP3-CR-R	GGCTATTGAAAAGGCAGT	
STP4- <i>Bsa</i> I-R	GGCTACGGTCTCGAAACTCCGCCAT TTCTTTGATTTTGACCAATGTTGCTCC C	

STP4-CR-F	TCTGCTCTGTTTGTCTGA	Used with STP4-CR-R to screen CRISPR-Cas9-mediated mutagenesis
STP4-CR-R	ATGGCTCCATTGAGGTT	
TurboID-F	TTCTGGCTCAGTCGACGCTAGCAAAG ACAATACTGTGCCTC	Used with mVenus-R to amplify TurboID-mVenus
mVenus-R	TGTTTGAACGATCGGACGTCTCACTT GTACAGCTCGTCCATG	
P_{UBQ10} -F	GGCCAGTGCCAAGCTTCGACGAGTCA GTAATAAACGG	Used with P_{UBQ10} -R to amplify P_{UBQ10}
P_{UBQ10} -R	TGATAGCTTGCGCGCCCTGTTAATC AGAAAACTCAGATT	
<i>attL2</i> -F	AGGATCCTGAATTCGACCCAGCTTTC TTG	Used with <i>attL5</i> -R to delete P_{AtU6} :gRNA in plasmid pYPQ141A
<i>attL5</i> -R	CGAATTCAGGATCCTGCGTTATCTAG AGGG	
Cas9i-D10A-F	GTACTIONTATCGGACTTGCTATTGGTA CGAACTCAGTTGG	Used with Cas9i-H840A-R to mutate D10 and H840 of Cas9i
Cas9i-H840A-R	GAGGGACAATCGCATCCACATCATAG TCGGAGAGT	
Cas9i-H840A-F	TGTGGATGCGATTGTCCCTCAATCTTT CCTGAAG	Used with Cas9i-R to mutate H840 of Cas9i
Cas9i-R	AGAATTCGGTCTCACTGAGTCACCAC CCAACCTGCGA	
pGGC-F	TCAGTGAGACCGAATTCTCG	Used with Cas9-N-terminal-R to amplify pUC19 based entry vector
Cas9-N-terminal-R	AGCAAGTCCGATAGAGTACTTCTTAT C	
GS-linker-F	GTCTCATCAGGTGGAGGCGGTTCAGG AGGTGGC	Used with mVenus-NLS-R to amplify TurboID-mVenus
mVenus-NLS-R	GGTAAAGGTTATCTAAACCTTTCTCT TCTTCTTTGGCTTGACAGCTCGTCCA TG	
pGGD-F	TAGATAACCTTTACCTTCATTCCCT	Used with pGGD-R to amplify pUC19 based entry vector
pGGD-R	TCCACCTGATGAGACCAAGC	
<i>PaqCI</i> -trRNA-F	CCCGAGTTAACGAGTCGGCGGCAGGT GAACACCTGCGCTCGTTTTAGAGCTA GAAATAGC	Used with trRNA- <i>AtIlue</i> -R to amplify <i>PaqCI</i> -trRNA
trRNA- <i>AtIlue</i> -R	TGAGCTACGGGAGCTCGCACCGACTC GGTGCCACTT	
P_{STP13} -agtc	AGTCTAAGTTAAAGAGACCATTGG	Used with P_{STP13} -aaac to create the 20 bp crRNA protospacer for inserting into TRV-RNA2- $P_{PEBV}:trRNA-tRNA^{AtIleu}$
P_{STP13} -aaac	AAACCCAATGGTCTCTTAACTTA	

Table A2. Bacterial and fungal strains used in this study

Resource	Source	Identifier
<i>E. coli</i> TOP10 Competent Cells	Thermo Fisher Scientific	C404003
<i>E. coli</i> Stellar™ Competent Cells	Takara	Cat# 636763
<i>A. tumefaciens</i> GV3101 Competent Cells	Lab stock	N/A
<i>Pseudomonas syringae</i> pv. <i>tomato</i> DC3000	Jane Parker's lab, Max Planck Institute for Plant Breeding Research, Germany	N/A
<i>Pseudomonas syringae</i> pv. <i>tomato</i> DC3000 <i>hrpL</i> ⁻	Jane Parker's lab, Max Planck Institute for Plant Breeding Research, Germany	N/A
<i>Pseudomonas syringae</i> pv. <i>tomato</i> DC3000 <i>scrB</i> ^{cr}	This study	N/A
<i>Pseudomonas syringae</i> pv. <i>tomato</i> DC3000 <i>scry</i> ^{cr}	This study	N/A
<i>B. cinerea</i> B05.10	Department of Plant-Microbe Interactions, Max Planck Institute for Plant Breeding Research, Germany	N/A

Table A3. Arabidopsis lines used in this study

Resource	Source	Identifier
<i>Arabidopsis thaliana</i> Col-0	Lab stock	CS76778
<i>Arabidopsis thaliana</i> Col-0 <i>cinv1</i>	Nottingham Arabidopsis Stock Centre	SALK_095807
<i>Arabidopsis thaliana</i> Col-0 <i>sweet11;12;13</i>	Li-Qing Chen's Lab, University of Illinois at Urbana-Champaign, United States	SALK_073269 SALK_031696 SALK_087791
<i>Arabidopsis thaliana</i> Col-0 <i>c/vif1;2</i> ^{cr}	This study	N/A
<i>Arabidopsis thaliana</i> Col-0 <i>stp3;4</i> ^{cr}	This study	N/A
<i>Arabidopsis thaliana</i> Col-0 <i>suc1;3</i> ^{cr}	This study	N/A
<i>Arabidopsis thaliana</i> Col-0 <i>sweet2;17</i> ^{cr}	This study	N/A
<i>Arabidopsis thaliana</i> Col-0 <i>vin1;2</i> ^{cr}	This study	N/A
<i>Arabidopsis thaliana</i> Col-0 <i>cinv1</i> P _{CIN1} :CIN1-P2A-eGFP-GUS#2	This study	N/A
<i>Arabidopsis thaliana</i> Col-0 P _{CIN2} :CIN2-P2A-eGFP-GUS#10	This study	N/A
<i>Arabidopsis thaliana</i> Col-0 P _{C/VIF1} :C/VIF1-P2A-eGFP-GUS#4	This study	N/A
<i>Arabidopsis thaliana</i> Col-0 P _{C/VIF2} :C/VIF2-P2A-eGFP-GUS#5	This study	N/A
<i>Arabidopsis thaliana</i> Col-0 P _{CWIN1} :CWIN1-P2A-eGFP-GUS#1	This study	N/A
<i>Arabidopsis thaliana</i> Col-0 P _{STP1} :STP1-P2A-eGFP-GUS#1	This study	N/A
<i>Arabidopsis thaliana</i> Col-0 P _{STP3} :STP3-P2A-eGFP-GUS#1	This study	N/A
<i>Arabidopsis thaliana</i> Col-0 P _{STP4} :STP4-P2A-eGFP-GUS#1	This study	N/A
<i>Arabidopsis thaliana</i> Col-0 P _{STP13} :STP13-P2A-eGFP-GUS#2	This study	N/A
<i>Arabidopsis thaliana</i> Col-0 P _{SUC1} :SUC1-P2A-eGFP-GUS#1	This study	N/A
<i>Arabidopsis thaliana</i> Col-0 P _{SUC3} :SUC3-P2A-eGFP-GUS#2	This study	N/A
<i>Arabidopsis thaliana</i> Col-0 P _{SWEET2} :SWEET2-GUS#2,8	Chen et al., 2015a	N/A
<i>Arabidopsis thaliana</i> Col-0 P _{SWEET4} :SWEET4-GUS#2,3,5,6	This study	N/A
<i>Arabidopsis thaliana</i> Col-0 P _{SWEET4} :SWEET4-eGFP#1	This study	N/A
<i>Arabidopsis thaliana</i> Col-0 P _{SWEET5} :SWEET5-GUS#1,3,5,8	This study	N/A
<i>Arabidopsis thaliana</i> Col-0 P _{SWEET7} :SWEET7-GUS#6,9,10,12	This study	N/A
<i>Arabidopsis thaliana</i> Col-0 P _{SWEET8} :SWEET8-GUS#1,4,7	This study	N/A
<i>Arabidopsis thaliana</i> Col-0 P _{SWEET12} :SWEET12-GUS#14	Chen et al., 2012	N/A
<i>Arabidopsis thaliana</i> Col-0 P _{SWEET12} :SWEET12-GFP#3	Chen et al., 2012	N/A
<i>Arabidopsis thaliana</i> Col-0 P _{SWEET17} :SWEET17-GUS#5,9	Guo et al., 2014	N/A
<i>Arabidopsis thaliana</i> Col-0 P _{VIN1} :VIN1-P2A-eGFP-GUS#5	This study	N/A

<i>Arabidopsis thaliana</i> Col-0 P _{VIN2} :VIN2-P2A-eGFP-GUS#2	This study	N/A
<i>Arabidopsis thaliana</i> Col-0 P _{UBQ10} :dCas9-TurboID-mVenus	This study	N/A
<i>Arabidopsis thaliana</i> Col-0 P _{CaMV35S} :XVE-P _{LexA} :dCas9i-TurboID-mVenus	This study	N/A

Table A4. Significantly enriched proteins in *Pst* DC3000 or mock samples ($p < 0.05$)

Representative protein ID	Ordered locus names	log ₂ FC (<i>Pst</i> DC3000 /mock)	<i>p</i> -value
Q87VS5	PSPTO_4860	10.00	0.044
Q42523	AT1G03090	-1.40	0.049
Q42533	AT5G16390	-1.54	0.016
P27140	AT3G01500	-2.52	0.002
P31414	AT1G15690	-2.61	0.033
P59259	AT1G07660 AT1G07820 AT2G28740 AT3G45930 AT3G46320	-2.70	0.049
Q9S7M0	AT5G54270	-2.71	0.027
P38418	AT3G45140	-2.77	0.000
Q9SUI4	AT4G12800	-2.88	0.033
Q8VZ87	AT1G29910 AT1G29920	-3.01	0.025
Q9XF91	AT1G44575	-3.06	0.008
Q9FMU6	AT5G14040	-3.10	0.004
Q9LZT0	AT3G46030	-3.11	0.015
P31167	AT3G08580	-3.11	0.001
Q9S831	AT4G28750	-3.25	0.036
Q9SHE8	AT1G31330	-3.44	0.016
Q9S7J7	AT2G05070	-3.51	0.025
P56761	ATCG00270	-3.51	0.011
Q8RUC6	AT2G35635	-3.51	0.002
Q9C944	AT1G52740	-3.58	0.011
Q42547	AT1G20620	-3.83	0.007
P93004	AT4G35100	-3.90	0.013
Q07473	AT5G01530	-3.99	0.031
Q9LRS0	AT3G14415	-4.08	0.002
O23255	AT4G13940	-4.09	0.001
Q944G9	AT4G38970	-4.13	0.014
Q9LMQ2	AT1G15820	-4.13	0.014
Q9S7N7	AT1G55670	-4.15	0.016
P25071	AT2G41100	-4.21	0.004
Q01667	AT3G54890	-4.26	0.049
O82660	AT5G23120	-4.33	0.002
Q9LRR9	AT3G14420	-4.36	0.001
Q9M1P5	AT3G62290	-4.37	0.015
P56767	ATCG00340	-4.42	0.010
P51419	AT4G15000	-4.47	0.012
P56777	ATCG00680	-4.48	0.013

P10798	AT5G38410	-4.53	0.007
P19366	ATCG00480	-4.56	0.001
O04616	AT4G01150	-4.57	0.013
P83755	ATCG00020	-4.79	0.022
O04019	AT1G09100	-4.83	0.007
Q9XF88	AT3G08940	-4.97	0.037
B6EUB3	AT5G47690	-5.03	0.023
O23654	AT1G78900	-5.08	0.001
P56778	ATCG00280	-5.23	0.017
Q9C9W5	AT1G68010	-5.38	0.003
P56757	ATCG00120	-5.42	0.001
O03042	ATCG00490	-5.46	0.008
Q06611	AT2G45960	-5.46	0.004
Q08770	AT1G26910	-5.51	0.000
P41916	AT5G20010	-5.52	0.019
P56779	ATCG00580	-5.56	0.011
P17745	AT4G20360	-5.56	0.000
P27521	AT3G47470	-5.57	0.018
Q9SY97	AT1G61520	-5.59	0.025
Q9XF89	AT4G10340	-5.69	0.011
Q8W4H7	AT1G07920 AT1G07930 AT1G07940 AT5G60390	-5.81	0.001
P56771	ATCG00540	-5.97	0.008
Q9SIH0	AT2G36160	-5.99	0.004
Q9LZR5	AT5G03740	-6.02	0.033
P49209	AT1G33120 AT1G33140	-6.03	0.007
Q9LR30	AT1G23310	-6.05	0.008
Q9LXG1	AT5G15200	-6.09	0.005
P56773	ATCG00720	-6.12	0.013
P56799	ATCG00380	-6.20	0.002
Q9LX88	AT3G46040	-6.21	0.001
P43286	AT3G53420	-6.27	0.011
Q43127	AT5G35630	-6.37	0.001
Q8VYF1	AT4G17390	-6.43	0.046
P56759	ATCG00130	-6.44	0.005
P10896	AT2G39730	-6.45	0.000
Q9SIP7	AT2G31610	-6.73	0.001
P46286	AT2G18020	-6.91	0.001
P17094	AT1G43170	-7.00	0.012
Q01908	AT4G04640	-7.04	0.006
O50008	AT5G17920	-7.15	0.004
Q9FVQ1	AT1G48920	-7.18	0.012
Q56YA5	AT2G13360	-7.18	0.010

Q8RWV0	AT3G60750	-7.23	0.001
P23321	AT5G66570	-7.23	0.008
P25856	AT3G26650	-7.63	0.005
Q9LD57	AT3G12780	-7.74	0.000
Q9SZJ5	AT4G37930	-8.59	0.000
Q41932	AT4G05180	-10.00	0.000
Q9FX54	AT1G13440	-10.00	0.000
O49299	AT1G23190	-10.00	0.000
Q9ZR03	AT4G03280	-10.00	0.000
P56792	ATCG00780	-10.00	0.000
F4IMB5	AT2G07698	-10.00	0.000
P22953	AT5G02500	-10.00	0.000
Q9SRU7	AT3G02320	-10.00	0.000
P49688	AT2G41840	-10.00	0.000
Q93VG5	AT5G20290	-10.00	0.001
P56801	ATCG00770	-10.00	0.001
O80480	AT1G09270	-10.00	0.001
Q9LFF8	AT3G52930	-10.00	0.001
P56802	ATCG00750	-10.00	0.001
P16181	AT3G48930	-10.00	0.001
Q9SMX3	AT5G15090	-10.00	0.001
P51430	AT5G10360	-10.00	0.001
Q9LR64	AT1G03600	-10.00	0.001
Q9FVE6	AT3G44750	-10.00	0.001
Q9C9C6	AT1G74060	-10.00	0.001
Q9LJE4	AT3G13470	-10.00	0.001
Q9STW6	AT4G24280	-10.00	0.001
Q9STF2	AT3G46780	-10.00	0.001
Q56WH4	AT5G22650	-10.00	0.001
Q9M047	AT3G55770	-10.00	0.001
Q9LFH5	AT3G53430	-10.00	0.001
Q9FN48	AT5G23060	-10.00	0.002
Q9SAJ4	AT1G79550	-10.00	0.002
P09468	ATCG00470	-10.00	0.002
O24456	AT1G18080	-10.00	0.002
Q9LR33	AT1G23290	-10.00	0.002
P49200	AT3G45030	-10.00	0.002
Q8VZ68	AT5G62300 AT1G52670	-10.00	0.002
P25857	AT1G42970	-10.00	0.003
Q9T043	AT4G27090	-10.00	0.003
Q9LR75	AT1G03475	-10.00	0.004
P29513	AT1G20010	-10.00	0.004
Q93VH9	AT2G17360	-10.00	0.004

P34788	AT1G22780 AT1G34030 AT4G09800	-10.00	0.004
F4HS99	AT1G01320	-10.00	0.004
Q9ZQ80	AT2G03440	-10.00	0.004
O65719	AT3G09440	-10.00	0.005
Q9LFN6	AT5G11170 AT5G11200	-10.00	0.007
P21218	AT4G27440	-10.00	0.007
P51818	AT5G56010	-10.00	0.007
Q5GM68	AT2G42600	-10.00	0.007
Q9SA52	AT1G09340	-10.00	0.008
Q9LPW0	AT1G12900	-10.00	0.008
P93014	AT2G33800	-10.00	0.008
Q9XFT3	AT4G21280	-10.00	0.008
Q9LNB6	AT1G12270	-10.00	0.008
F4JL11	AT4G16143	-10.00	0.008
P51407	AT2G27720	-10.00	0.008
Q8LBI1	AT3G25520	-10.00	0.009
P21238	AT2G28000	-10.00	0.010
P41376	AT3G13920	-10.00	0.010
Q9SSS9	AT4G09650	-10.00	0.010
Q42139	AT4G32260	-10.00	0.011
Q08682	AT1G72370	-10.00	0.011
Q96250	AT2G33040	-10.00	0.011
O04204	AT2G40010	-10.00	0.011
P25851	AT3G54050	-10.00	0.011
Q9SKX4	AT2G43030	-10.00	0.012
P55852	AT4G26840	-10.00	0.012
P56793	ATCG00790	-10.00	0.014
Q9ZVL6	AT1G54780	-10.00	0.013
P42825	AT5G22060	-10.00	0.014
Q9T029	AT4G39200	-10.00	0.014
Q96266	AT2G47730	-10.00	0.014
O23174	AT4G37120	-10.00	0.014
Q9FE65	AT1G69620	-10.00	0.014
O80653	AT1G77180	-10.00	0.015
Q9S714	AT2G20260	-10.00	0.015
Q9C9I7	AT1G71500	-10.00	0.015
F4JP43	AT4G17330	-10.00	0.015
Q9MAB3	AT3G05060	-10.00	0.016
Q9LQI9	AT1G17370	-10.00	0.016
Q9FI56	AT5G50920	-10.00	0.017
Q9SK69	AT2G20330	-10.00	0.017
Q9XI93	AT1G13930	-10.00	0.017
Q9ZP05	AT5G09660	-10.00	0.017

O65396	AT1G11860	-10.00	0.017
Q9ZNZ7	AT5G04140	-10.00	0.018
O23049	AT1G05190	-10.00	0.018
Q9FM47	AT5G40490	-10.00	0.018
Q9M158	AT4G01050	-10.00	0.018
P46283	AT3G55800	-10.00	0.018
Q9ASR1	AT1G56070	-10.00	0.018
Q9FKW6	AT5G66190	-10.00	0.019
Q9ASS2	AT1G20110	-10.00	0.019
Q8GUP3	AT4G31880	-10.00	0.020
Q93W03	AT3G56130	-10.00	0.021
Q0WNJ6	AT3G11130	-10.00	0.022
Q38953	AT3G26560	-10.00	0.022
Q9LUT2	AT3G17390	-10.00	0.023
Q9FND0	AT5G43960	-10.00	0.023
Q940B0	AT5G27850	-10.00	0.023
Q9CA67	AT1G74470	-10.00	0.024
Q9SRX2	AT1G02780	-10.00	0.025
P46645	AT5G19550	-10.00	0.025
O04983	AT5G35360	-10.00	0.025
Q9LU74	AT5G57120	-10.00	0.026
O23553	AT4G17090	-10.00	0.026
O80860	AT2G30950	-10.00	0.026
Q9SZY1	AT4G10480	-10.00	0.026
Q9SH88	AT2G37990	-10.00	0.028
P92948	AT1G09770	-10.00	0.029
Q8VZ31	AT1G04530	-10.00	0.031
A4FVN8	AT1G10580	-10.00	0.032
Q9LQ55	AT1G59610	-10.00	0.033
Q8L611	AT3G63460	-10.00	0.038
Q9LZQ9	AT3G62310	-10.00	0.038
Q9M2D8	AT3G61260	-10.00	0.041
O65655	AT4G39680	-10.00	0.042
Q8L4S3	AT5G09390	-10.00	0.044
Q9STN3	AT4G08350	-10.00	0.044
P42697	AT5G42080	-10.00	0.045
P38666	AT3G53020	-10.00	0.046
Q9LVK6	AT3G13940	-10.00	0.047
P10796	AT5G38430	-10.00	0.049
Q56WK6	AT1G72150	-10.00	0.049
Q9ZUP3	AT2G19480	-10.00	0.049

I declare under oath that I have produced my thesis independently and without any undue assistance by third parties under consideration of the 'Principles for the Safeguarding of Good Scientific Practice at Heinrich Heine University Düsseldorf'.